NBSIR 77-853
CONS-3800-1

HELIUM RESEARCH IN SUPPORT OF SUPERCONDUCTING POWER TRANSMISSION

ANNUAL REPORT

(July 1975 - September 1976)

CRYOGENICS DIVISION
INSTITUTE FOR BASIC STANDARDS
NATIONAL BUREAU OF STANDARDS
BOULDER, COLORADO 80302

PREPARED FOR

THE U.S. ENERGY RESEARCH AND DEVELOPMENT ADMINISTRATION
OFFICE OF CONSERVATION
DIVISION OF ELECTRIC ENERGY SYSTEMS
UNDER CONTRACT NO. E(49-1)-3800

February 1977

NBSIR 77-853
CONS-3800-1

HELIUM RESEARCH IN SUPPORT OF SUPERCONDUCTING POWER TRANSMISSION

ANNUAL REPORT

(July 1975 - September 1976)

M.C. JONES, V.D. ARP, W.R. PARRISH,
D.E. DANEY, P.R. LUDTKE, N.V. FREDERICK
AND B.A. HANDS*

CRYOGENICS DIVISION
INSTITUTE FOR BASIC STANDARDS
NATIONAL BUREAU OF STANDARDS
BOULDER, COLORADO 80302

(*Guest Worker from Department of Engineering Sciences,
University of Oxford)

PREPARED FOR

THE U.S. ENERGY RESEARCH AND DEVELOPMENT ADMINISTRATION
OFFICE OF CONSERVATION
DIVISION OF ELECTRIC ENERGY SYSTEMS
UNDER CONTRACT NO. E(49-1)-3800

February 1977

U.S. DEPARTMENT OF COMMERCE, Juanita M. Kreps, Secretary

Dr. Betsy Ancker-Johnson, Assistant Secretary for Science and Technology

NATIONAL BUREAU OF STANDARDS, Ernest Ambler, Acting Director

FOREWORD

In order to bring superconducting electric power transmission for ulilities application from its conceptual stage to a practical realization, developments were needed in several fields apart from the conductor itself. These included electrical insulations, economical of space, which would function at the low temperatures of the conductor; cable designs to withstand the thermal stress accompanying cooldown; refrigeration machinery of heretofore unheard of reliability; and low-cost, reliable cryogenic envelopes to house and thermally insulate the low-temperature cables. But, in addition to these, it was recognized that the circulation of helium at temperatures and pressures required to refrigerate superconductors in channels kilometers long presented a unique thermal-hydraulic situation; no such flow system had been operated prior to the inception of this cable development work.

The combination of cable refrigerant channels, whose walls have low thermal capacitance at liquid helium temperatures, and the strongly temperature dependent density of the helium at the thermodynamic states encountered in the refrigeration of the superconductor could be shown on theoretical grounds to lead to flow instabilities in some circumstances. This situation was compounded by the fact that available instrumentation for basic helium measurements were either unavailable or primitive and some special problems resulted from the high voltages present in the cable.

These are the general problems addressed by the current program of research at the Cryogenics Division of the National Bureau of Standards. The goals are to identify the conditions under which stable flow and temperature of the refrigerant can be expected in order to maintain the conductor at its proper working temperature, notwithstanding the perturbing effect of network fault currents; further, to conduct such research and development on measurement techniques as to ensure that the performance of model and prototype cables and their refrigeration systems can be intelligently monitored.

CONTENTS

LIST OF FIGURES

List of Figures (continued) Page

List of Figures (continued) Page

ABSTRACT

This report is the second annual report of research on helium related problems in support of superconducting power transmission development. The report is in four sections.

In the first section; results are presented from experimental and computer modeling of the performance of current leads cooled with supercritical helium gas. Performance characteristics studied are burn-out conditions and existence of oscillation in the helium gas.

The second section, on helium measurements, reports some conclusions on the feasibility of data transmission from high-voltage regions to grounded read-out instrumentation, on thermometry and on helium impurity measurements. A major part of this section is a detailed description with test results of microwave cavity pressure transducers for use at helium temperatures.

A third section, on helium properties, reports some improvements in computer codes for helium properties and discusses some recent data on the thermal conductivity of helium.

In the final section, a description is given of a recently completed flow facility which has been built for research on flow and heat transfer dynamics of supercritical helium in channels of high aspect ratio modeling superconducting power transmission line channels.

Key Words: Burn-out; helium-cooled current leads; helium flow facility; helium impurities; microwave pressure transducer; thermal-acoustic oscillations.

1.0. CURRENT LEADS COOLED WITH SUPERCRITICAL HELIUM FOR SUPERCONDUCTING POWER TRANSMISSION LINE TERMINATIONS

1.1. Introduction

Much has appeared in the literature on the thermodynamic optimization of current leads, but it becomes increasingly clear for electric power applications that considerations of efficiency must give way to those of reliability, safety and operability. This has been the emphasis of the NBS program. High voltage aspects have not concerned us, however, since these are under study elsewhere and the thermal performance appears to be a separable problem.

Our concern at the outset was that, although helium-cooled current leads were common everyday accessories in many laboratories, almost all of them were of the self-sustained type cooled by boil-off helium from a dewar at a little over atmospheric pressure. SPTL leads would require the use of high pressure helium and the gas flow would be set independently of current. This had implications as far as thermal runaway, or burn-out, is concerned, and we also had some concerns about the possibility of thermal acoustic oscillations in the helium, a commonly observed phenomenon in tube penetrations into liquid helium dewars. Our approach, therefore, was to build small models of candidate designs and to run these at current densities and helium conditions typical of proposed SPTL leads.

Unfortunately, at the time we began this work, only one such lead had been designed for this application and this was of the conventional Efferson braid type adapted to a.c. conditions by having transposed braids. We therefore chose basic model geometries whose operational characteristics, if not detailed construction, could be scaled up to desired capacity.

Four models of different design were studied; the essential features of each are given in table 1 and figure 1. The first two leads were designed to encompass a wide variation in flow and heat transfer characteristics. Thus in no. 1 - a simple tubular conductor - the gas friction factor and heat transfer coefficient for a given Reynolds number should be the lowest limit achievable, as should also the heat transfer area per unit length in relation to the conductor cross section. In lead no. 2 - a braided lead in an annular space - these factors were expected to be about as high as can be achieved. The heat transfer aspects of a lead, as shown below in section 1.2, are characterized by the dimensionless group $H = hPL^2/kA$, where h is the heat transfer coefficient, P the wetted perimeter (or heat transfer surface area per unit length), L the lead length, k the conductor thermal conductivity at reference conditions and A the cross sectional area of the conductor. This factor based on an unenhanced laminar flow heat transfer coefficient is also listed in table 1.1.

Lead no. 3 is a special tapered lead design of larger capacity constructed by the Los Alamos Scientific Laboratory. A large heat transfer area is obtained in this case by soldering an externally threaded copper tube in the center of a hollow conductor generating three parallel spiral channels against the bore, the central passage being plugged.

While we had tested nos. 1 and 2 with a return lead which was similar in construction to no. 2, we needed a new return lead of greater length and capacity for use with no. 3. We chose a length of copper heat exchanger tubing consisting of a coiled copper spiral ribbon insert soldered between a central core and an outer tube used as the conductor. We also tested this lead as no. 4. This choice had one advantage that heat transfer and pressure drop characteristics were well documented [1] as well as its being naturally an efficient heat transfer device. Tests on leads 3 and 4 were restricted to one pressure (1 MPa) and an inlet helium temperature range of 4.5-6 K while those for nos. 1 and 2 covered the range from 0.25 to 1.5 MPa and 4.5 to 12 K.

TABLE 1.1. LEAD SPECIFICATIONS

	Lead No. 1	Lead No. 2	Lead No. 3	Lead No. 4
Construction	Simple Tube 0.48 cm I.D. X 0.026 cm wall	Braided Wire in Annulus (192 strands, 34 gauge) Annulus: 0.425 cm O.D., 0.274 cm I.D.	Tapered Tube with Spiral Insert 1.562-1.016 cm O.D., 0.952 cm I.D.	Heat Exchanger Tubing; Spiral Ribbon Insert 1.70 cm O.D.; 1.257 cm I.D. 0.32 cm diameter core
Length (cm)	45.7	45.7	100.3	100.0
Material	Phosphorized Copper (refrigeration tubing)	ETP Copper	Relatively Pure Copper	Phosphorized Copper
Resistance Ratio ($\frac{R293K}{R4K}$)	5.93	53.8	Tube 90; Insert 8.92	5.4
Conductor Area (cm^2)	0.0413	0.0385	Top 1.376; Bottom 0.276; Insert 0.177	1.023
Hydraulic Diameter (cm)	0.48	0.0184	0.19	0.167
Flow Area (cm^2)	0.142	0.0445	0.112 perpendicular to flow 0.312 perpendicular to axis	0.84
Porosity (%)	NA	54	NA	72
Surface Area Per Unit Length (cm)	1.51	9.65	6.14	20.12
Optimum Helium Flow (g/s)	0.003	0.088	0.025	0.048
Optimum Current (A)	51	190	675	800
H^* 6K	57	7,600	218	360
300K	330	44,000	330	2100

*Based on Nu = 4.36.

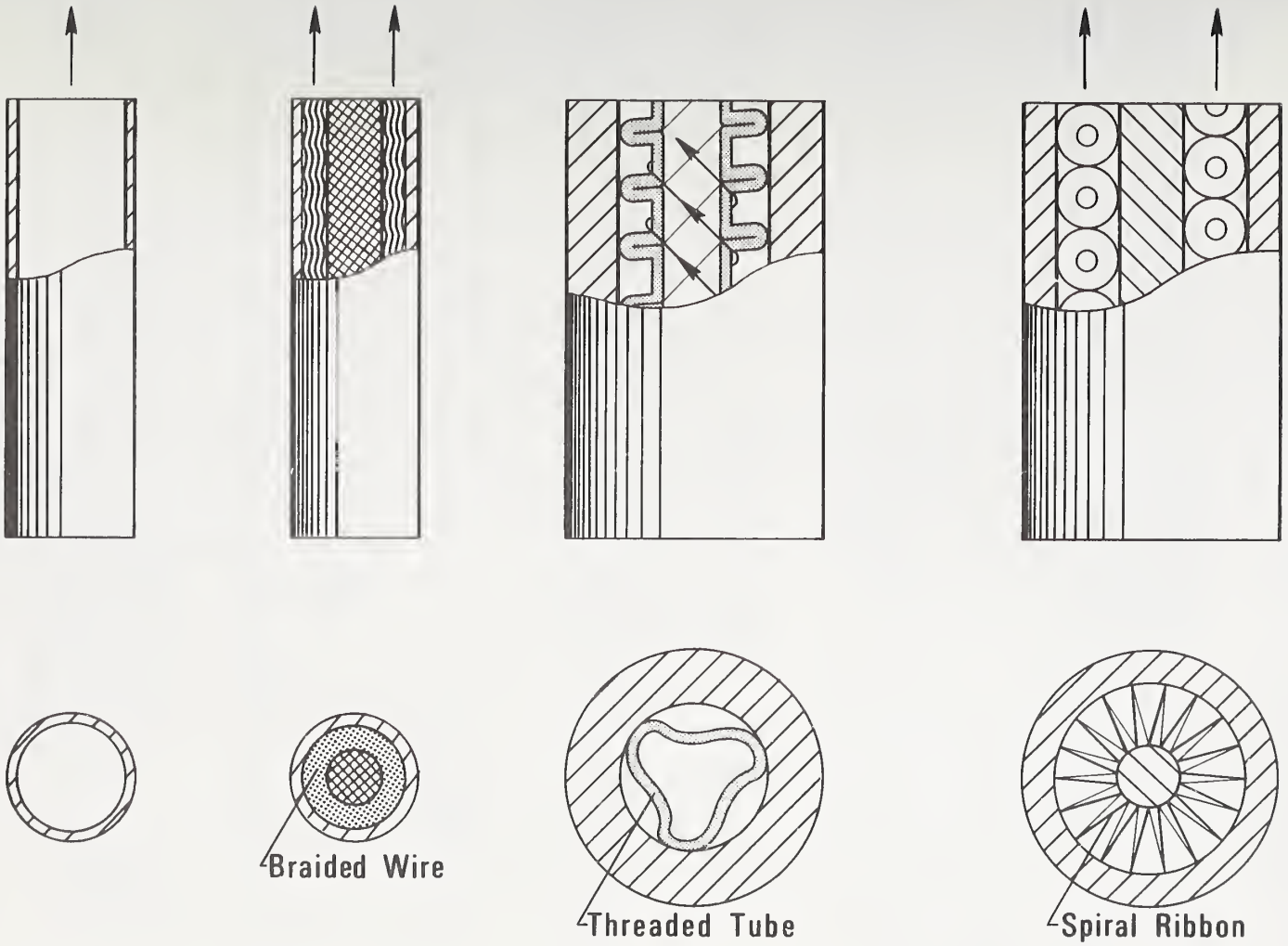

Figure 1.1. Sketch showing model lead construction.

In section 1.2 we discuss the similarity laws for current leads. After a brief description of the experimental details of our test apparatus in section 1.3, we discuss our observations of thermal runaway and computations of this phenomenon in 1.4. In section 1.5 oscillatory behavior observed in testing the leads is discussed. Finally, in section 1.6 we list some recommendations for lead design resulting from this study.

1.2 Similarity Considerations

It is useful to consider under what conditions a model and full scale current lead can have identical temperature profiles. This can be done by a dimensional analysis of the governing differential equations and boundary conditions. We assume that the temperature boundary conditions at the lead ends (both conductor and gas) are the same and that the same material is used for the conductor. This analysis does not depend upon the often used simplifications that the Wiedemann-Franz law is obeyed, or that the thermal conductivity is a constant, or that the heat transfer coefficient and specific heat of the gas is a constant. Furthermore, a variable conductor cross sectional area may be admitted.

For a given construction and conductor material with thermal conductivity $k(T)$, resistivity $\rho(T)$, cross sectional area $A(x)$, operating between the lower and upper temperatures T_o and T_u for the conductor and θ_o and θ_u for the gas, the governing differential equations for one dimensional heat flow in the conductor and gas are

$$\frac{d}{dx}\left(kA\,\frac{dT}{dx}\right) - \frac{dQ}{dx} + \frac{\rho I^2}{A} = 0 \qquad (1.1)$$

$$\dot{m}C_p\,\frac{d\theta}{dx} = \frac{dQ}{dx} = Ph\,(T-\theta)\,, \qquad (1.2)$$

dQ/dx is the lateral heat transfer to the gas per unit length, $\dot{m}$ the gas flow rate and P the perimeter of the conductor in contact with gas.

We now define reference values (eg. at T_u), denoted by asterisks, for the temperature dependent quantities k, C_p, h. We also define dimensionless distance η by $d\eta = \frac{k^*A^*}{kAL}\,dx$ and,

$$\eta_L = \frac{k^*A^*}{L}\int_o^L \frac{dx}{kA} \qquad (1.3)$$

where L is the length of the lead. Then the differential equations may be written

$$\frac{d}{d\eta}\left(\frac{dT}{d\eta}\right) - \left(\frac{kA}{k^*A^*}\right)\left(\frac{h}{h^*}\right)\left(\frac{Ph^*L^2}{k^*A^*}\right)(T-\theta) + \left(\frac{k\rho}{L_oT}\right)\left(\frac{L_oL^2I^2}{k^{*2}A^{*2}}\right)T = 0 \qquad (1.4)$$

$$\frac{d\theta}{d\eta} = \left(\frac{Ph^*L}{\dot{m}C_p^*}\right)\left(\frac{C_p^*}{C_o}\right)\left(\frac{h}{h^*}\right)\frac{kA}{k^*A^*}\,(T-\theta) \qquad (1.5)$$

where we have introduced the Lorenz constant L_o ($\propto k\rho/T$). Insofar as $\frac{h}{h^*}$, $\frac{kA}{k^*A^*}$, $\frac{C_p}{C_p^*}$ and $\frac{k\rho}{L_oT}$ are dimensionless functions of η, T and θ, the solutions

for T and θ must have as sole parameters the three dimensionless quantities

$$J = \frac{L_o^{1/2} LI}{k^* A^*}, \quad M' = \frac{\dot{m} C_p^*}{Ph^* L} \quad \text{and} \quad H = \frac{Ph^* L^2}{k^* A^*}$$

or, alternatively, we can choose the equivalent three parameters J, $M = \frac{\dot{m} C_p^* L}{k^* A^*}$ and $H' = \frac{Ph^* L}{L_o^{1/2} I}$. For a given conductor material, therefore, to achieve identical temperature profiles in a model and full scale lead we must preserve the ratios IL/A^*, $\dot{m}L/A^*$ (or $\dot{m}/I$) and $Ph^* L^2/A^*$ (or $Ph^* L/I$).

We will consider now what the implications are for scale-up, for the optimum operating condition and for the burn-out, or thermal runaway condition.

i) Scale-up. The first two parameters J and M give the fairly obvious requirements that, for the same length, current scales with cross sectional area and mass flow rate with current. Alternatively, if cross section is to be held constant, current and mass flow must scale as the inverse of the length. The consequences of the third parameter H may be best illustrated by considering the scale-up of a lead without change in length. In this case $h^* \sim k_G^*/D_H$ if hydrodynamic similarity is maintained, or the the flow is laminar, where k_G^* is the thermal conductivity of the gas at reference conditions and D_H is the mean hydraulic diameter. Thus, one class of lead that may always be scaled up is the matrix (eg., bundles of wires, braids, sintered spheres) simply by maintaining the same diameter filament or sphere with the same packing density. A simple tubular conductor scales up into many identical tubes, but not into a larger tube. A finned conductor will scale-up if the fin dimensions and conductor radial thickness are held constant. If H is large enough, say $H > 10{,}000$, we have ideal heat transfer. Then θ T and a temperature profile for given material and end temperatures is determined by J and M alone making scale-up straightforward for any such lead.

ii) Optimum Operating Conditions. If one is not constrained by the performance characteristics of an already existing refrigerator a lead must be optimized by minimizing the ideal Carnot work required to both refrigerate the cold end and supply the cooling gas. The optimum condition then corresponds to a particular temperature profile. If we neglect the electrical energy lost in the lead through Joule heating it is a profile with zero temperature gradient at the warm end as shown by Lock [2] for self-sustained leads with ideal heat transfer, by Pippard [3] for the more general gas-cooled lead with ideal heat transfer, and by Agsten [4] for a lead cooled in a thermodynamically optimum manner. But whether we neglect the Joule heating or not a fixed profile in dimensionless form results. However, it is not clear that the same profile still holds for less than ideal heat transfer.

Again, if we are to run both the model and full-scale lead at optimum conditions, this can be achieved by preserving the ratios IL/A^*, $\dot{m}/I$ and $h^* PL/I$. The Carnot work for the cold gas is simply proportional to $\dot{m}$ which is proportional to I, and the Carnot work for the cold end refrigeration is proportional to $A \left.\frac{dT}{dx}\right|_{x=0}$. The latter can be obtained from the optimum dimensionless profile: $\left.\frac{AdT}{dx}\right|_{x=0} \sim \frac{A^*}{L} \left.\frac{dT}{d\eta}\right|_{\eta=0}$. Therefore the optimum cold end refrigeration is also proportional to the optimum I. As is well known, if heat exchange approaches the ideal case, optimum total refrigeration per ampere should be independent of the lead geometry. It also follows in this

case that the mass flow per ampere and the factor IL/A* should be the same for all optimized leads of the same material operating between the same temperatures.

iii) Burn-out Conditions. Burn-out of a lead corresponds to a singularity in the temperature for certain combinations of J and M. Experimentally, above a certain current for fixed mass flow rate the lead temperature rises at ever increasing rate, or runs away, instead of approaching a limit. The question is, for the purposes of this work, if we know burn-out conditions for a model lead can they be predicted for the full scale? Since again burn-out is related to a property of the temperature profile we simply have to preserve the same three scaling ratios. However, this case differs from the consideration of optimum conditions in that burn-out can occur at some current for all values of $\dot{m}$ for a given lead, so we need to determine the burn-out relation I vs. $\dot{m}$. More generally, at burn-out M is a function of J with H as parameter, but note that H may be a function of M. The general case has not been tackled, but Bejan and Cluss[5] have recently computed the relations for the simple model of constant thermal conductivity, and resistivity linear with temperature. In the absence of a more general solution, burn-out must be modeled with a lead of the same material and same end temperatures with the same H. Alternatively, exact numerical calculations can be made for a given material if the thermal conductivity and electrical resistivity are known as functions of temperature and if the heat transfer coefficient and its flow dependence are known.

In summary, similarity considerations lead us to the laws of scale-up applicable to a model and full scale lead of the same material, and hence to the prediction of the optimum operating point and the burn-out curve once these are known for the model.

1.3. Experimental Details

A description and flow scheme for the experimental arrangement for testing the model leads appeared in our previous annual report.[6] In view of some minor modifications a revised flow scheme is given in figure 1.2. The major revision is the addition of a small circulating pump to spray liquid helium at 4 K onto the cold bus bar which connects the two current leads under test. This was found to be necessary because of inadequate heat exchange between the cold end of the leads and the helium supply pressure vessel. The pump together with a heater on the pressure vessel allowed flexibility in running the cold end of the leads from 4.5 to 15 K.

The leads were instrumented with six or ten thermocouples evenly spaced along their length and referenced at the cold end to a germanium resistance thermometer mounted in a heavy copper fitting. This also formed the electrical end of the lead. Each lead had its own separate vacuum jacket and the whole assembly plus the return lead assembly was soldered into a 15 liter pressure vessel with a heavy copper bus bar connecting the two leads at the base. Detailed drawings showing the mounting of the four model leads are given in figures 1.3, 1.4, 1.5 and 1.6 respectively. The lead no. 3 was supplied to us with two alternatives for electrical connection. In the first, shown in figure 1.5, the electrical connection was directly to a boss at the end of the outer copper conductor. In the second alternative, current was supplied via an extension on which was wound a niobium-tin superconducting wire. This was then soldered onto the helical passages for 25 cm up into the lead as shown in figure 1.7. Both modes of connection were used in comparative tests.

Helium gas was supplied to the pressure vessel from a tube trailer via purification and heat exchange systems. The temperature of this vessel could be controlled by a flow splitting valve which directed up to 100 percent of the stream through a liquid helium heat exchanger. On account of the large

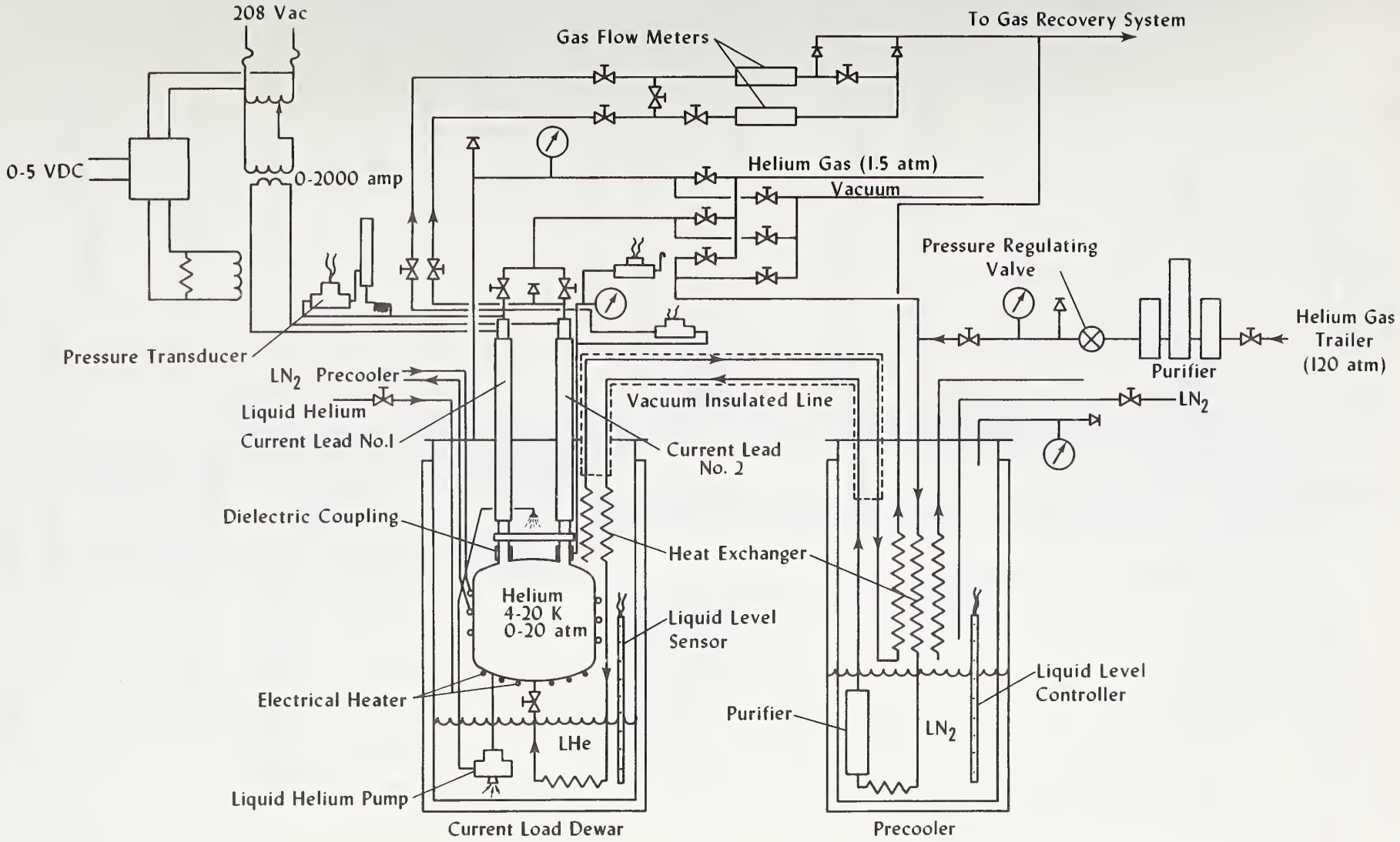

Figure 1.2. Flow schematic of lead test apparatus.

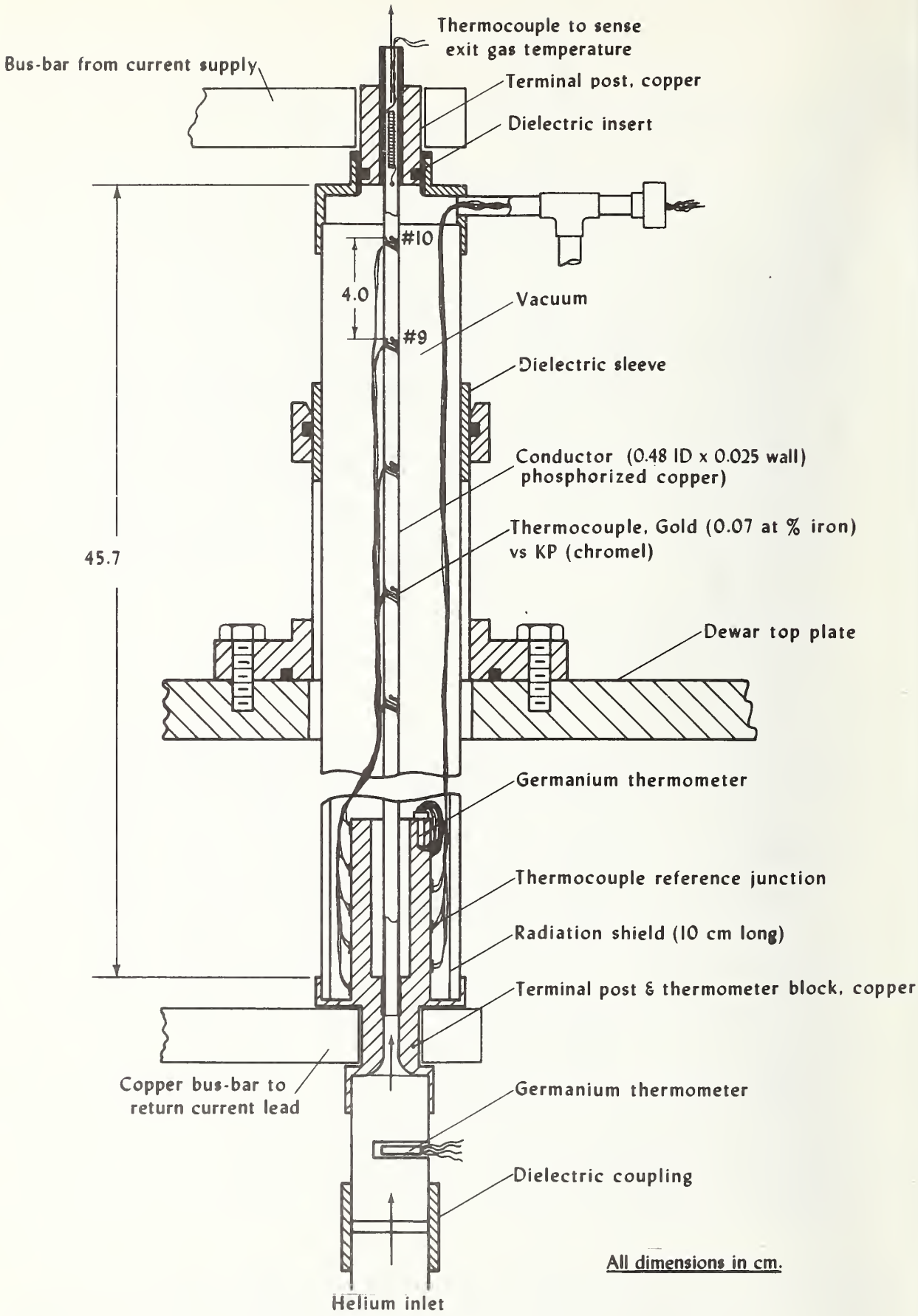

Figure 1.3. Installation of lead no. 1.

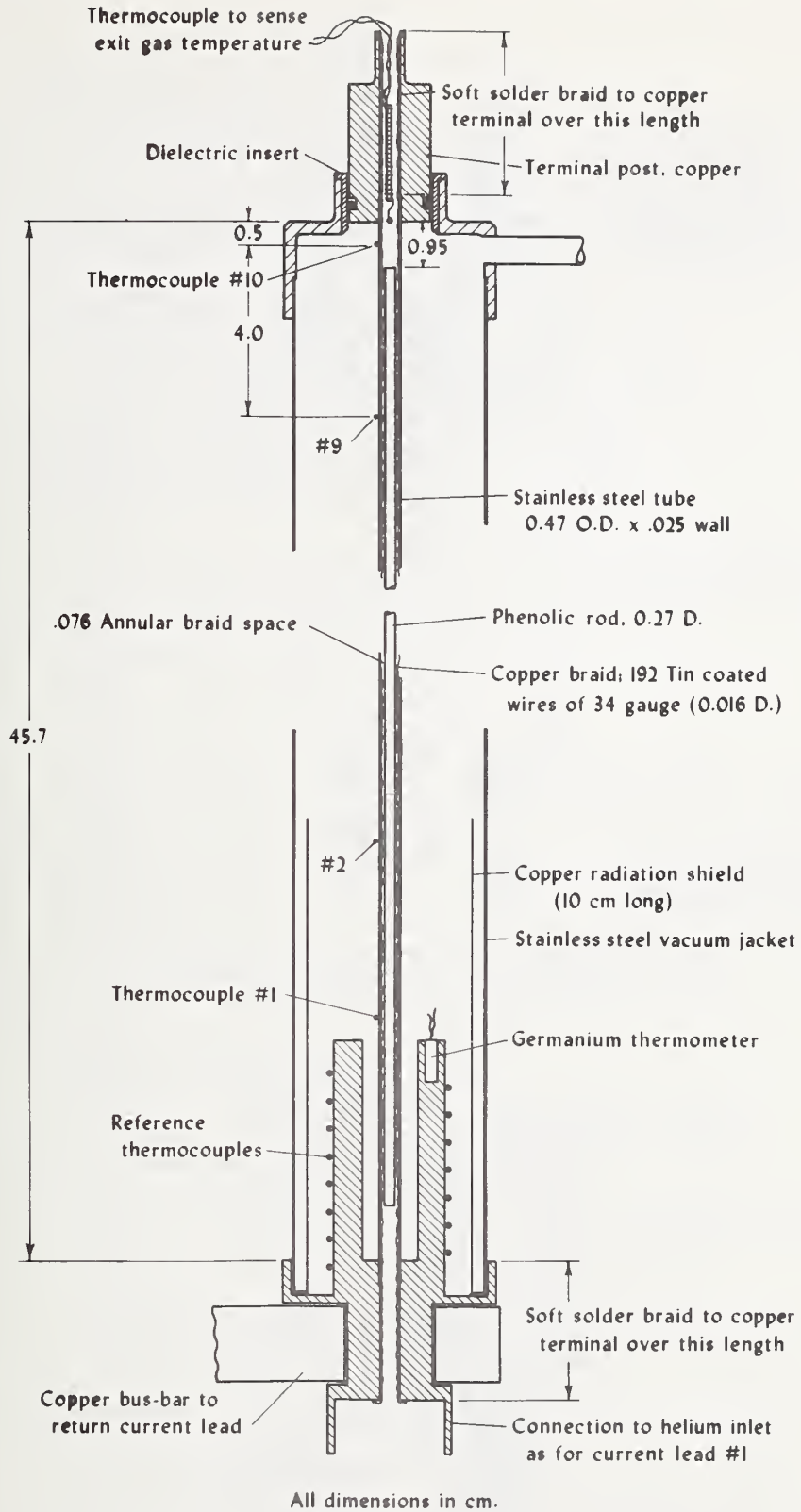

Figure 1.4. Installation of lead no. 2.

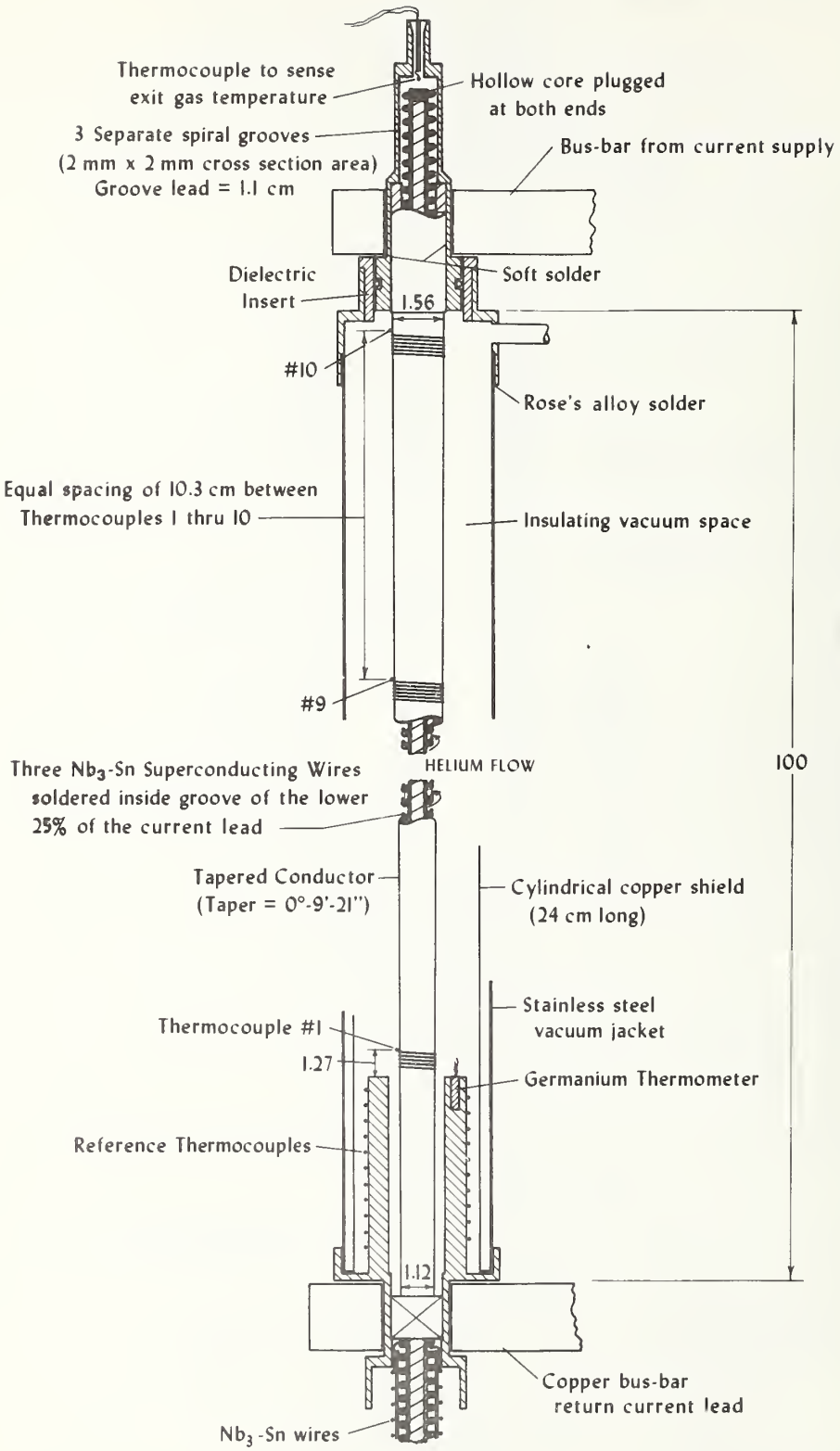

All dimensions in cm.

Figure 1.5. Installation of lead no. 3.

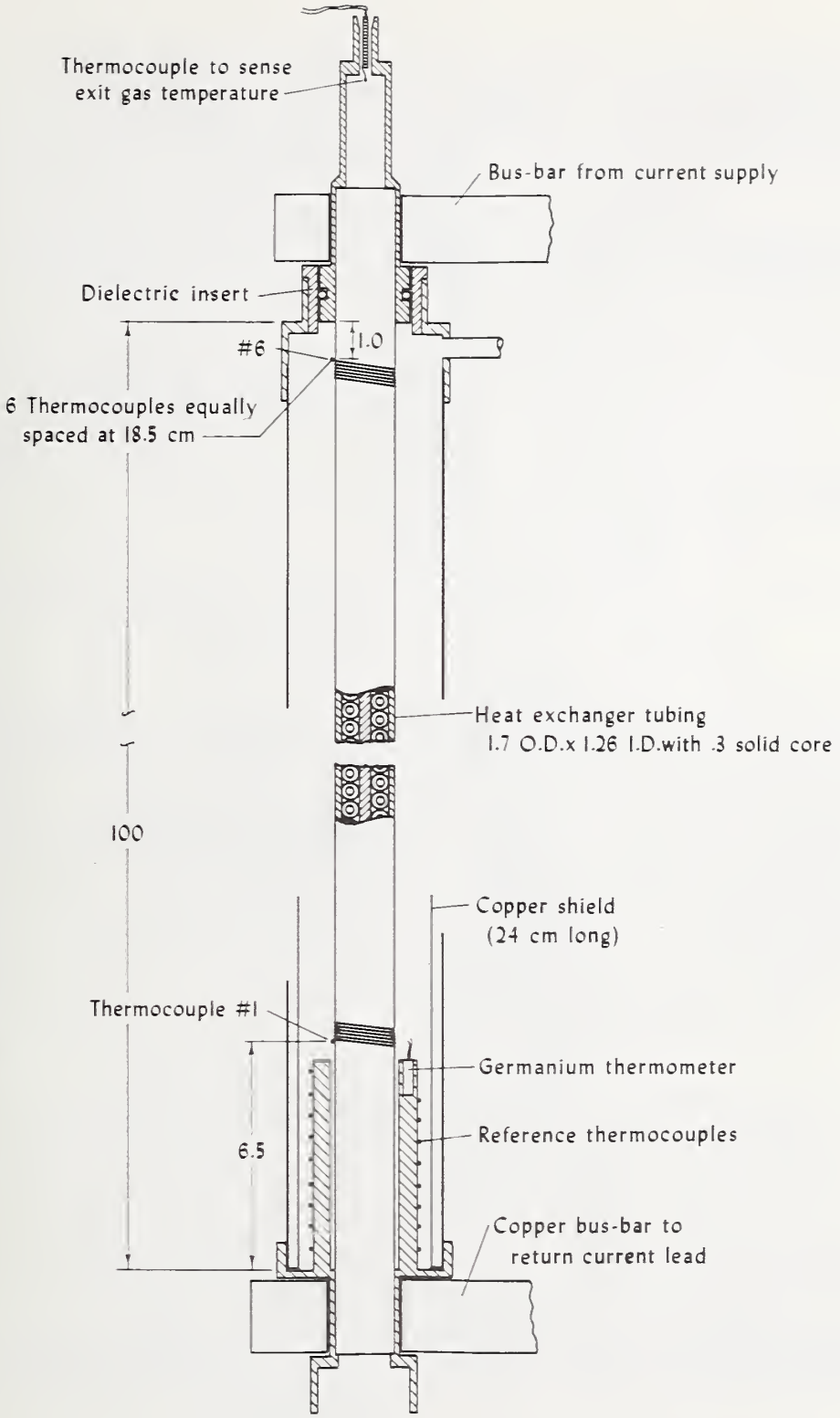

All dimensions in cm.

Figure 1.6. Installation of lead no. 4.

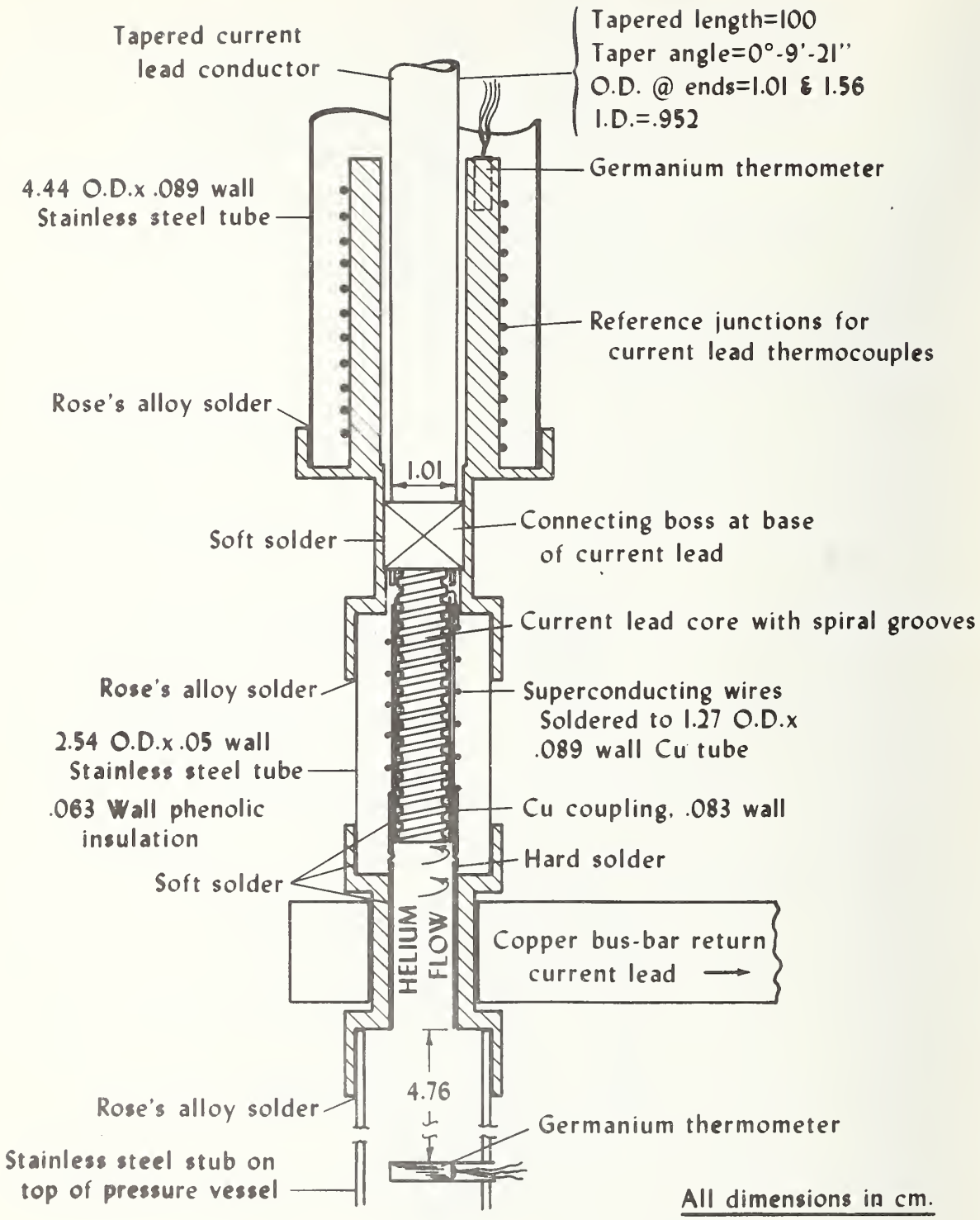

Figure 1.7. Alternative installation of lead no. 3.

reservoir capacity and low flow rates, measurements could be made with gas inlet to the reservoir closed. The flow through the test leads was regulated manually by a valve in the warm gas exit piping. At this valve gas pressure was reduced to essentially atmospheric. Finally, both ac current to 2000 A and dc to 600 A could be supplied via bus bars to the warm end of the lead.

The following measurements were made during each test.

1. Conductor and helium warm exit gas temperatures: Gold (0.07 at % iron) vs. KP (chromel) thermocouples. Estimated total error between $\pm$ 0.05 K at 4 K and $\pm$ K at t 300 K.

2. Helium inlet gas temperature: Germanium resistance thermometer. Estimated total error $\pm$ 0.01 K.

3. Helium mass flow rate through lead: Thermal flow meter. Estimated total error $\pm$ 0.001 g/s.

4. Helium reservoir pressure: Magnetic reluctance transducer. Estimated total error $\pm$ 0.01 MPa.

5. Pressure oscillation at lead warm end: Magnetic reluctance transducer. Frequency range as installed 0.1-200 Hz.

6. Lead current ($\pm$ 3% ac, $\pm$ 1-1/2% dc).

Representative temperature profiles for lead nos. 1, 3 and 4 are given in figures 1.8 through 1.13. In figures 1.14 and 1.15 a comparison of profiles for lead no. 3 is shown with the alternative methods of connection at the cold end. The use of the superconducting current path does not appear to have been of benefit; however, we feel that design of the cold end connection may not have been optimum for the heat flow in the case which utilized the niobium-tin superconductor. Comparison of profiles for leads 3 and 4 should take into account the much greater purity of the conductor for no. 3 as evidenced by the greater residual resistivity ratio. Further evaluation of this lead is being conducted by the Los Alamos Scientific Laboratory.

Lead no. 2 was selected for a detailed study of thermal run-away and temperature profiles are given and data discussed in section 1.4.

1.4 Thermal Runaway Studies

While the analysis and verification of optimum operating conditions for helium-cooled current leads has received a great deal of attention, the problem of thermal runaway, or the accidental burn-out of a lead, has been neglected with the exception of the work at MIT. For current leads cooled with supercritical helium gas at, say, 1.0-1.5 MPa, the helium flow rate may be set independently of the lead current and so the "flow choking" mechanism of burn-out suggested by Thullen, et al.[7] is not relevant. These authors correctly note that pressure drop increases with reduction in mass flow rate when currents are greater than a critical value. If the majority of the available pressure drop is taken across the lead itself the flow is unstable and must reduce indefinitely if the current parameter J is greater than π. For leads designed for SPTLs, however, or any system where high pressure helium is used, the flow will be stabilized by taking the majority of the pressure drop across a control valve.

For the SPTL application, the analysis of Bejan and Cluss[5] is more appropriate although this is based on the constant conductivity/linear resistivity model and is thus approximate for most coppers that would be considered in a lead. However, one new feature of this analysis is that it is

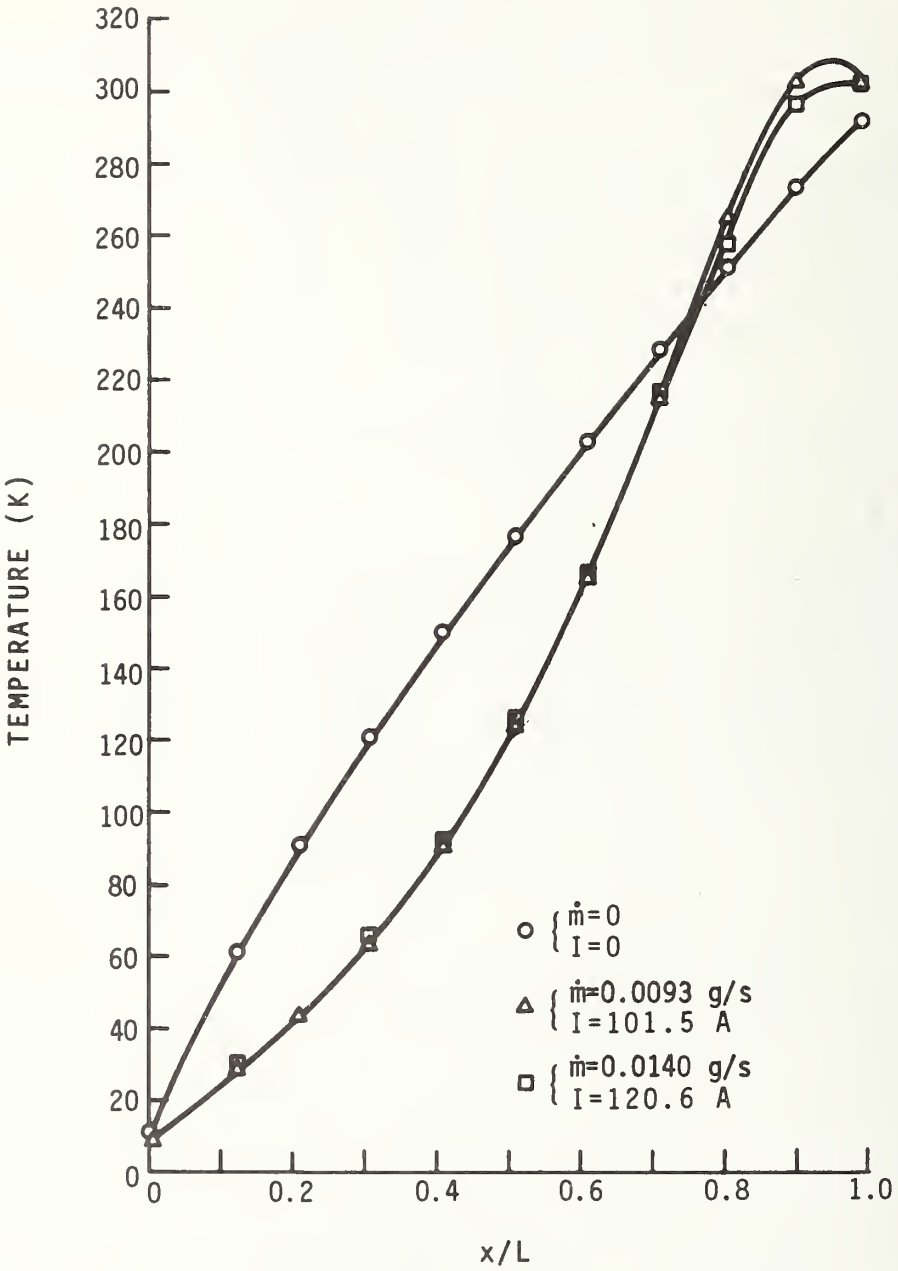

Figure 1.8. Temperature profiles for lead no. 1.

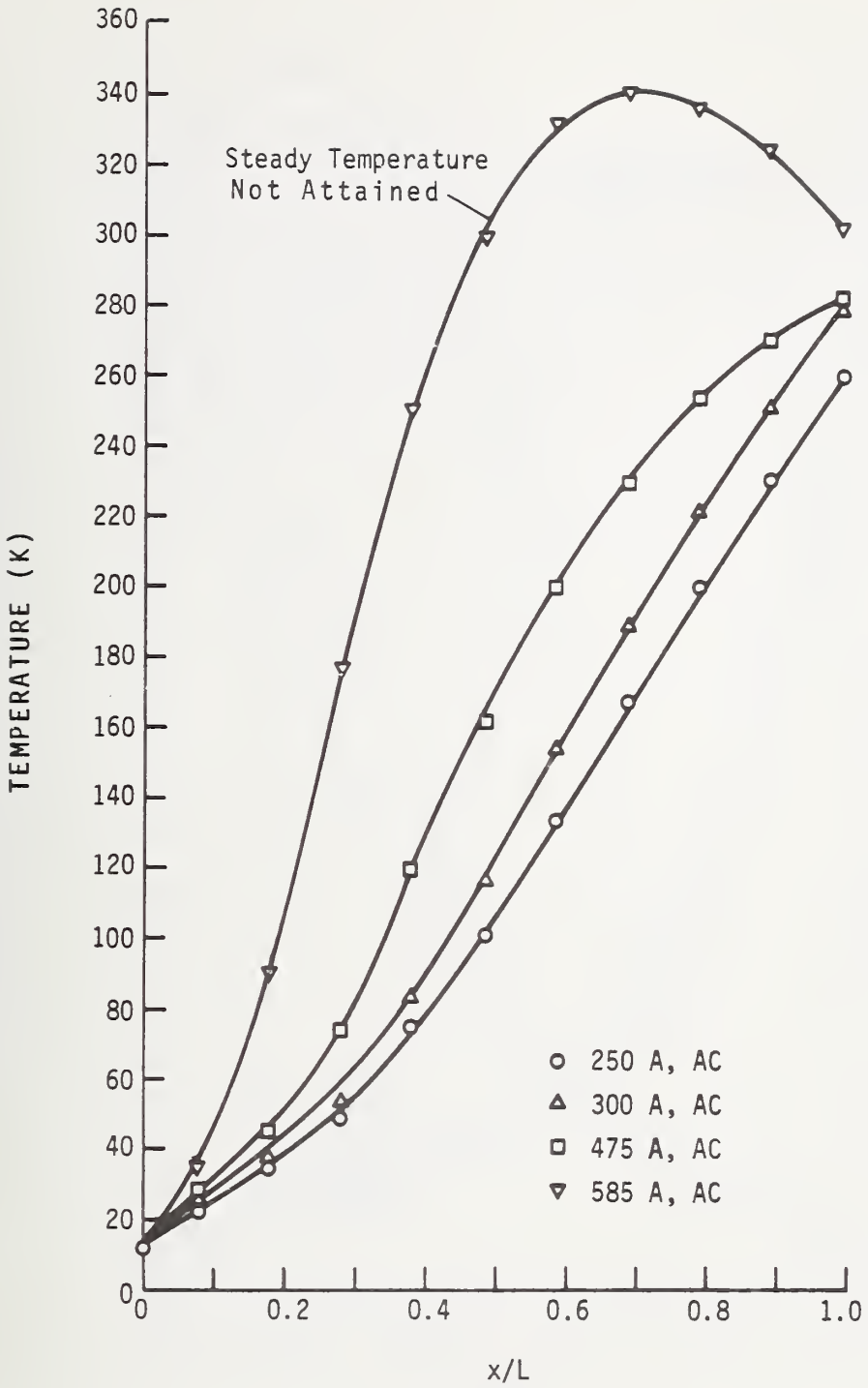

Figure 1.9. Temperature profiles for lead no. 3. Helium flow rate 0.0117 g/s, pressure 1.0 MPa, helium inlet temperature 4.5-6 K.

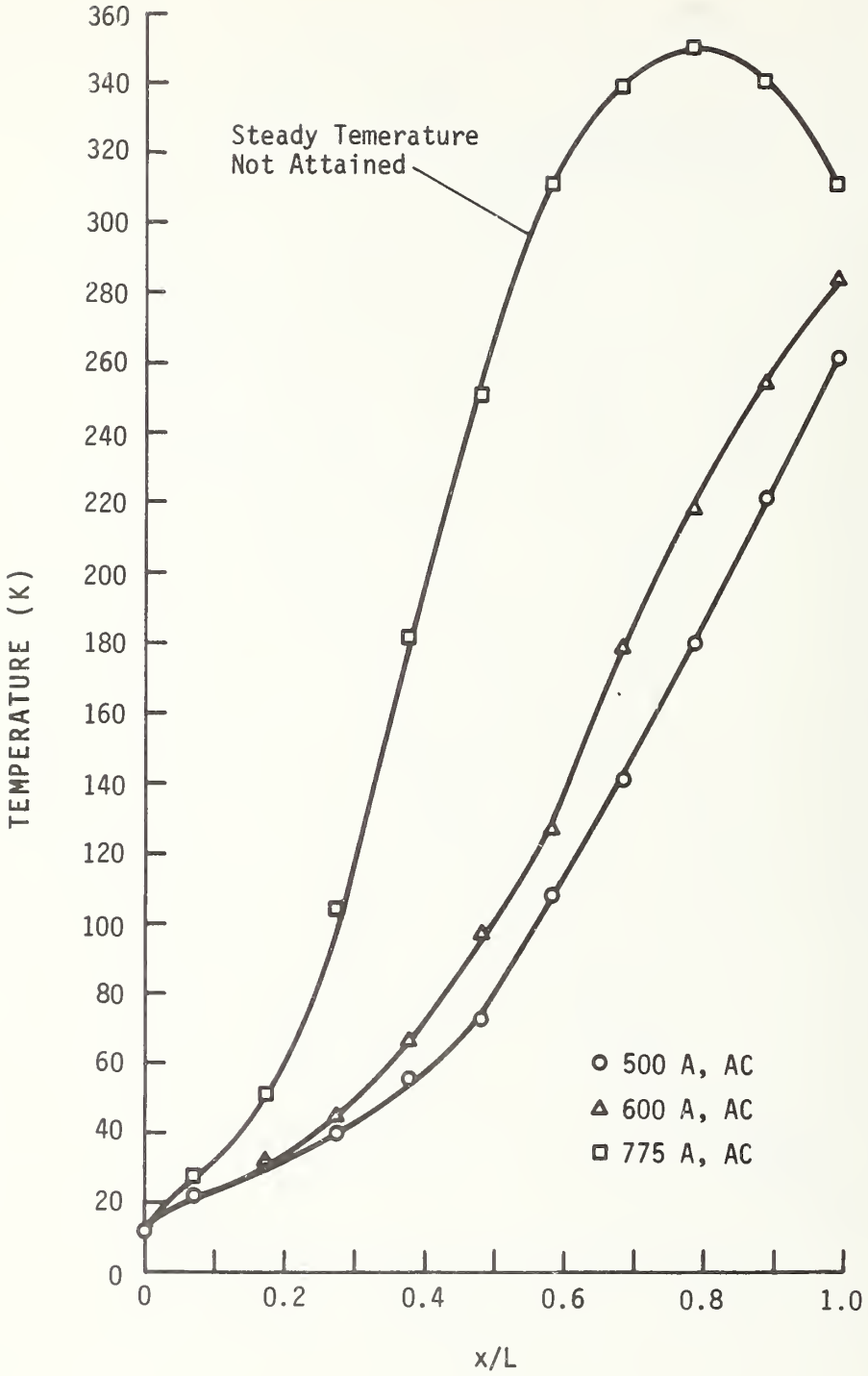

Figure 1.10. Temperature profiles for lead no. 3. Helium flow rate 0.0233 g/s, other conditions as for figure 1.9.

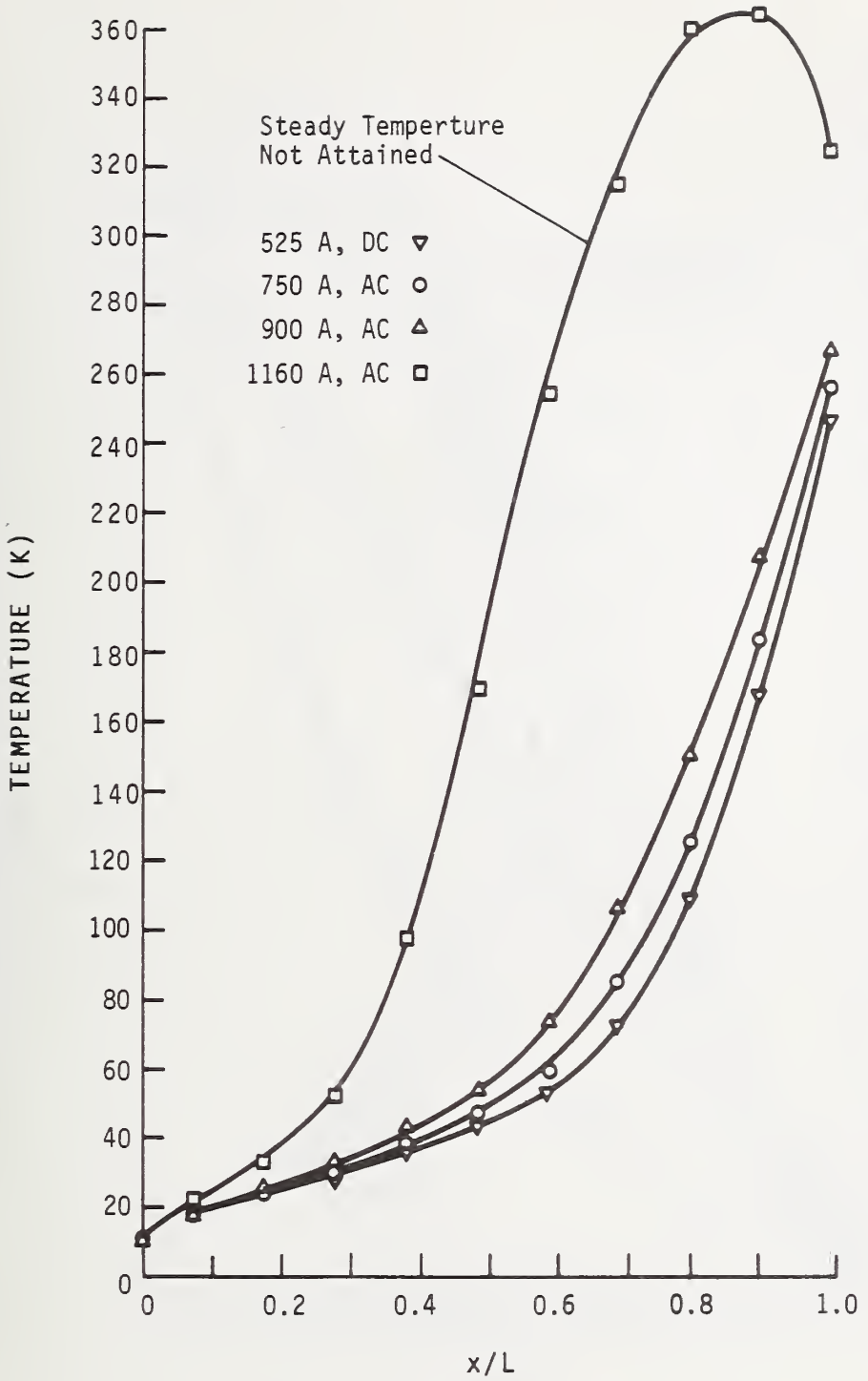

Figure 1.11. Temperature profiles for lead no. 3. Helium flow rate 0.0457 g/s, other conditions as for figure 1.9.

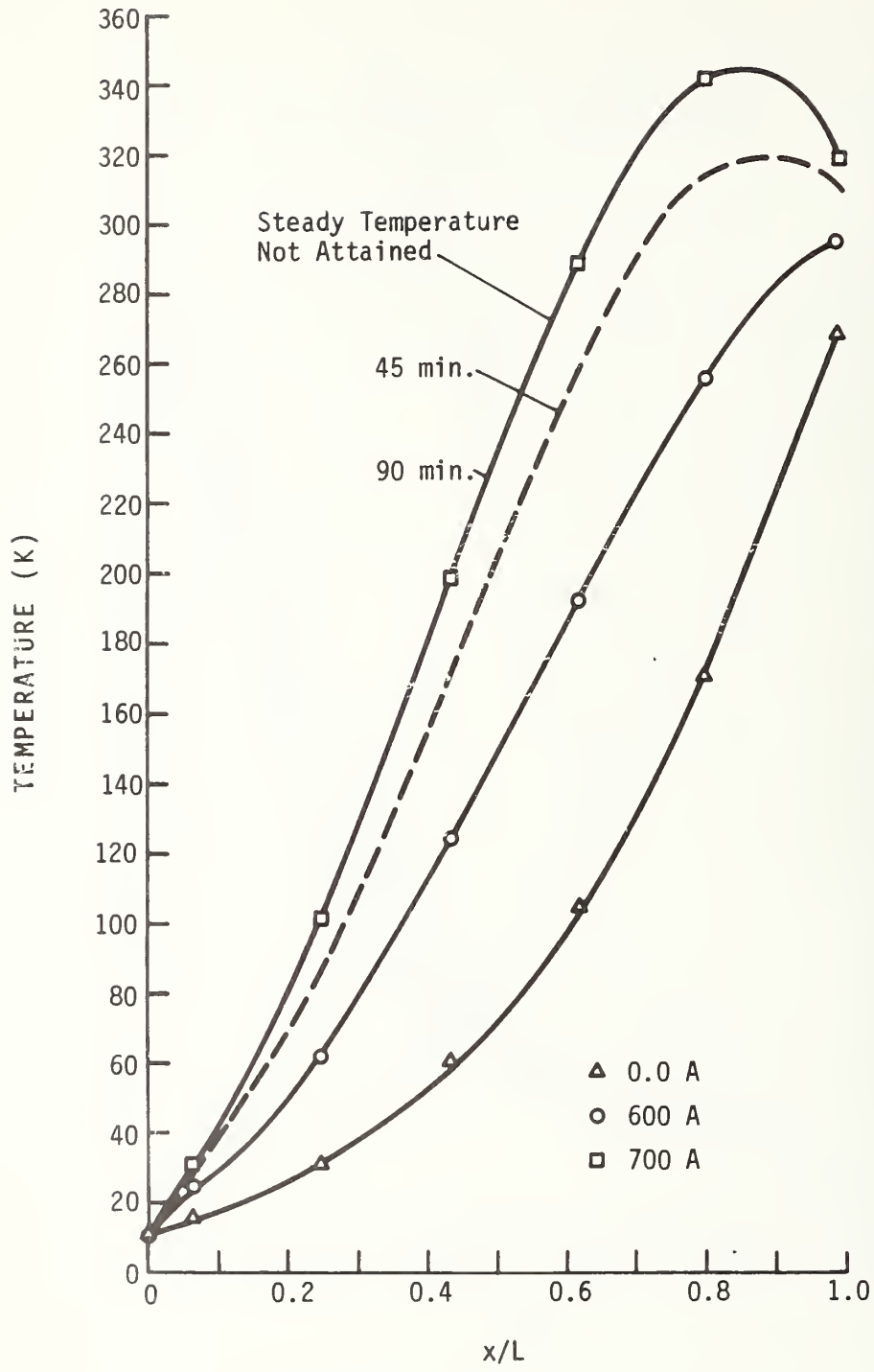

Figure 1.12. Temperature profiles for lead no. 4. Helium flow rate 0.0233 g/s, other conditions as for figure 1.9.

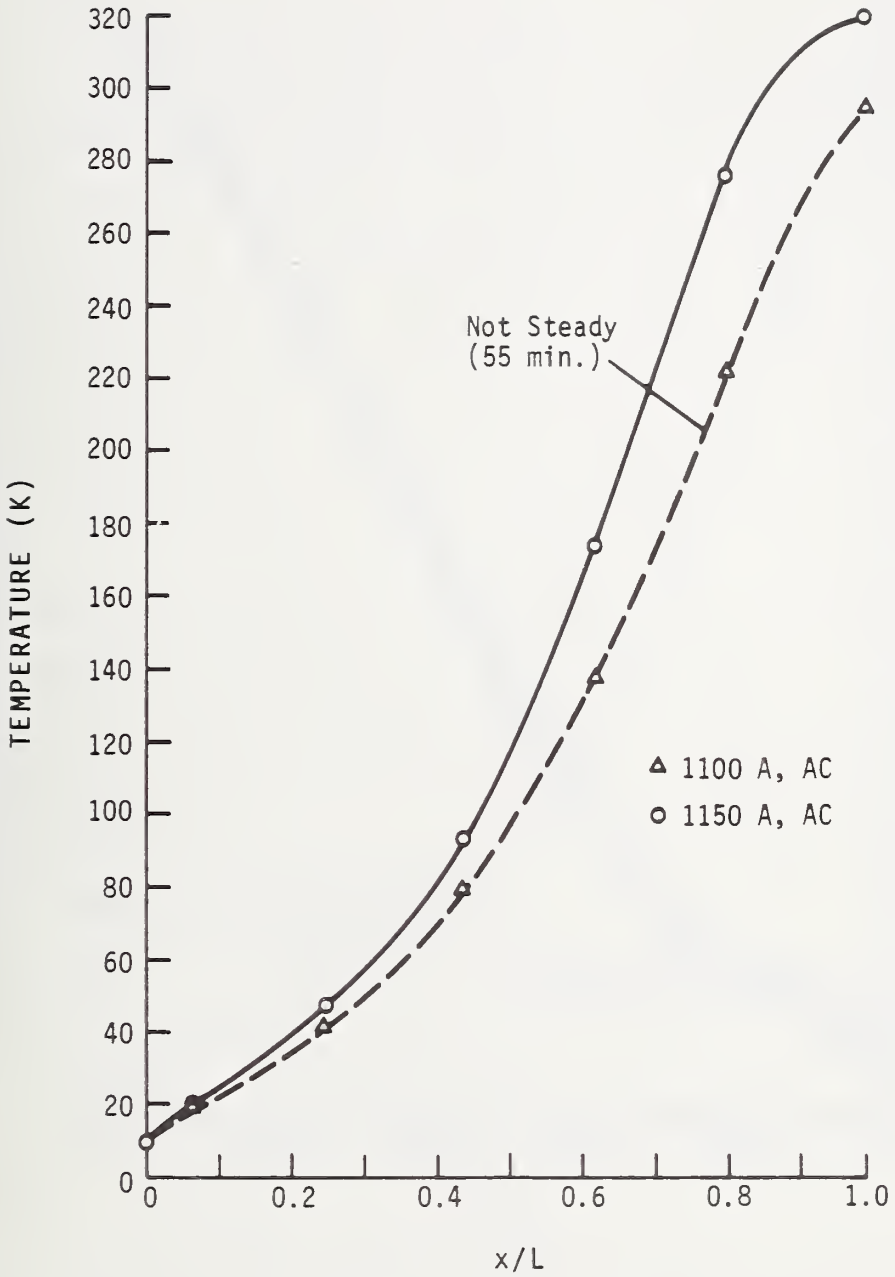

Figure 1.13. Temperature profiles for lead no. 4. Helium flow rate 0.070 g/s, other conditions as for figure 1.9.

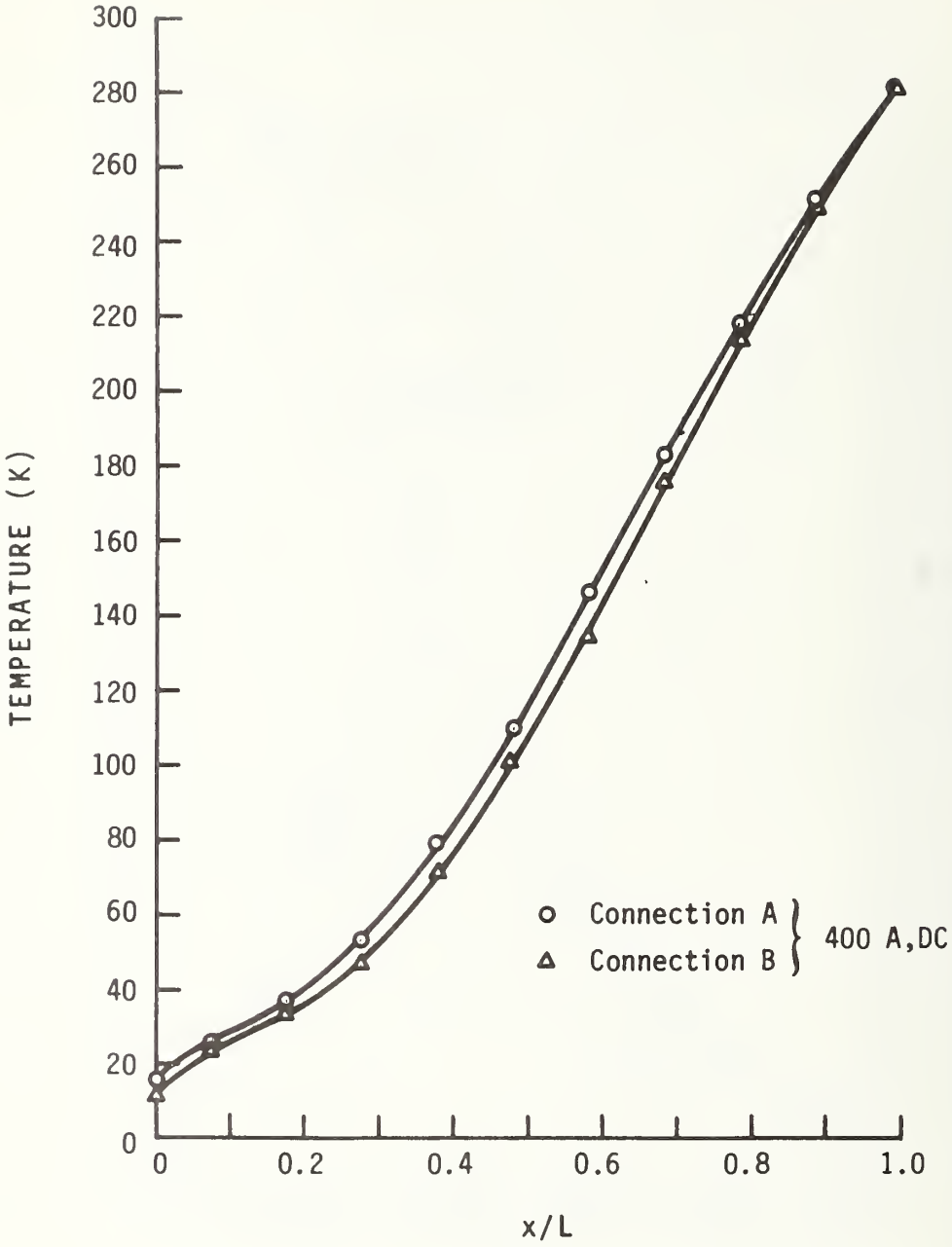

Figure 1.14. Comparison of temperature profiles for lead no. 3. Connection A as for figure 1.5; connection B as for figure 1.7. Helium flow rate 0.0168 g/s, other conditions as for figure 1.9.

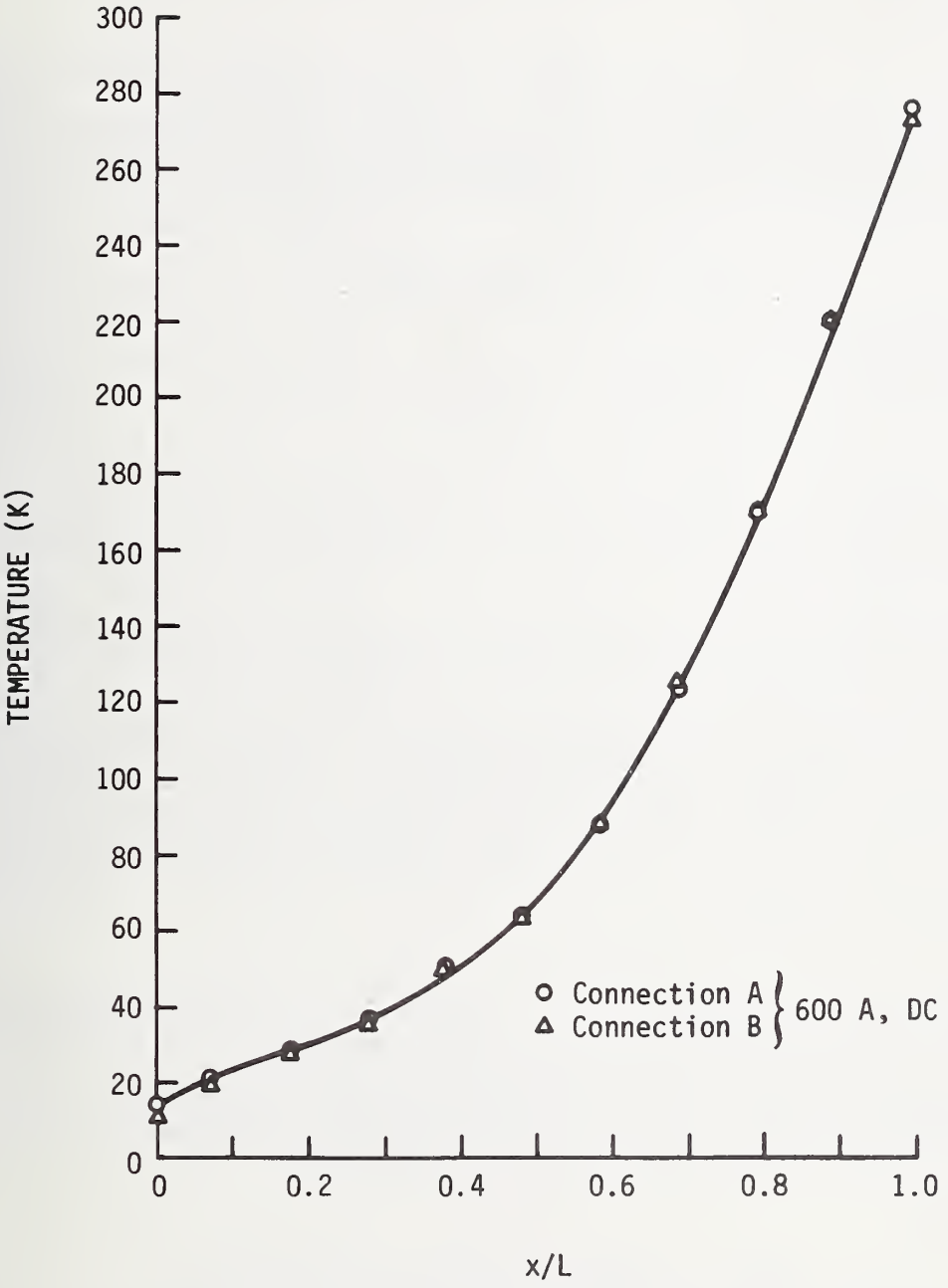

Figure 1.15. Comparison of temperature profiles for lead no. 3. Helium flow rate 0.0308 g/s, other conditions as for figure 1.14.

applied to the case of imperfect heat transfer and the burn-out predictions for J are given as a function not only of M but H also. From these results one can at least see how large H must be for burn-out to be independent of H; practically speaking if H is greater than about 10^4 burn-out occurs at the ideal heat exchange criterion

$$J^2 - \left(\frac{M}{2}\right)^2 = \pi^2 \tag{1.6}$$

This relationship is only true for constant thermal conductivity, linear resistivity, but it is helpful in interpreting experimental results. For if in the general real property case we define the dimensionless lead length as

$$\eta_L = \frac{A^*k^*}{L} \int_o^L \frac{dx}{A(x)k(T)} \tag{1.7}$$

the criterion now becomes

$$J^2 - \left(\frac{M}{2}\right)^2 = \left(\frac{\pi}{\eta_L}\right)^2 \tag{1.8}$$

and if $k(T) > k^*$ for all T (RRR $> \simeq 50$) then for a constant area lead $\eta_L < 1$ and burn-out occurs at higher values of J for given M. For some commercial non-electrical coppers, $k(T) < k$ for all T, $\eta_L > 1$, and we may expect burn-out to occur at lower J. This would be for RRR $< \simeq 9$ and it leaves a grey area between. One cannot be more quantitative without knowing the temperature profile at burn-out. This then becomes a difficult iterative process.

In order to be able to shed light on our experimental results we decided that an accurate and general calculation should be available, which invariably means that one resorts to a numerical method. The computer program described in the next section was, we thought, as general as one could make it since none of the common approximations are made. Comparison with experimental results, as will be seen, revealed that even this was not enough and there may be some aspects of real leads which simply are not well enough known until they are tested.

1.4.1. Computer Program for Lead Performance

The computer program simultaneously integrates the exact one-dimensional momentum and energy equations given by Arp [8] for the helium gas, and the one-dimensional heat conduction equation for the conductor. This is then coupled to the helium energy equation by the heat transfer term. A combined Runge-Kutta, Adams-Moulton predictor-corrector method is used with complete property updating and error checking for both helium and conductor at every step. Thus we have the simultaneous set of equations:

Helium pressure:

$$\frac{dP}{dx} = \frac{p}{(1-\underline{M}^2)K}\left[(-1+\phi\underline{M}^2)\ F_1 - \phi\underline{M}^2 F_2\right] . \tag{1.9}$$

Helium enthalpy:

$$\frac{dH}{dx} = \frac{C^2}{(1-\underline{M}^2)}\left[(-1+\phi)\underline{M}^2 F_1 + \left(1-(1+\phi)\underline{M}^2\ F_2\right)\right]. \tag{1.10}$$

Conductor temperature:

$$\frac{dT}{dx} = Y . \tag{1.11}$$

Conductor heat flow:

$$\frac{dY}{dx} = \frac{1}{k_s}\left(\lambda - \frac{I^2\rho}{A^2} - Y^2\frac{dk_s}{dT}\right). \qquad (1.12)$$

To commence the integration at x = 0 initial values of p, H, T and Y are given. In these equations, p is the helium pressure, H the helium enthalpy (not to be confused with the heat transfer parameter H defined above), $\underline{M}$ is the Mach no., C the adiabatic sound velocity, $K = \frac{p}{\rho}\left(\frac{\partial\rho}{\partial p}\right)_s$, and ϕ is the Gruneisen parameter $= \frac{\rho}{T}\left(\frac{\partial T}{\partial\rho}\right)_s$. $F_1 = \frac{P}{2A_G}\underline{M}|\underline{M}|f$ with A_G = helium gas flow cross sectional area, P the wetted perimeter and f the Fanning friction factor; $F_2 = \lambda/\dot{m}C^2$ with λ the heat transfer per unit length $\frac{dQ}{dx}$. In the usual manner the integration is iterated on dT/dx at x = 0 until at x = L the required warm end temperature T_U is found. It will be noted that the thermodynamic state of the helium is calculated with coordinates p and H. From this the temperature θ and density ρ_G are determined from explicit functions $\theta(p,H)$ and $\rho_g(p,H)$ developed especially for fast computer evaluation as is required here. The derivatives ϕ, C and K are obtained from the equation of state of McCarty.[9]

The conductor properties may be strongly temperature dependent. In view of the large deviations from the Wiedemann-Franz Law for even moderate purity coppers - for example 50 percent at 40 K for RRR = 100 - we decided not to invoke the Law except for the imperfection contribution k_o, but to compute k_s and ρ separately. For ρ we used Matthiessen's rule, $\rho = \rho_o + \rho_I$ and calculated the residual resistivity ρ_o from the specified RRR and the ideal lattice resistivity ρ_I from the data given by White and Woods.[10] Our curve, fitted to those data, is

$$\ln(\rho_I \times 10^8) = -9.600976 - 12.52445\ \ln T + 8.309361(\ln T)^2 - 1.583458(\ln T)^3 + 0.0993132(\ln T)^4. \qquad (1.13)$$

The deviation from the data is no more than two percent. This equation is used up to 300 K, after which ρ_I is assumed proportional to T.

For the conductor thermal conductivity k_s we used the approach followed by Lock.[2] In this approach an analogue of Matthiessen's rule is used. Thus we take

$$\frac{1}{k_s} = \frac{1}{k_o} + \frac{1}{k_I}. \qquad (1.14)$$

This is a compromise between accuracy and computational efficiency. The procedure is known not to be accurate above 10 K (the error can reach 10 percent) for the thermal resistivity, but for engineering purposes the possibility of computing the thermal conductivity from a single property - RRR - is very appealing. We calculate k_o from L_oT/ρ_o using an average experimental value for L_o of $2.1 \times 10^{-8} V^2/K^2$. The lattice contribution to thermal resistivity $1/k_I$ was assumed to be independent of purity and calculated from the data of Powell, et al.[11] for a sample of RRR = 110. Thus we compute k_I from the expression

$$k_I = T \exp \sum_1^5 C_i/T^i \qquad (1.15)$$

with $C_1 = 146.587$,
$C_2 = 269.117$,
$C_3 = 16956.6$,
$C_4 = 101324.0$,
$C_5 = -171156.0$.

This expression is used up to 150 K after which the thermal conductivity is assumed to be constant at its 150 K value. The fit generally predicts the thermal conductivity data of Powell to better than five percent but is low by 14 percent at 40 K. Nevertheless, considering the complex nature of the temperature dependence of the thermal conductivity and its variation by orders of magnitude at low temperatures, this analytical representation gives a very realistic and economical representation. This is illustrated in figure 1.16 where we have compared some of our computed curves with experimental data for which RRR was known and was of comparable magnitude.

In calculating the heat transfer term λ we put as usual $\lambda = Ph(T-\theta)$. We calculate h based on the mean hydraulic diameter $D_H = 4A_G/P$ and appropriate expressions for laminar and turbulent flow in pipes as appropriate to the calculated Reynolds number. In most cases Reynolds numbers indicated flow would be laminar and we used the flow independent Nusselt number, $Nu = hD_H/k_G = 4.364$. It was felt that in cases other than a simple tube the Nusselt number would be enhanced by tortuous geometry so that this approach should be conservative and not overestimate the heat transfer term.

As a demonstration of the computer program we first used it to calculate the optimum operating conditions for a lead of the design of no. 2 with RRR = 50 and operating between 6 and 300 K. In figure 1.17 we plot the total specific Carnot work W_T/I vs. the specific gas flow $\dot{m}/I$ and in figure 1.18 we show W_T/I vs. IL/A. The procedure was to vary IL/A and find the minimum Carnot work for fixed $\dot{m}$. These minima are then plotted showing that the absolute minimum W_T/I for this lead is 0.270 W/A and occurs at IL/A = 2.25×10^5 A/cm and $\dot{m}/I = 4.62 \times 10^{-5}$ g/As. It is interesting to compare this result with the values given by Güsewell and Haebel [13] for a slotted finned rod with RRR = 57. The corresponding figures are $W_T/I = 0.333$ W/A, IL/A = 2.6×10^5 A/cm and $\dot{m}/I = 4.9 \times 10^{-5}$ g/As. Agsten gives $W_T/I = 0.340$ W/A for a Wiedemann-Franz material operating between 4.2 and 300 K as the absolute thermodynamic optimum. The differences appear to be chiefly a result of operating the cold end at 6 K in our case compared to 4.4 K and 4.2 K respectively. This permits a relatively greater amount of heat to be removed at the cold end through the alleviation of the Carnot factor and thus less gas is used.

The program was next used to investigate thermal runaway. We attempted to duplicate the experimental data described in the next section. Here, the procedure was to compute temperature profiles for a fixed mass flow rate, incrementing I until a solution could no longer be obtained, or excessively high conductor temperatures were encountered. The results will be discussed in section 1.4.3.

1.4.2. Experimental Results

A careful study of thermal runaway was made on lead no. 2. This lead had previously burned out during exploratory runaway tests, but was repaired

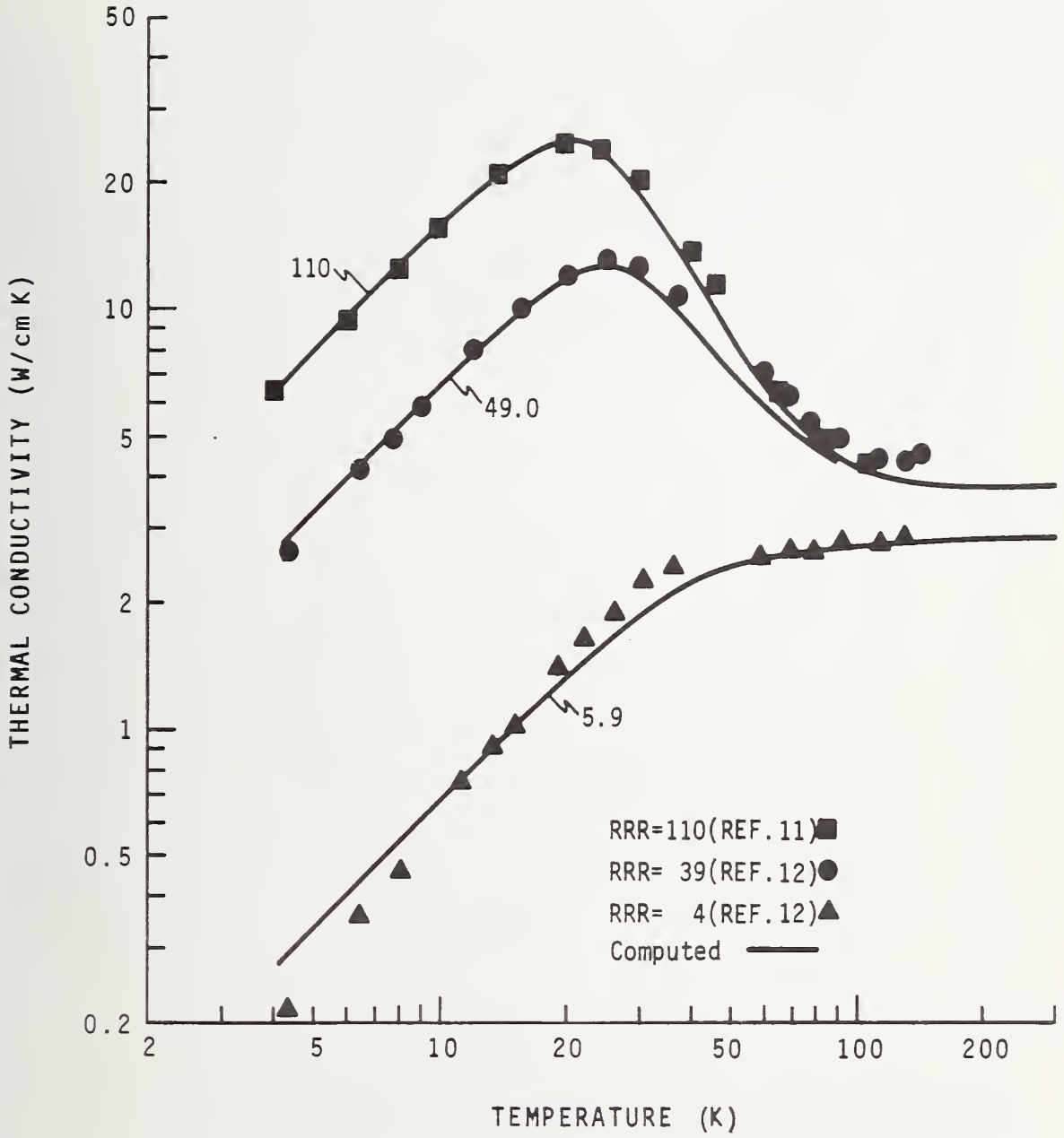

Figure 1.16. Comparison of computed thermal conductivity of copper with experimental data.

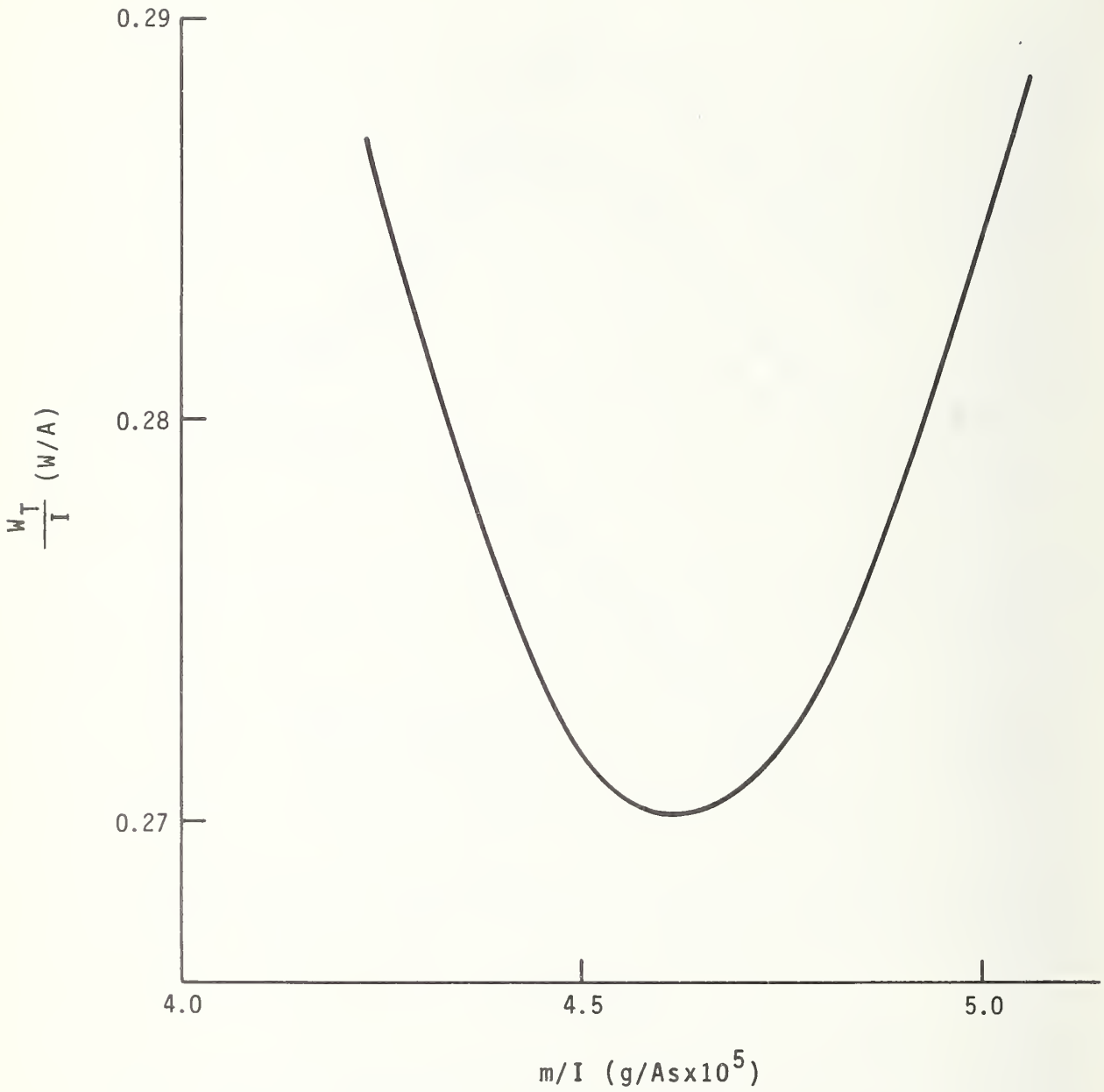

Figure 1.17. Total Carnot work per ampere of lead current vs $\dot{m}/I$.

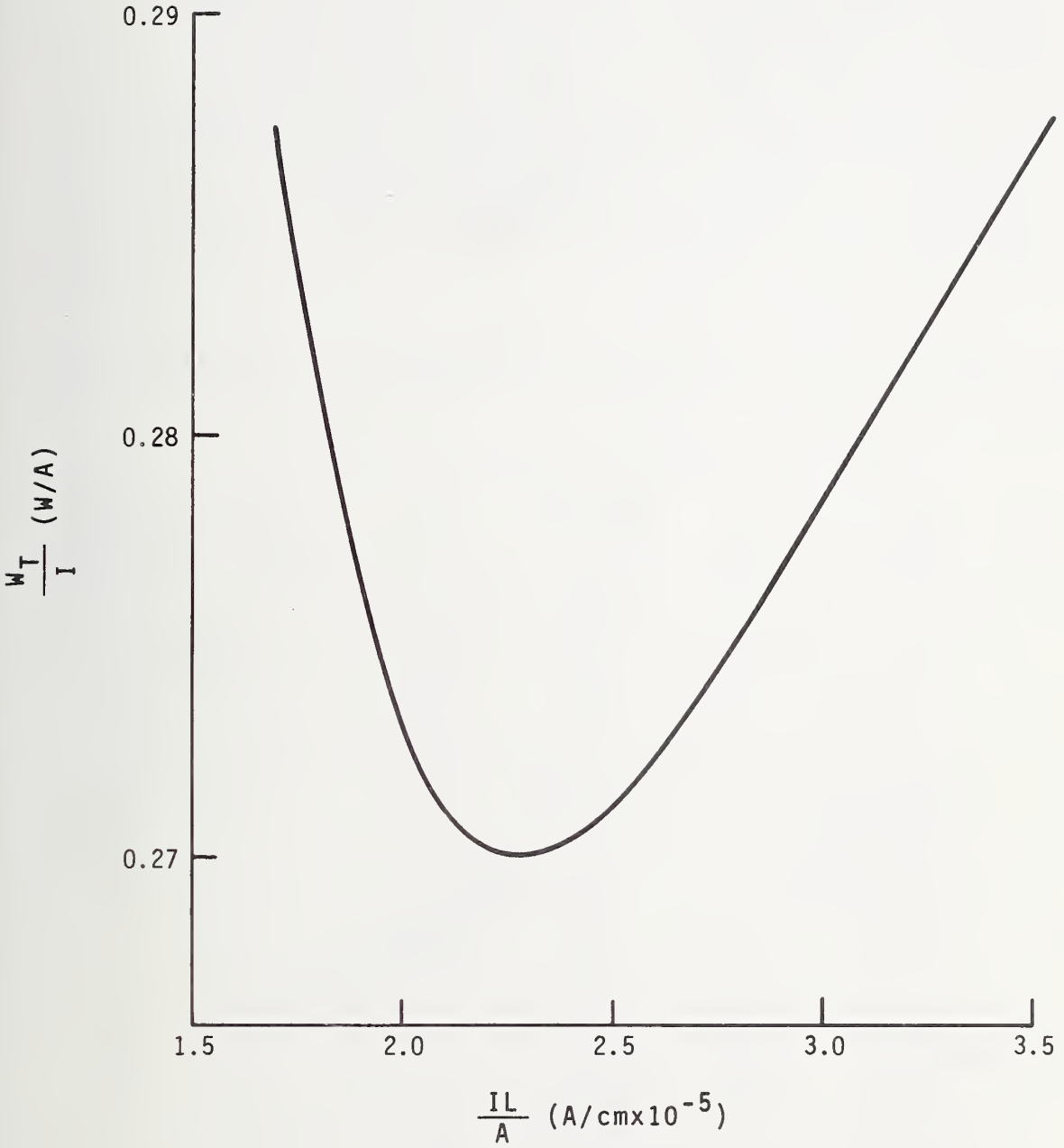

Figure 1.18. Total Carnot work per ampere of lead current vs IL/A.

by replacing part of the burned-out stainless steel tubing and by completely replacing the braid. We also extended the phenolic resin rod by a little over a centimeter since there was evidence of poor thermal anchoring at the warm end.

The lead was run at three mass flow rates: 0.0047 g/s, 0.0093 g/s and 0.0149 g/s. The middle value was close to what we had determined to be the mass flow rate under optimum conditions. For each flow rate the current was increased in increments of five or ten amperes. When at a particular setting the temperature profile had stabilized it was recorded. When for a given setting the temperature profile still continued to increase with no sign of slowing down after 10 minutes, or an excessive temperature had been reached (360 K), the test was terminated and the last two currents were assumed to bracket the critical burn-out current. In this way the burn-out current has been established to within at most five percent. The tests were carried out at 0.4, 1.0 and 1.5 MPa and the results are given in table 1.2. Temperature profiles for the three flow rates at 1.0 MPa are given in figures 1.19, 1.20, and 1.21. Pressure in fact made little difference. In all of these tests the lead cold end temperature was held at 6 K while the gas inlet temperature was 4.5 K.

In addition to measuring temperature profiles we also measured the lead resistance and the values are also given in table 1.2. It is clear that this could be a useful indicator of approach to thermal runaway, but only at a fixed helium flow rate.

Table 1.2. Thermal Runaway Tests. Lead No. 2.

Pressure	Flow Rate (g/s)	$\frac{M}{2}$	Current (A)	$\frac{2J}{M}$	Stable or Unstable	Lead Resistance (μ ohm)
0.4	0.0047	3.59	115	1.49	S	947
			125	1.61	U	956
	0.0093	7.18	185	1.16	S	748
			190	1.20	U	750
	0.0149	11.48	250	1.01	S	307
			260	1.05	U	588
1.0	0.0047	3.59	110	1.42	S	857
			115	1.49	U	1039
	0.0093	7.18	190	1.23	S	628
			195	1.26	U	704
	0.0149	11.48	265	1.07	S	374
			270	1.09	U	549
1.5	0.0047	3.59	115	1.49	S	849
			120	1.55	U	1010
	0.0093	7.18	190	1.23	S	532
			195	1.26	U	697
	0.0149	11.48	265	1.07	S	430
			270	1.09	U	574

Conditions of Tests: d.c. current, helium inlet temperature 4.5 K, conductor cold end temperature 6.0 K.

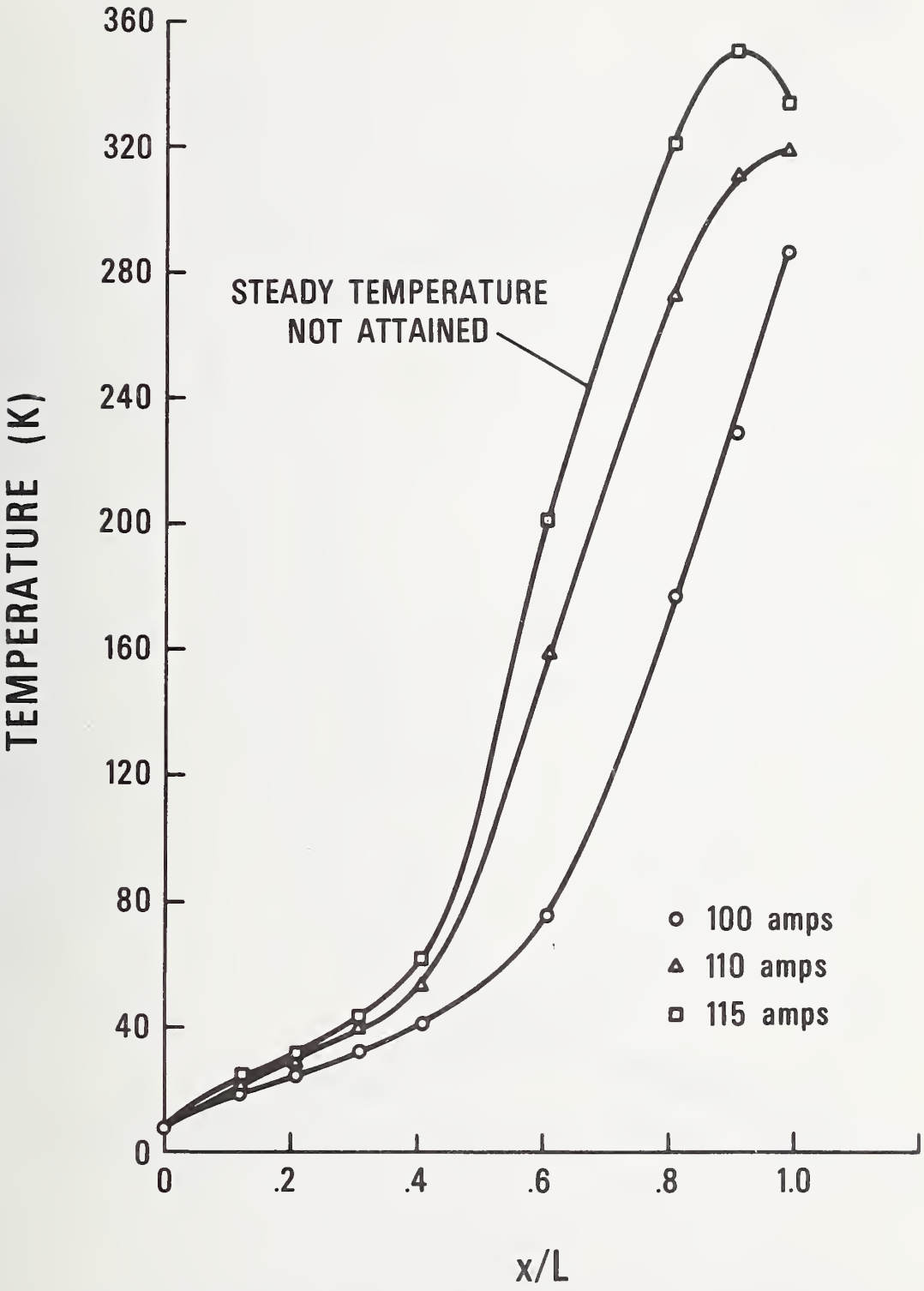

Figure 1.19. Thermal runaway tests for lead no. 2. Helium flow rate 0.005 g/s, pressure 1.0 MPa, helium inlet temperature 4.5 K.

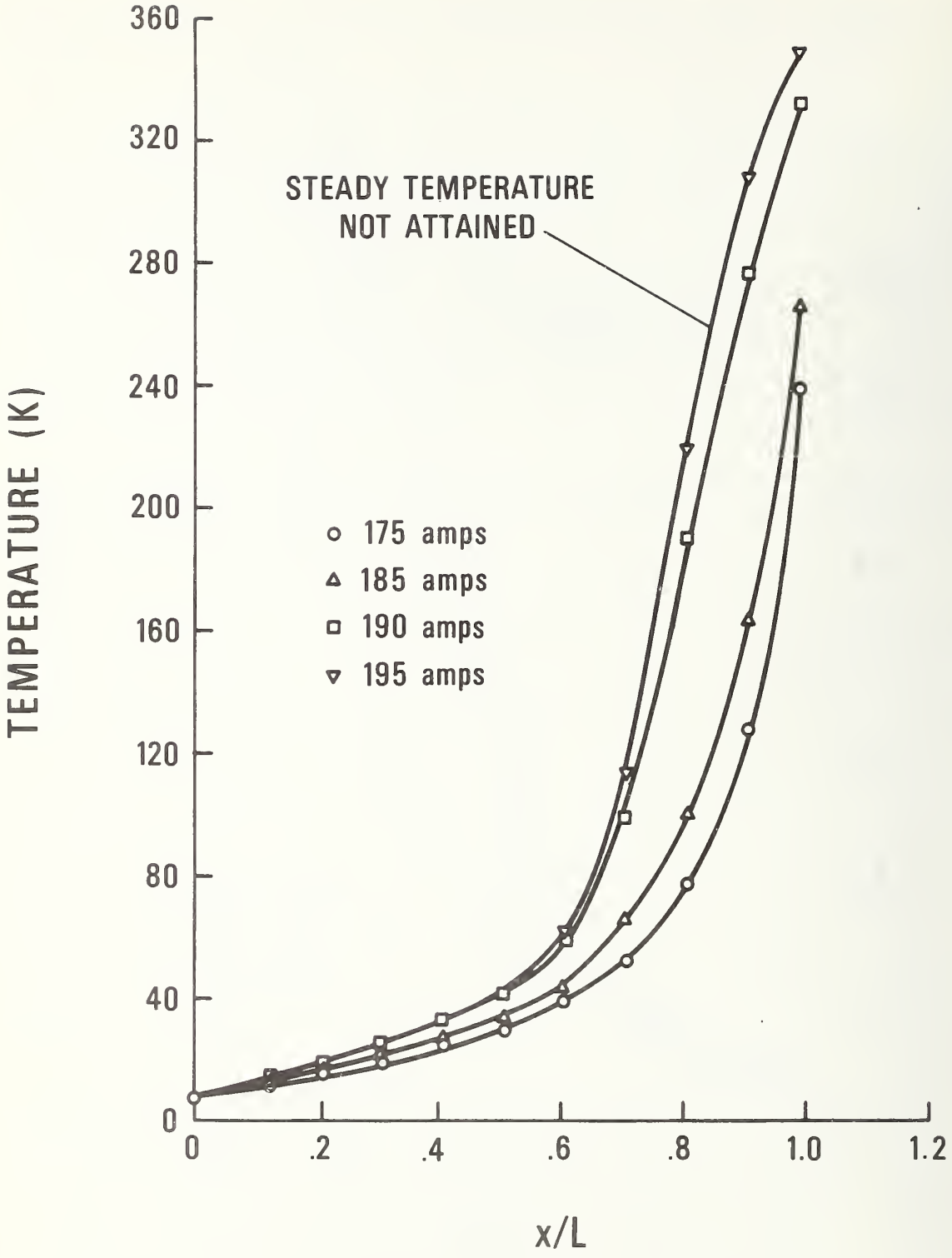

Figure 1.20. Thermal runaway tests for lead no. 2. Helium flow rate 0.0093 g/s, other conditions as for figure 1.19.

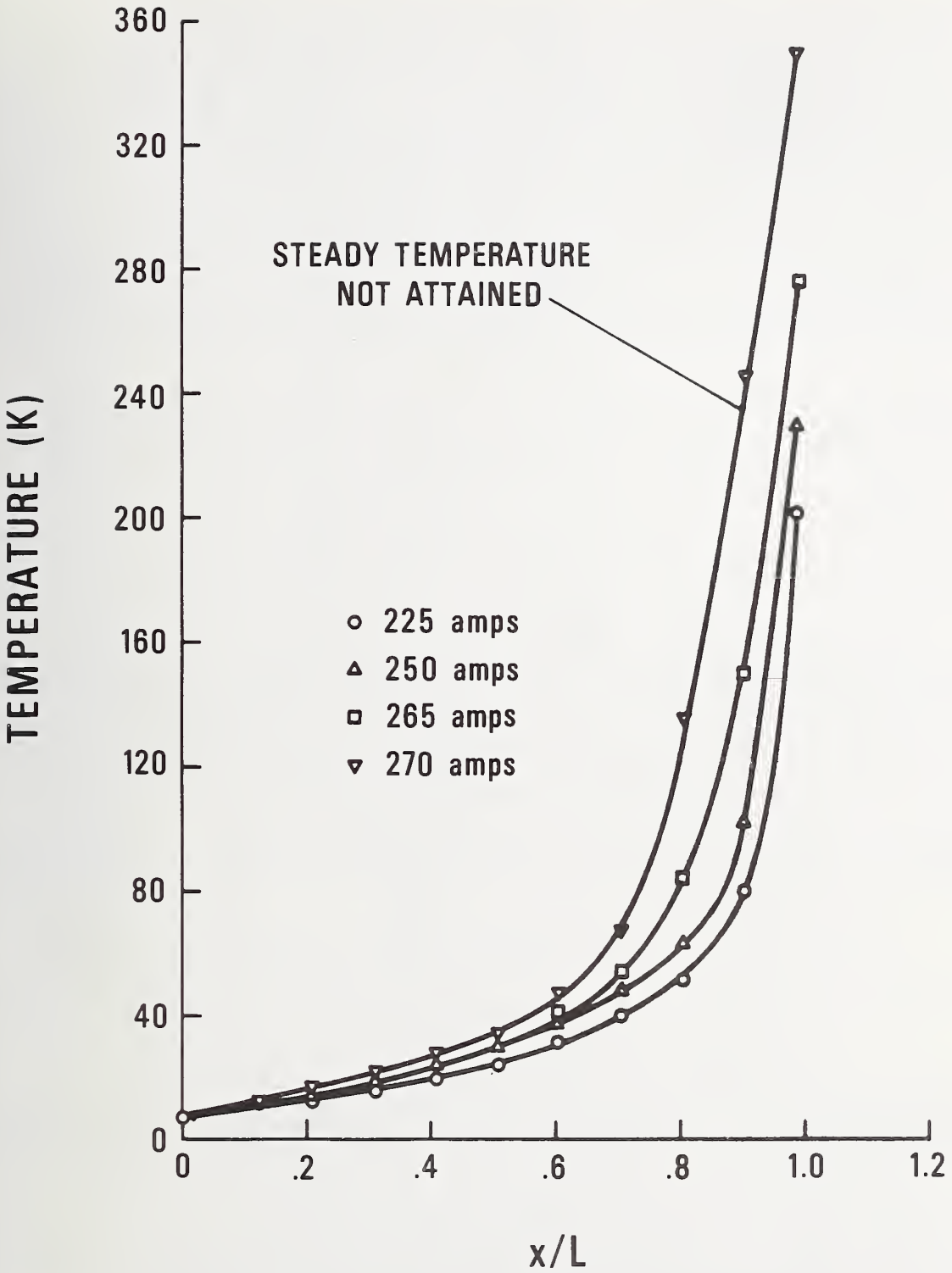

Figure 1.21. Thermal runaway tests for lead no. 2. Helium flow rate 0.0149 g/s, other conditions as for figure 1.19.

In the course of running a series of tests for the LASL lead, no. 3, we encountered runaway conditions and this allowed us to obtain a rather coarse but nonetheless useful bracketing of the runaway conditions for both leads 3 and 4. The data are given in tables 1.3 and 1.4. The response time of these two leads is very much greater than for nos. 1 and 2 making this kind of test difficult; it was necessary to wait on the order of one hour for the establishment of equilibrium for nos. 3 and 4 compared with ten minutes for lead no. 2. No thermal runaway tests were carried out on lead no. 1.

Table 1.3. Thermal Runaway Tests. Lead No. 3.

Pressure (MPa)	Flow Rate (g/s)	Current (A)	Stable or Unstable
1.0	0.0117	475	S
		585	?
	0.0168	625	S
		775	U
	0.0233	600	S
		775	U
	0.0308	720	S
		930	U
	0.0457	900	S
		1160	U

Conditions of Test: a.c. current, helium inlet temperature 4.5-6 K, conductor cold end temperature 10.0 K.

Table 1.4. Thermal Runaway Tests. Lead No. 4.

Pressure (MPa)	Flow Rate (g/s)	$\frac{M}{2}$	Current (A)	$\frac{2J}{M}$	Stable or Unstable
1.0	0.023	1.98	600	1.55	S
			700	1.80	U
	0.047	3.87	900	1.18	S
	0.070	5.92	1150	0.99	S
			1378	1.186	U

Conditions of Test: a.c. current, helium inlet temperature 4.5-5 K, conductor cold end temperature 10 K.

1.4.3. Discussion of Results and Comparison with Theory

The most obvious thing about the temperature profiles that we did not anticipate is that they give evidence of incomplete thermal anchoring at the warm end despite the modification to the phenolic resin core referred to above. To get a really ideal experimental setup for comparison with theoretical calculations it is apparently necessary to employ water cooling or some such remedy except at the adiabatic warm-end condition. Nevertheless, from computer simulation we do not believe in these experiments that the lack of thermal anchoring changed the burn-out condition significantly. The second

point to notice is that the thermal runaway condition only involves temperature profiles with maxima at the lower flow rates. But this, as we shall see is not unexpected. A third point is that in all of these tests the lead was unstable at some level of current. In computer simulations we have observed two distinct modes of burn-out. The one is a definite instability; above a certain current no solution can be found and a plot of lead temperature vs. current has infinite slope at this current. In this case the burn-out current occurs at the adiabatic warm end condition and it is also the condition of minimum Carnot work. In the other case, lead temperature becomes very sensitive to current and the profile has a maximum, but a solution can always be found though the temperature may be unacceptably high. This latter case we associate with poor heat transfer, but we have not been able to explore all parameters sufficiently to make generalizations. For the present case, computer simulation indicated definite instability, but we would caution that experimentally the two would be difficult to distinquish, especially with large capacity leads of long time constant.

The crucial point is whether these temperature profiles and thermal runaway conditions are predictable. In figure 1.22 we have plotted the thermal runaway condition, equation (1.6), for the simple constant conductivity, linear resistivity case with ideal heat transfer. We plot 2J/M vs. M/2 using for k*, 4.0 W/cm K which should be applicable to lead no. 2 between 150 and 300 K. The measured RRR for this lead was 49 and leads one to expect that burn-out will occur above the line. When we plot the bracketed burn-out points using symbols larger than the implied uncertainty we see that this is indeed so for most of the points. We have also plotted a single datum point for lead no. 2 for an actual accidental burn-out at high flow rate and we see that this is quite low, but not inconsistent with the other data. Departures from the ideal heat transfer case are accentuated at high flow rate according to Bejan and Cluss and it is possible to draw a smooth curve through all data for lead no. 2 which would correspond to a heat transfer factor H somewhat less than 2000. On the same graph we have plotted the 2J/M vs. M/2 relationship for adiabatic warm end according to the constant conductivity-linear resistivity model. This shows that, indeed as observed, temperature maxima are only expected for lower flow rates for this model.

There is no unambiguous way of plotting the burn-out data for the tapered lead no. 3 on this plot, but we have plotted no. 4. As expected, for the low resistance ratio of no. 4 (RRR = 5.4) the data fall below the computed line.

When we made computer simulations of the burn-out conditions for lead no. 2, however, we found that the computer program overpredicted the burn-out for given mass flow as seen in figure 1.22. Far more noticeably, for a given current and mass flow, the temperature profiles were too low.

We apparently did not know one or more of the lead parameters well enough for modeling purposes for this lead as tested. Realizing that others may find themselves confronted with the same situation, we felt that it would be worth pursuing this point to narrow down the causes. We have since rerun computer simulations for this lead with various parameters varied in turn to look for a plausible explanation. These included resistance ratio, total resistance, conductor cross-sectional area, thermal impedance to the thermal ground at the warm end, inlet temperature and, finally, the heat transfer factor H through variation of the product Ph. Only the latter is capable of modifying the computed results sufficiently through a reasonable variation. We find that about a twenty-fold reduction in this factor in needed from the flow-independent (Nu = 4.364) value for laminar flow and we illustrate this in figure 1.23 where we have shown an experimental profile with several computed profiles for differend Ph. Taking the closest curve it is also apparent that some further temperature dependence of the heat

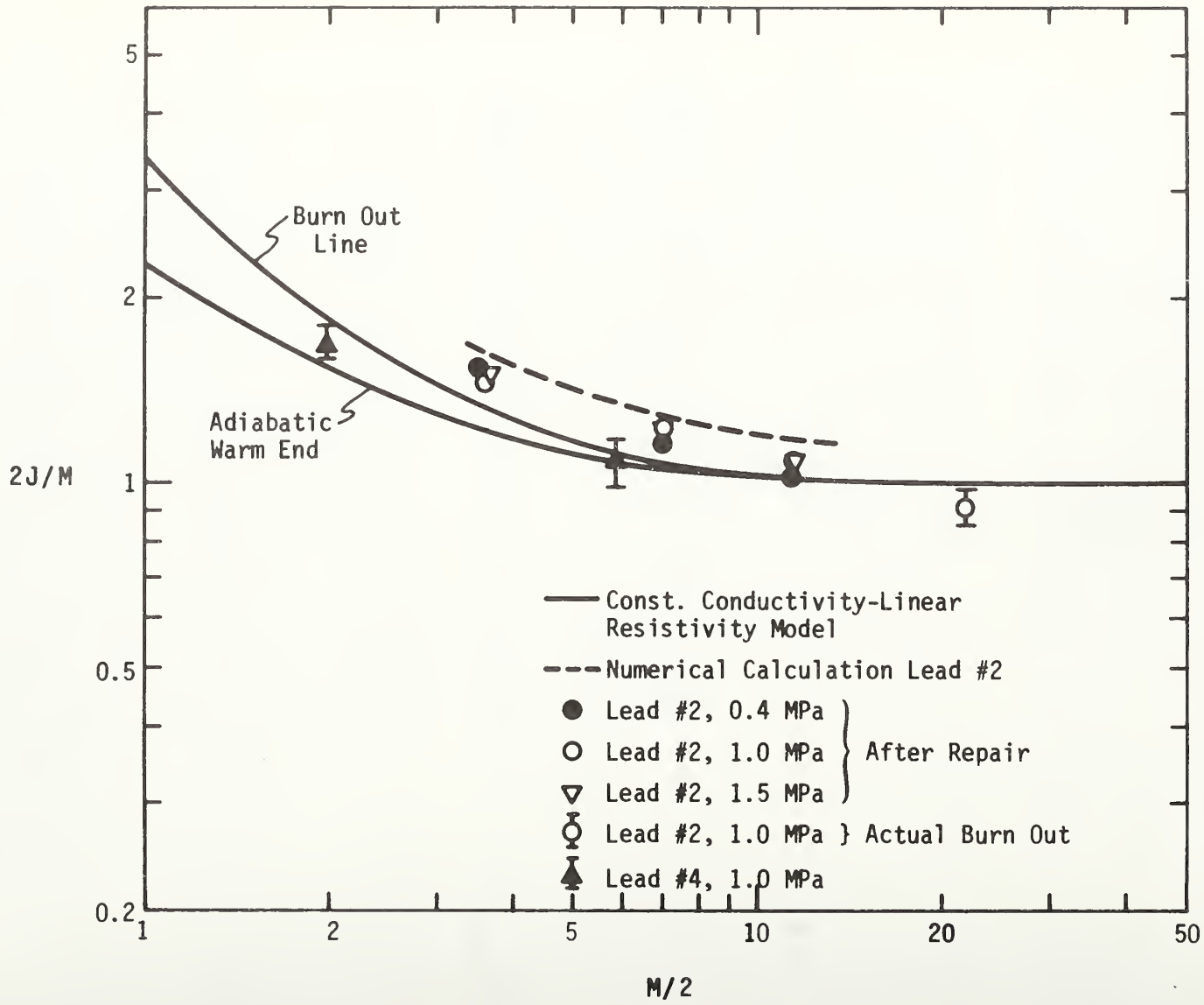

Figure 1.22. Generalized plot of thermal runaway results.

transfer factor should have been allowed, probably by incorporating flow dependence of the Nusselt number; the Reynolds number decreases up the tube due to the temperature dependence of viscosity.

In addition, we have dismantled the lead and examined it for likely cause. The braid was in good condition. The resistance ratio was remeasured and found to be, in fact, a little higher (RRR = 58) than our previous measurement on a sample from the same spool. But the total room temperature resistance before unsoldering the braid differed from the expected braid resistance (2.54 milli ohm cf. 2.0 milli ohm) indicating a significant contact resistance at the soldered junctions. Certainly, heat generation at the warm end would cause premature thermal runaway, but considering the great disproportion between the thermal conductance to the heavy copper fittings and that to the braid it would appear that this could only be a minor effect.

One final piece of evidence we feel makes the poor heat transfer argument conclusive. The measured helium outlet temperature for the run in figure 1.23 was 15 K below the conductor temperature compared with about 1 K for the original calculation. For the curve with hP = 0.174 in figure 1.23 the calculated temperature difference was much more realistic at 11 K.

We thus come to a not-too-surprising conclusion: a current lead is a heat exchange device and to predict its performance accurately one would be well advised to base his estimates on measured heat transfer coefficients. In the case studied the approach of using a mean hydraulic diameter and therefore assuming a uniform distribution of flow channels is simply not correct.

1.5 Oscillatory Behavior

1.5.1 General Description of Observed Oscillation

Pressure oscillations were observed in all four leads tested, no. 1 being the most prone to oscillate, the others were in the order no. 3, no. 4 and no. 2. It is interesting to note that no. 2, having suffered a burn-out failure during testing, was repaired for further testing. The repair involved patching the outer stainless steel sheath, replacement of the braid and slight lengthening of the phenolic resin core. After this modification, the weak oscillations which had been observed could no longer be repeated. By these changes we appear to have tipped the balance from marginally unstable to stable behavior.

The dependence of pressure oscillations on the independent parameters for a given lead may be generalized as follows:

1. Amplitude decreased with decreasing gas flow rate going to zero at some small finite value. Oscillations always ceased when the gas flow through the lead was shut off.

2. Amplitude decreased with increasing current and could be reduced to zero above a critical current for leads 1 and 2, but not for leads 3 and 4.

3. Amplitude decreased with gas inlet temperature, again going to zero at a critical value depending on the pressure and gas flow rate.

4. Amplitude decreased with increasing pressure for lead no. 1. The opposite is true however for lead no. 2.

The oscillation amplitude vs. lead current is shown in figure 1.24 for lead no. 1 operating at the given conditions, and the dependence of the critical current (the maximum at which oscillations occurred) on gas flow rate with pressure as a parameter is shown in figure 1.25.

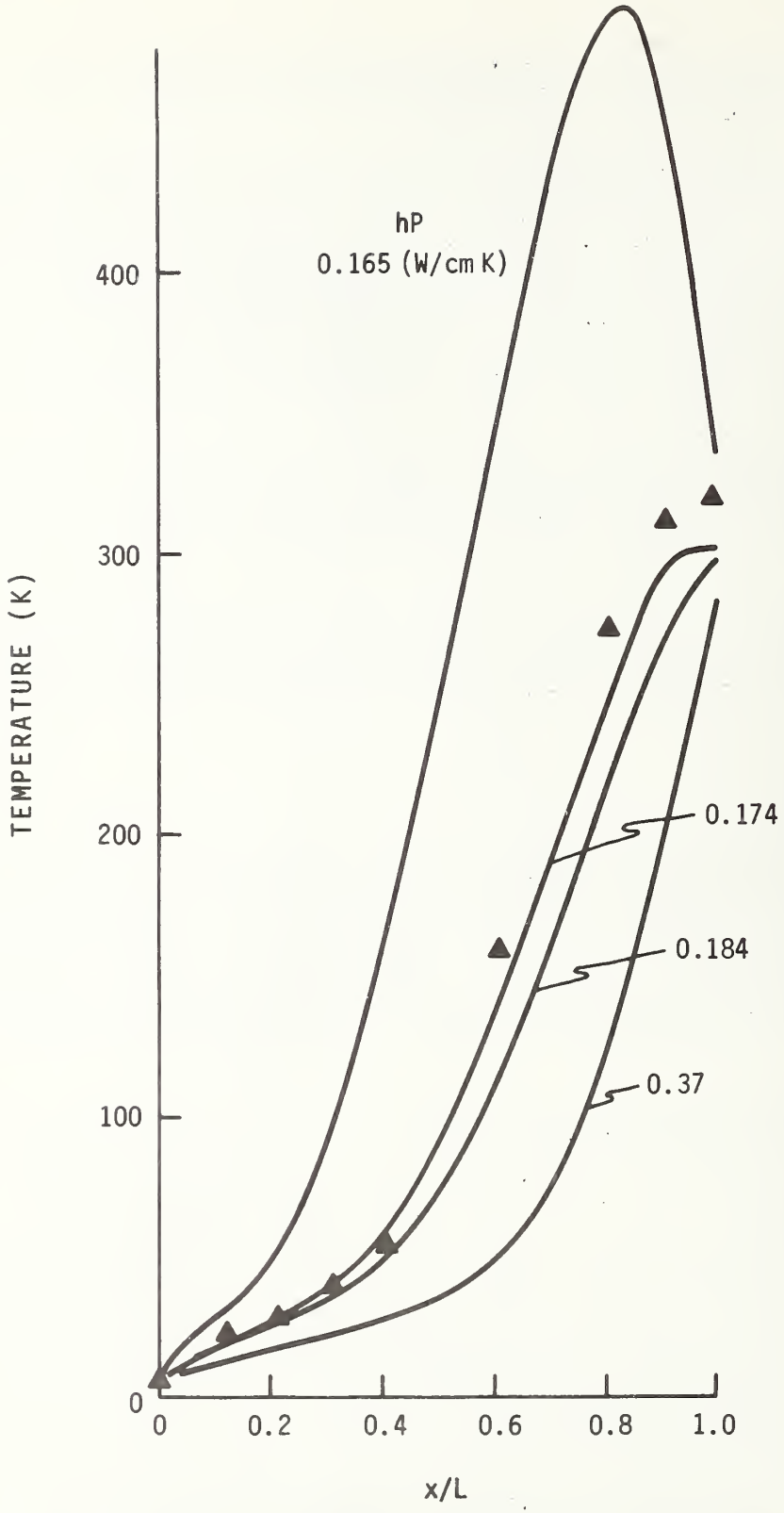

Figure 1.23. Comparison of experimental steady state temperature profile with calculations for various hP.

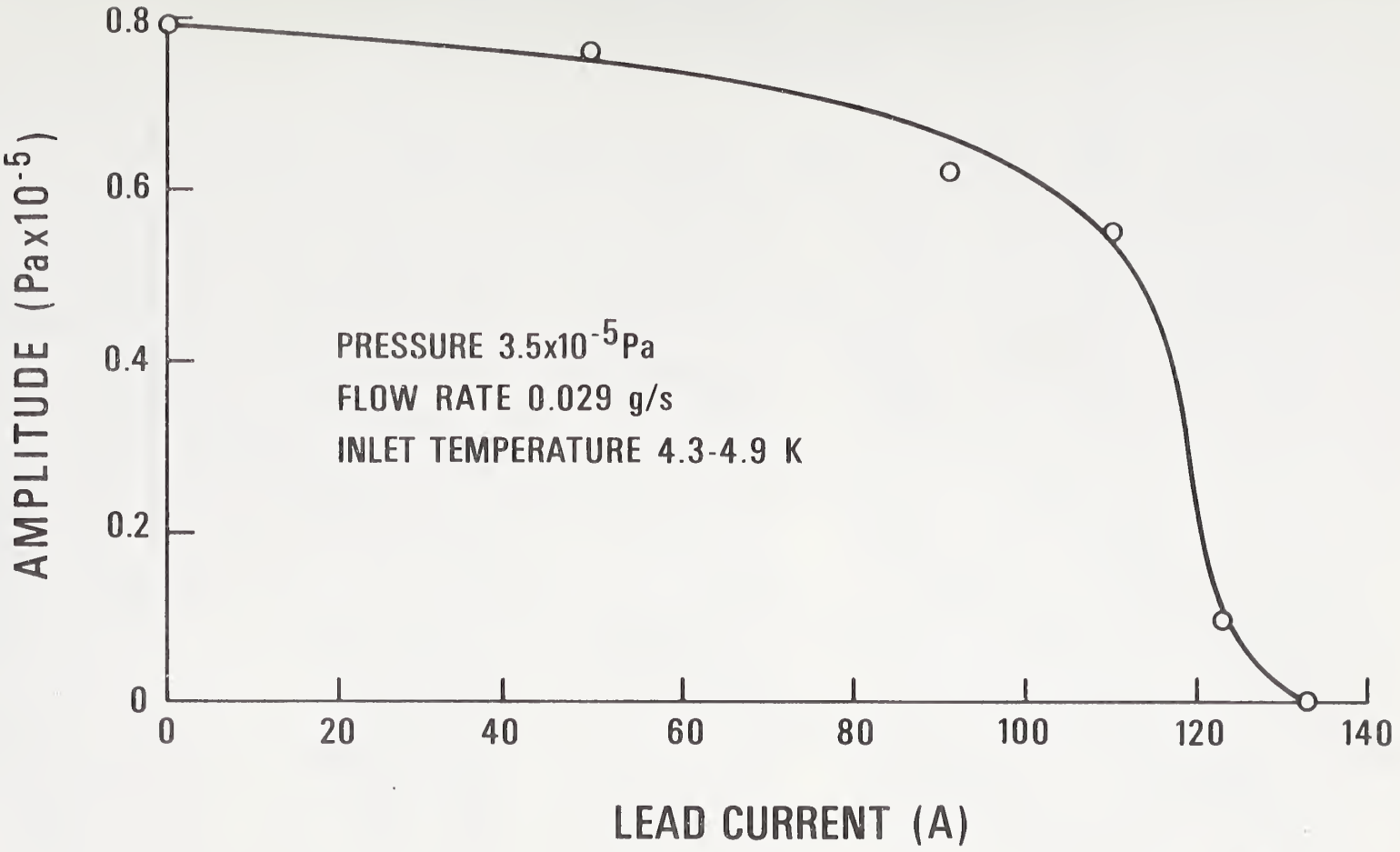

Figure 1.24. Oscillation amplitude vs. lead current for lead no. 1.

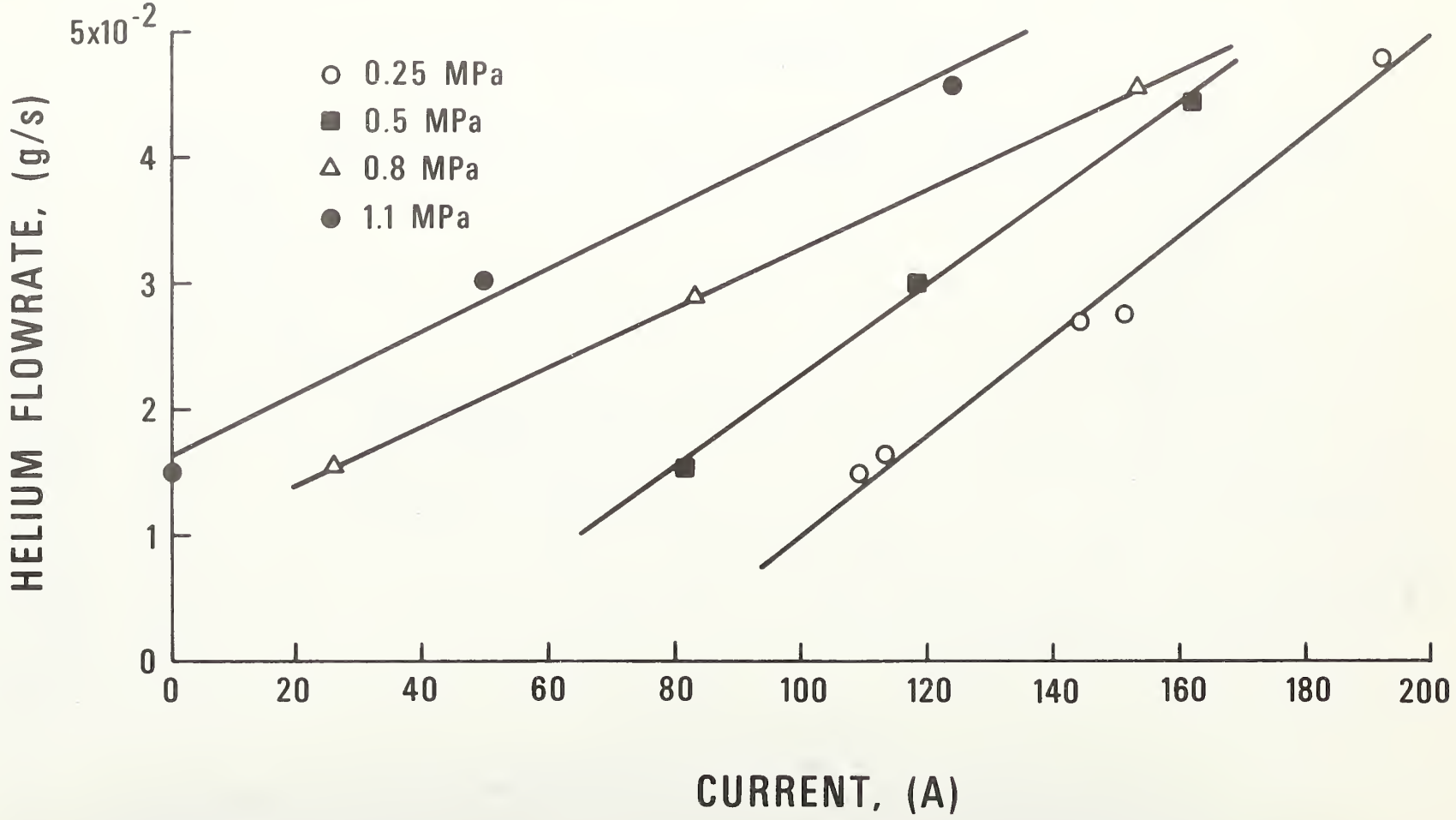

Figure 1.25. Current-flow rate conditions necessary to eliminate oscillations in lead no. 1 for a helium inlet temperature 4.3-4.5 K. The family of lines shifts to the left for higher inlet temperatures.

Additional observations of importance are:

5. Pressure oscillations could not be detected in the gas supply reservoir.

6. Oscillations could be eliminated by connecting a warm gas reservoir of about 1 liter capacity at the exit of the lead.

7. The oscillation frequencies were in the range 22-55 Hz. The only dependence found for frequency was on the inlet gas density and is illustrated in figure 1.26 for lead nos. 1 and 2.

8. In the case of lead no. 1 only, a low frequency modulation of the pressure oscillation was observed with a frequency of about 0.1 to 0.5 Hz. This was accompanied by temperature oscillations of the same frequency which could achieve amplitudes as high as 19 K at the cold end.

9. There was no basic difference observed between oscillatory behavior above and below the critical pressure. In the latter case it is fairly certain that the liquid phase did not enter the lead.

For lead nos. 1 and 2, where we explored the widest range of parameters, the existence of oscillations in the pressure-temperature plane for the helium entering the leads, is shown in figures 1.27 and 1.28. In the case of lead no. 2 this applied to the lead before repair as mentioned above.

1.5.2. Discussion of Oscillations

As a practical matter one might first inquire as to the amplitude of the pressure oscillations. Maximum peak-to-peak amplitudes observed under any of the conditions of our tests were about 0.1 MPa at 0.5 MPa for no. 1, 0.01 MPa at 1 MPa for no. 2, 0.016 MPa at 1 MPa for no. 3 and 0.008 MPa at 1 MPa for no. 4. We feel that although in the latter three cases these may not be serious perturbations one should not draw comfort from the results until some understanding of the governing parameters has been obtained, especially considering the limited range of the tests for nos. 3 and 4 and the possibility of attendant heat flow which could not be measured in these experiments.

Considering the observed frequency and the configurations of the leads it appears that the oscillations are of the thermally driven acoustic type commonly observed in tubes inserted into helium dewars. Here, one normally has an open cold end and a closed warm end giving rise to a standing wave with a pressure node at the open end and an antinode at the closed end - thus a 1/4 wave. In our case there are some differences, chiefly that the warm end was not closed and there was always a flow of gas when oscillations were observed. Nevertheless, with a considerable flow restriction in the warm gas exit piping where most of the pressure drop to atmospheric pressure was taken, we believe the slow flow of gas would not affect the oscillation - except insofar as the temperature profile is determined by the flow rates as will be discussed.

The driving mechanism of such oscillations is well understood and has been given greatest analytical clarity by Rott [14]. According to this accepted mechanism, when an acoustic standing wave of infinitesimal magnitude exists in the presence of a temperature gradient, an oscillating heat flux from the tube wall to the gas accompanies it. If the temperature gradient is such that the gas is heated in that part of the oscillation where it is moving towards the pressure antinode and cooled when moving away, then the oscillation can be enhanced and may grow in time to become an observable sustained oscillation. The temperature must therefore increase from pressure node to antinode - the conditions which existed in our lead tests. When the 1 liter reservoir was connected to the warm gas exit piping this end was apparently converted to a pressure node so that only the 1/2 wave standing wave could exist and the conditions for growth did not exist over half of the lead.

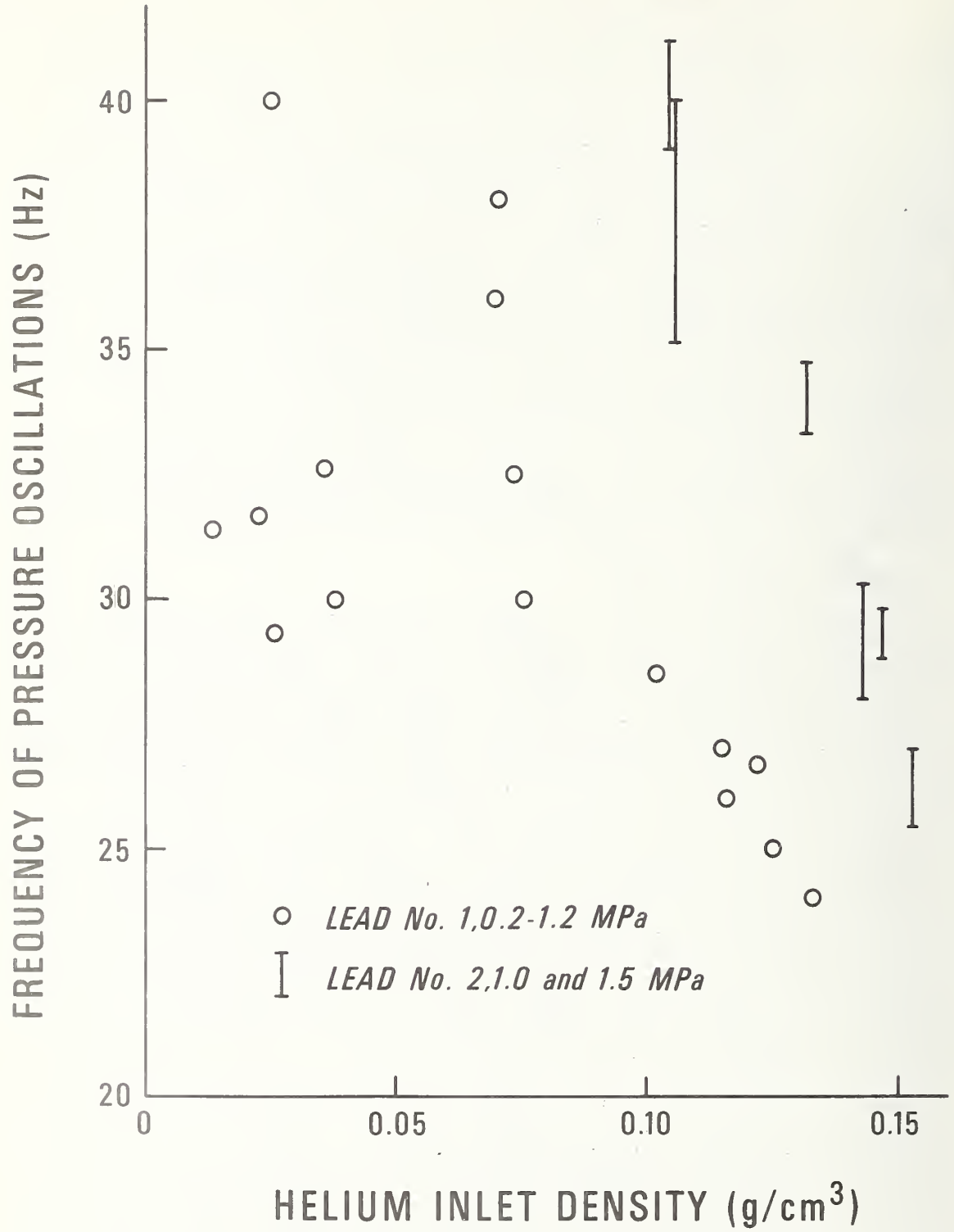

Figure 1.26. Frequency of oscillations as a function of inlet helium density.

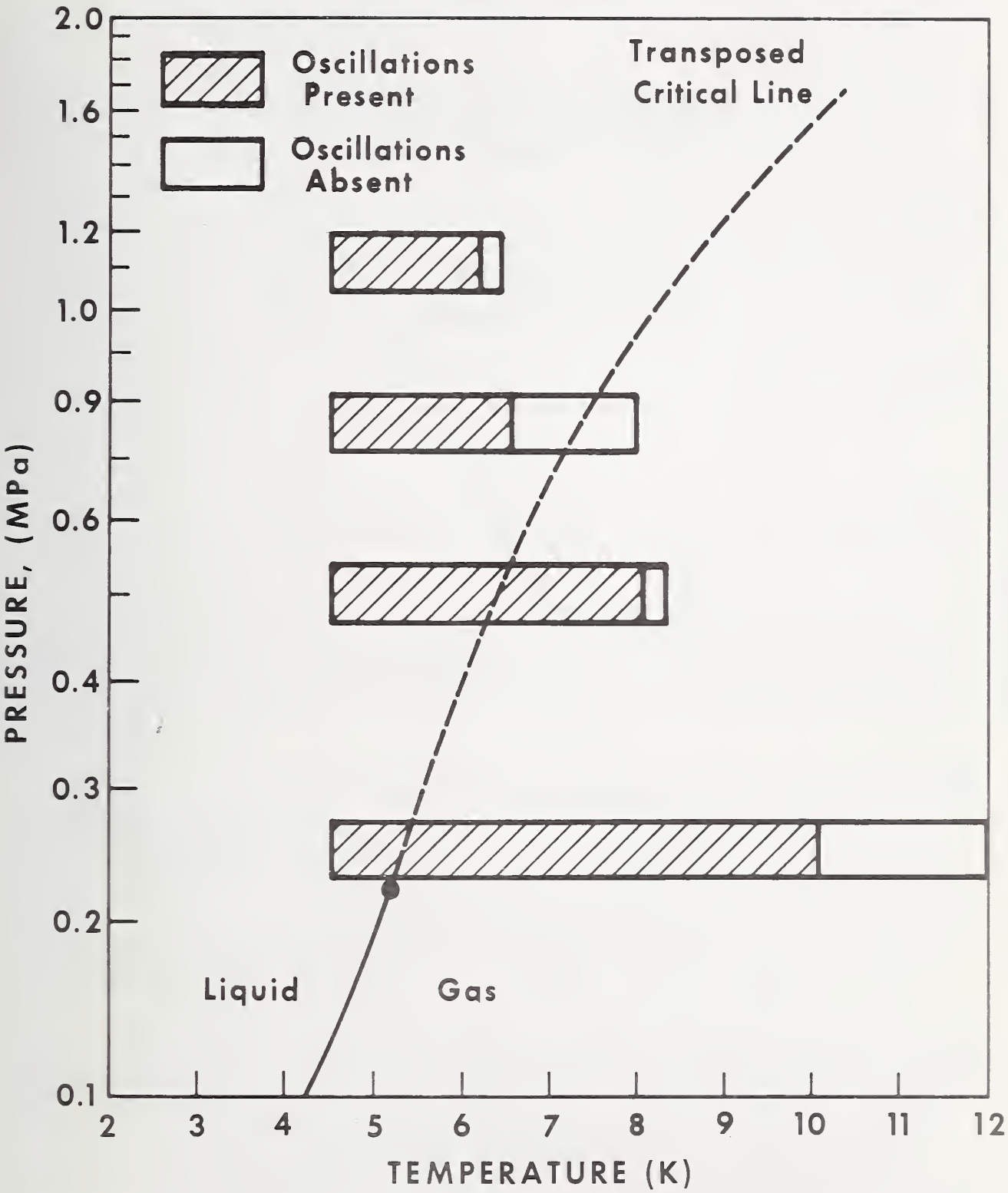

Figure 1.27. p,T regions in which oscillations were observed for lead no. 1.

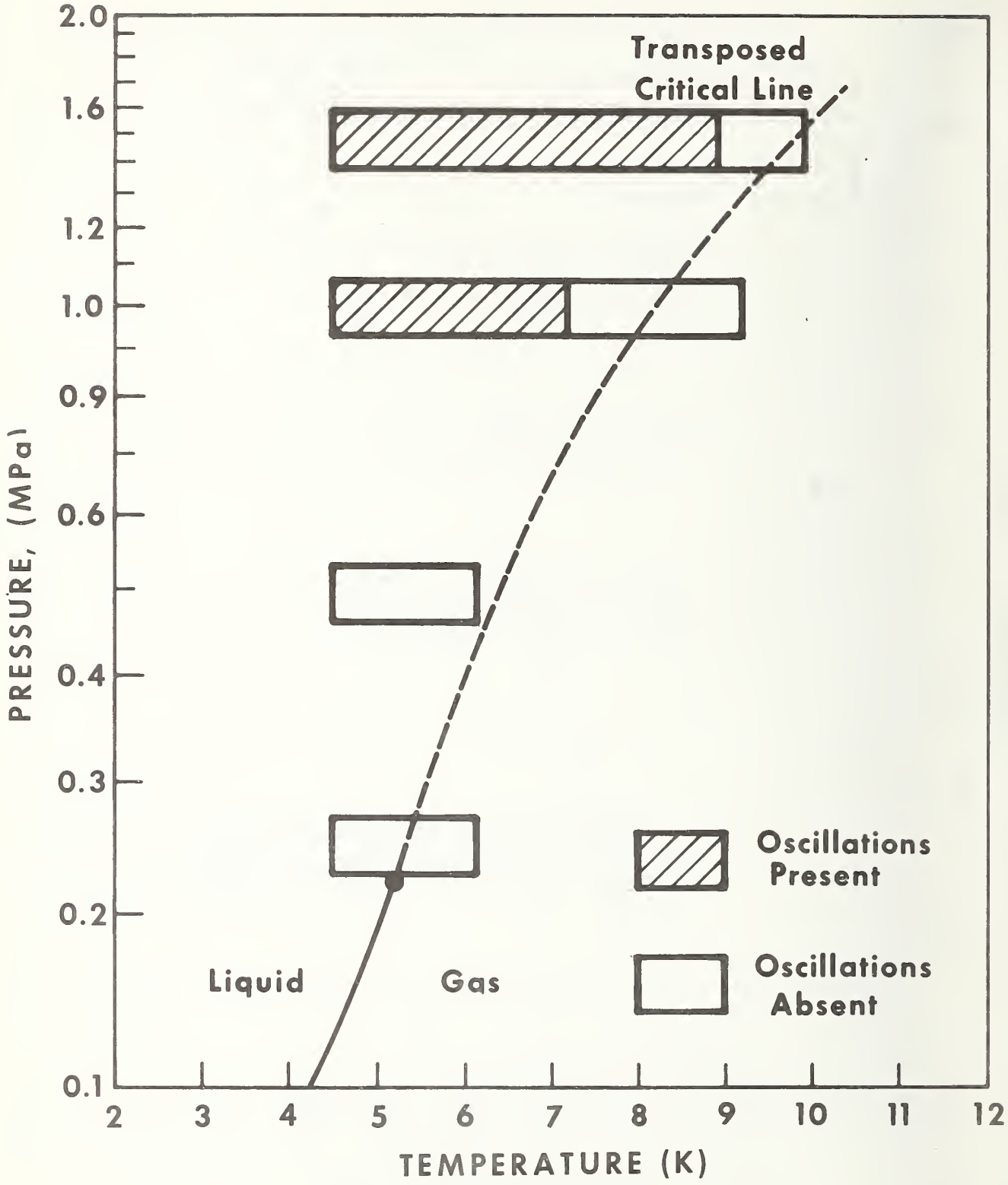

Figure 1.28. p,T regions in which oscillations were observed for lead no. 2.

We would like to be able to predict for any lead design and for various operating conditions when oscillations can be expected. The dependence of the existence of the oscillations on current and flow rate appears to be a complex function of resulting temperature profiles. However, the dependence on the helium thermodynamic state - i.e., whether oscillations can exist for any current and flow rate for given helium states - appears to be broadly predictable from the theory and stability computations worked out by Rott for a simple model. This model is of a simple tube, with an open end in a helium dewar at T_C and a closed end at room temperature T_H. The temperature profile is assumed to be that of a discontinuous change in temperature between two isothermal zones. Solving the one-dimensional wave equation for the pressure under the assumptions of continuity of pressure and pressure gradient at the temperature discontinuity, but taking into account the two-dimensional aspects of momentum and heat transport in the vicinity of the tube wall, he was able to plot a critical temperature ratio for neutral stability $\alpha = T_H/T_C$ vs. the dimensionless ratio Y of the tube radius r to the ac boundary layer thickness, $(\nu_C/\omega)^{1/2}$, where ν_C is the kinematic viscosity in the cold zone end ω the angular frequency. A parameter of the plot was the ratio ξ of warm length to cold length, ℓ_C. A second plot gave the frequency, but von Hoffmann [15] et al. showed that the two could be combined into a single plot of α vs. $\Delta = Y/(\omega\ell_C/C_C)^{1/2} = r(C_C/\ell_C\nu_C)^{1/2}$ where C_C is the acoustic velocity in the gas at T_C. Now, the frequency is no longer explicit. We have reproduced this combined stability plot for various ξ in figure 1.29 from Rott's paper making good use of the asymptotes of the two branches of the neutral stability curve given in the paper.

The physical significance of the two branches is that to the right of and below the lower branch there is insufficient heating and cooling during a cycle to overcome the normal dissipation of the wave; this is the wide tube limit where, in both warm and cold parts, the tube radius is many times the ac boundary layer thickness. Above the upper branch the boundary layer in the warm part fills the entire tube and the pressure wave is heavily attenuated as in a capillary tube.

Now if we plot on the same graph the operating ranges of the ratios α and and Δ at constant pressure, interpreting the tube diameter in Rott's calculations as the mean hydraulic diameter of the lead, (4 X flow cross sectional area/wetted perimeter), we see a remarkable correspondence with our experimental observations, particularly the somewhat contrasting behavior of nos. 1 and 2 with pressure. For, considering lead no. 1, for any reasonable value of ξ (we estimate $\xi = 0.47$) at 0.25 MPa the oscillation should be excited for cold end temperatures up to somewhere between 8 and 12 K. The experimental value was 10 K. As the pressure is increased this temperature should reduce to about 5 K at 1.1 MPa where 6 K was observed. Thus we find an explanation of the behavior of figure 1.27.

Considering lead no. 2, we see that it cannot be unstable at 0.25 MPa for any temperature and any value of ξ (the curve for $\xi = 1$ is the furthest to the left) as observed. But at 1.0 and 1.5 MPa oscillations are possible, and for higher cold end temperatures at 1.5 MPa than at 1.0 MPa - again as observed and illustrated in figure 1.28. Precise stability boundaries are of course not predictable because of the need to interpret ξ for the case of helium cooled leads, where the change in temperature between warm and cold ends is certainly not discontinuous although it approaches it for low currents. The behavior noted in points no. 1 and 2 above is not predicted probably because for both high currents and low flows the temperature profiles become less

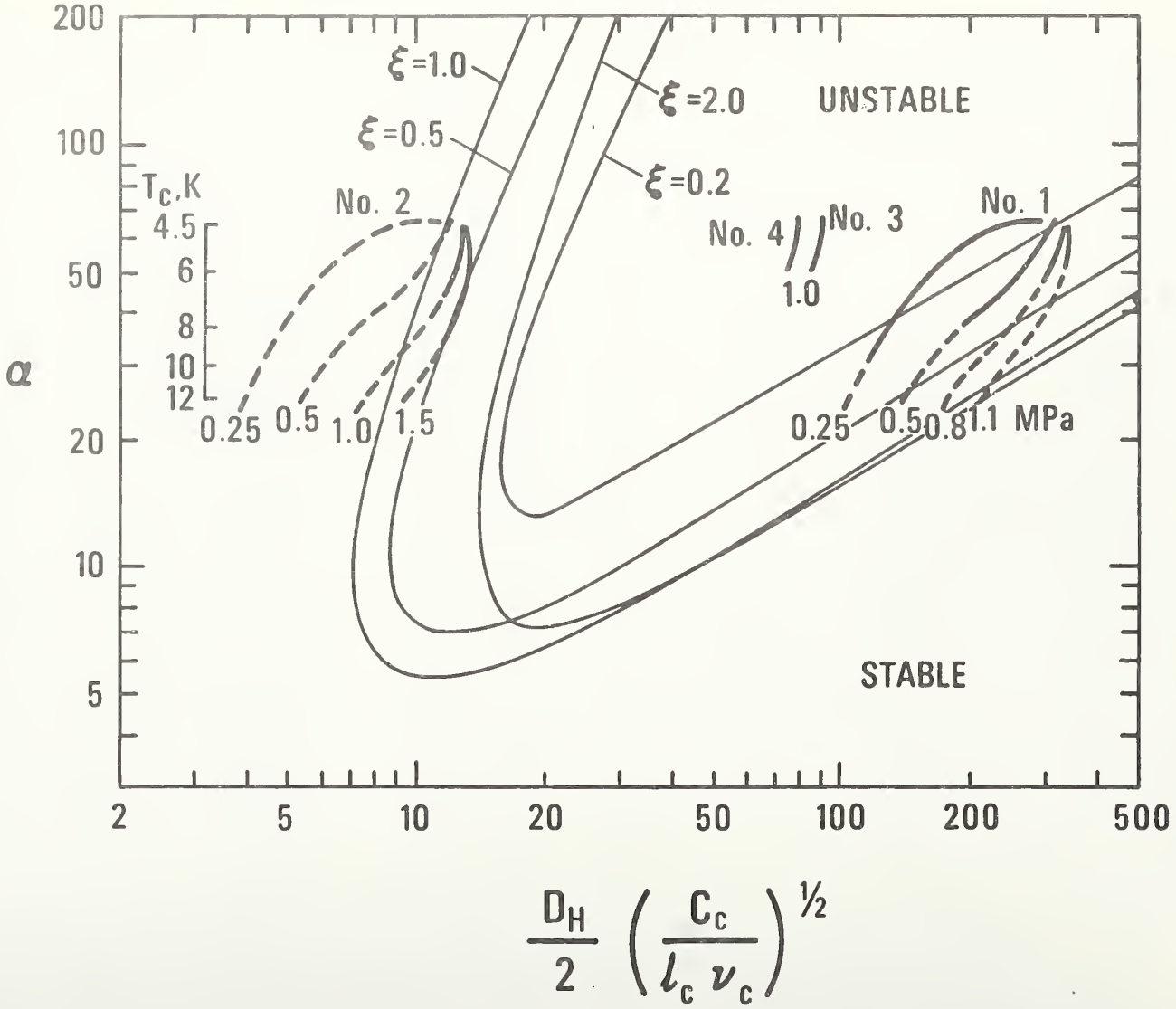

Figure 1.29. Stability boundaries from the calculations of Rott compared with observations of this work. The dashed lines represent experimental conditions where oscillations were not observed, the solid lines where oscillations were observed.

discontinuous and the model must break down. However, the position of the operating curves for lead nos. 3 and 4 are certainly consistent with the observation that for all currents oscillations were observed. By comparison with lead no. 1 one might guess that large amplitudes would have been observed had they been tested at lower pressures.

We see from this comparison of our results with Rott's theoretical calculations that the main design feature at our disposal to avoid oscillations for given thermodynamic states of the helium is the mean hydraulic diameter of the lead. We have two alternatives: to make this quantity no larger than in our lead no. 2, - a proven option - or to go in the opposite direction and use a mean hydraulic diameter at least a factor of two larger than in our lead no. 1. The former option is certainly compatible with a high heat transfer factor; it is not certain that this could be achieved with the latter since $H \approx 1/(D_H \cdot D_S)$ where D_S is the mean thickness of the conductor $(4A_s/P)$.

The possibility of changing the boundary conditions at the lead ends should also be considered. As we have seen, creating a pressure node at the warm gas exit by connecting a reservoir is effective, but perhaps not convenient in a high voltage environment. Creating a flow restriction at the lead inlet may result in a 1/2 wave or closed-closed standing wave. In this case heat addition and subtraction from the wall would not be effective in exciting oscillations in the lower half of the lead and may cancel the positive effect in the upper half. According to Rott's results some alleviation could be achieved by reducing ξ to a small value. This would imply placing a flow restriction immediately at the warm gas exit.

On a final note some of the limitations of Rott's calculations for our purposes should be noted. Apart from the simplicity of the model and the need to interpret his tube diameter as the mean hydraulic diameter of the complex lead structure, his calculations were carried out assuming zero penetration of the temperature wave in the tube wall material, or, constant wall temperature. This can certainly not be true in the cold part of the lead. In addition, calculations involved ideal gas equations, but the anomalous properties in the region of the transposed critical line lead to further uncertainties in the applicability of the results in that vicinity.

1.6. Conclusions and Recommendations

This study has been necessarily exploratory in nature and we have only been able to make a small beginning in several areas. Nevertheless some conclusions have already emerged.

1. From the point of view of lead installation we quickly learned that heat exchange to the entering helium gas alone was not enough to keep the cold end of the conductor temperature down to within a fraction of a kelvin of the entering helium. Some extraordinary cooling surface at the cold end must be provided in addition as was accomplished in our test by cooling the bus bar.

2. To be safe, in order to avoid burn-out, one should not exceed the adiabatic warm end condition.

3. The actual burn-out current per unit of mass flow is a function of conductor purity and heat transfer design. Based on our experience with lead no. 2 for RRR > 50 a safe criterion for operation seems to be $2J/M < 1.0$ if the mass flow is close to optimum or below. For flow rates above optimum this will only be true for leads with heat transfer factor H greater than about 10^4. Further work is needed on leads with low RRR.

4. The heat transfer factor for a braided lead of the design of no. 2 is much less than can be estimated from simple heat transfer concepts.

5. Accurate predictions of thermal runaway for a given lead design will only be possible if empirical knowledge of the heat transfer factor and its dependence on mass flow is available in addition to the RRR. The heat transfer factor should be measurable by less expensive room temperature experiments.

6. Oscillatory behavior can be expected in leads where the mean hydraulic diameter is greater than about 0.018 cm unless other precautions are taken. These precautions include the use of a warm-end reservoir or throttling of the helium coolant at the inlet to the lead. It is recommended that actual designs be tested for oscillations without current flow to establish the conditions for stable operation.

7. Future work should concentrate on specific candidate designs with demonstrated high heat transfer factors. Yet to be established is the safe operating current at which a lead may operate with the capability of withstanding fault currents. This should be amenable to calculation.

1.7 References

[1] Trumpler, P. R., and Dodge, B. F., The Design of Ribbon-Packed Exchangers for Low Temperature Air Separation Plants. Trans. Am. Inst. Chem. Eng. 43, 75 (1947).

[2] Lock, J. M., Optimization of Current Leads into a Cryostat. Cryogenics 9, 438 (1969).

[3] Pippard, A. B., Continuous Refrigeration of Current Leads. Cryogenics 5, 81 (1965).

[4] Agsten, R., Thermodynamic Optimization of Current Leads into Low Temperature Regions. Cryogenics 13, 141 (1973).

[5] Bejan, A. and Cluss, E. M., Criterion for Burn-up Conditions in Gas-cooled Cryogenic Current Leads. Cryogenics 16, 515 (1976).

[6] Arp, V. D., Daney, D. E., Frederick, N. V., Jones, M. C., Ludtke, P. R., Parrish, W. R., and Powell, R. L., Helium Research in Support of Superconducting Power Transmission. NBSIR 75-823, Nat. Bur. Stand. (U.S.), October 1975.

[7] Thullen, P., Stecher, R. W., and Bejan, A., Flow Instabilities in Gas-cooled Cryogenic Current Leads. Proceedings of the 1974 Applied Superconductivity Conf., IEEE Trans. on Magnetics MAG-11 (IEE Magnetics Society, 1975).

[8] Arp, V. D., Thermodynamics of Single-Phase, One-Dimensional Fluid Flow. Cryogenics 15, 285 (1975).

[9] McCarty, R. D., Thermodynamic Properties of Helium 4 from 2 to 1500 K at Pressures to 10^8 Pa. J. Phys. Chem. Ref. Data 2, No. 4, 923 (1973).

[10] White, G. K., and Woods, S. B., Electrical and Thermal Resistivity of Transition Elements at Low Temperatures. Phil. Trans. Roy. Soc. (London) A251, 273 (1959).

[11] Powell, R. L., Roder, H. M., and Hall, W. J., Low-Temperature Transport Properties of Copper and its Dilute Alloys: Pure Copper, Annealed and Drawn. Phys. Rev. 115, No. 2, 314 (1959).

[12] White, G. K., and Woods, S. B., Phil. Mag., 7, 45, 1343 (1954).

[13] Güsewell, D. and Haebel, E. V., Current Leads for Refrigerator-Cooled Large Superconducting Magnets. Proc. ICEC 3, Berlin, p. 187 (I.P.C. Science and Technology Press, Guildford, UK, 1970).

[14] Rott, N., Damped and Thermally Driven Acoustic Oscillations in Wide and Narrow Tubes. ZAMP 20, 230 (1969) and Thermally Drive Acoustic Oscillations, Part II, Stability Limit for Helium. ZAMP 24, 54 (1973).

[15] von Hoffman, T., Lienert, V. and Quack, H., Experiments on Thermally Driven Gas Oscillations. Cryogenics 13, 490 (1973).

2.0. HELIUM MEASUREMENTS

An important part of this report has been concerned with the measurement of those helium properties which monitor the performance of the cooling system. The NBS work for this year is divided into several catagories. The general problem of data transmission from the power line to ground potential is discussed in section 2.1. Comments on thermometry are given in section 2.2, which is a follow-up on a similar discussion in last year's report. Possible indirect methods for determining helium pressure are discussed in section 2.3, and work on a new form of pressure transducer is dicussed in section 2.4. Problems of impurity detection are discussed in section 2.5.

2.1 Data Transmission from the Superconducting Power Line to Ground Instrumentation

The generalized problem of transmitting the operational information (on pressure, temperature, flow, etc.) from the power line to the final readout condition at ground potential was discussed in some detail at the project review meeting in Boulder on January 27, 1976. At that meeting Dr. Rabinowitz of EPRI informed the group of an existing EPRI-sponsored contract related to signal transmission across a high voltage gap, and as a result it was concluded that our superconducting power line project should not initiate any experimental work in this direction at this time. However, the subject is important here in relating recommended measurement systems to the generalized constraints imposed by power line system operation.

A schematic outline of the signal path is shown in figure 2.1, assuming that the transducer and its electrical circuit will unavoidably ride essentially at the potential of the superconductor. Since this potential may be several hundred kilovolts above ground, special signal processing techniques are called for. As seen in figure 2.1, the power supplies, amplifiers, etc., used for signal detection are enclosed in a high voltage "cage" at the power line potential, and special equipment is used to transmit the information outside of the cage to recording equipment at ground potential. What limitations, problems, and costs are incurred through this signal path? It is convenient to divide the question into several categories: the power supply, amplifier and detector specifications, transmission to ground potential, and 60 Hz noise pickup from the power cable.

2.1.1 Power Supply

The power supply should provide instrumentation power during cooldown and electrical faults which temporarily open the line as well as during steady state operation. This could be achieved by using a rechargeable battery supply, and arranging a charging circuit inductively coupled to the current in the superconductor for recharging the battery during steady state operation. No new technology is required, but this does suggest that d.c. powered instrumentation may be most appropriate. Conversion to a.c. is possible, but it adds to the cost of the power supply.

2.1.2 Equipment Specifications

An important question is whether conventional electronic equipment - amplifiers, a to d converters, etc. - will operate as effectively and accurately within the high voltage "cage" as they do at ground potential. This point was discussed very carefully with Dr. Oskars Petersons and several of his staff at the NBS High Voltage Section in Gaithersburg. We had been concerned that miscellaneous power line transients could couple into the components and perturb sensitive circuits through small stray capacitances to ground. Dr. Petersons, a man of considerable practical experience, assures us that this will not be the case, and that ordinary components will meet their ordinary specifications when properly "grounded" to the cage.

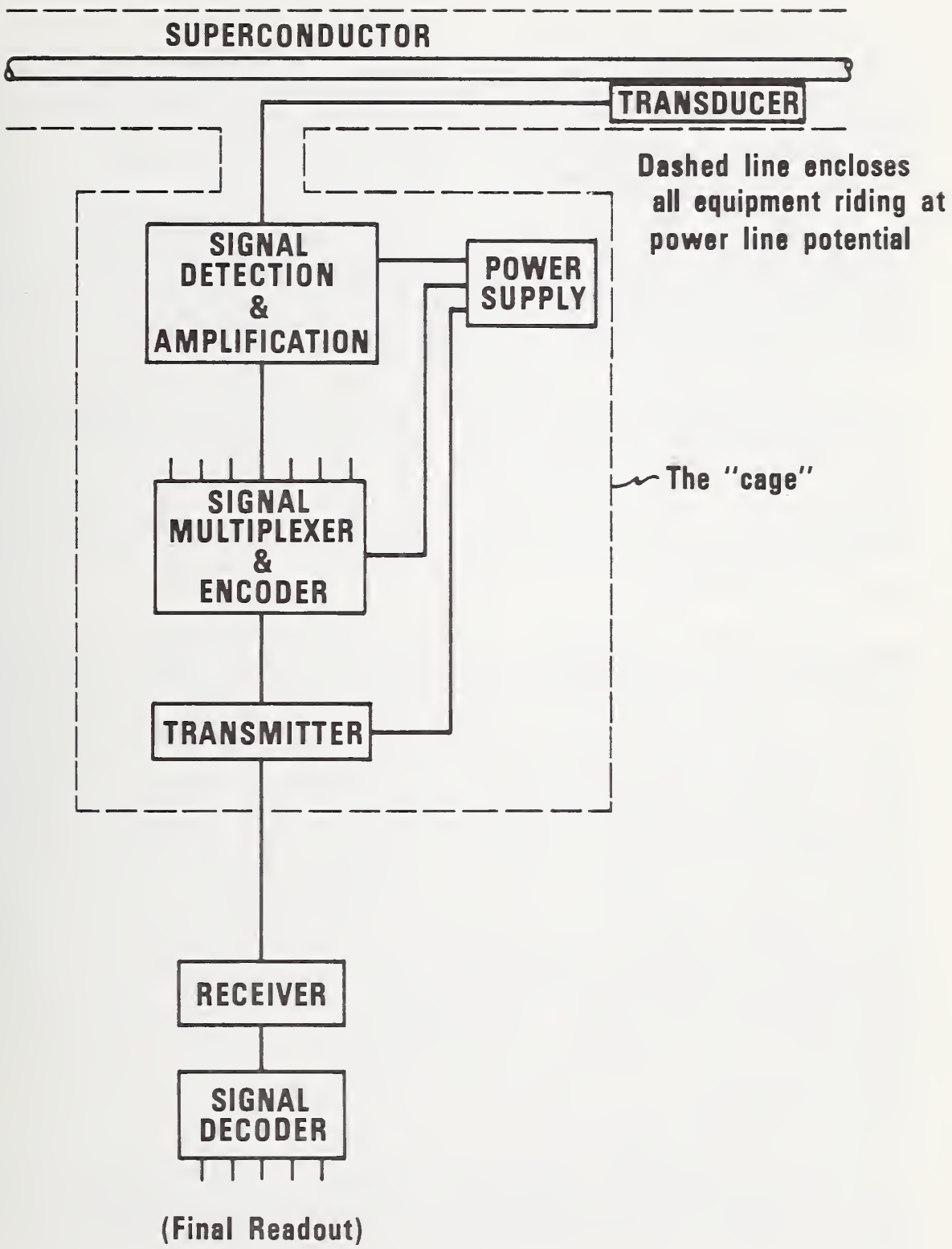

Figure 2.1. Schematic outline of the transducer signal path from high voltage to ground potential.

2.1.3 Transmission to Ground

The biggest question is how to transmit the transducer information out of the "cage" to ground potential. Here there are three basic alternatives to be considered: (1) a capacitive link, (2) a fiber-optical link, and (3) an f.m. radio link.

2.1.3.1 Capacitive Coupling

The use of conventional overhead high-voltage power lines for transmitting communications as well as power is standard within the industry, and techniques developed for the communication link may be applicable to our instrumentation problems. Frequencies in the range of 30 - 300 kHz have been employed for power line carrier purposes, as this range is high enough to be isolated from the 60 Hz power frequency and the noise it creates, yet not so high as to encounter excessive attenuation.

The accepted technique for transmitting the communications signal between ground and the high voltage line is to use a high voltage coupling capacitor, for which standards have been set up by the AIEE. From a discussion on this topic with Mr. Ray Fillenberg of the U.S. Bureau of Reclamation, the cost of such a unit is of order $8,000, though this may include certain filters and tuning circuits. We conclude that there should be no major technological barrier to the use of such a device for transmitting instrumentation signals to ground potential. Several carrier frequencies could be used simultaneously.

2.1.3.2 Fiber-optics

An alternative technique is to use fiber-optical data transmission between high voltage and ground. The basic advantage of such a link stems from its insensitivity to electromagnetic radiation from the power line, in particular, from the transients. In the early 1960's such a fiber-optical link was developed and marketed, but sales were disappointing (apparently) and it has been discontinued. Since that time, the Light Emitting Diode (LED) has been developed. In the high voltage research activities of Hydro-Quebec in Ottawa, LEDs and fiber-optical techniques have been combined for just such instrumentation links as are being considered here. This work was performed with private funding and has never been described in the open literature. A representative of a Canadian company tells us that they do not manufacture these as standard items, but would be willing to build one on special order. Various pulse-code modulation and/or frequency modulation techniques could be used. Amplitude modulation is less desirable because LEDs are quite nonlinear and also drift with age. A description of a proposed fiber-optical link for high-voltage systems has been given by Erez [1]. Fiber-optical links have also been used to control the firing times on the thyristors used in the d.c. power transmission systems between Southern California and the Bonneville Power Administration. In this case only a very small amount of information is transmitted (one firing pulse every sixtieth of a second), but possible problems of surface leakage and flash-over along the fiber-optics appear to have been solved.

2.1.3.3 Radio Transmission

A third alternative for the instrumentation link is to use radio transmission. Such a system, operating at about 100 MHz, has been described by Morse, et al. [2]. This reference also mentions a fiber-optical link, and it appears that the radio and fiber-optics offer comparable transmission capabilities.

2.2 Thermometry

The sensitivity of various types of thermometers to electromagnetic fields was summarized in our last year's report [3]. In discussing the subject with the Steering Committee (on May 7, 1975) prior to writing that report, it had been suggested that it would be desirable to place them, for example, in the high voltage insulation space, thereby exposing them to intense a.c. fields. This places stringent requirements on the thermometers, but several types were identified which should give temperature measurements substantially unaffected by these ambient fields.

This subject was further discussed in the Steering Committee meeting of January 27, 1976, this time in relation to the problem of induced voltages on the electrical leads from the thermometer to the power supply and sensing device. The general conclusion at this time was that thermometers would never be placed in such high-field regions because of the great difficulty with induced voltages on the leads and recording equipment. In other words, thermometer selection and sensing in SPTL's would not involve electromagnetic conditions significantly more stringent than in many other low temperature systems, though small size and fast response (in milliseconds) may be very desirable. On this basis we have not done any further study on thermometer systems.

At the time of this writing, neither our Laboratory nor the other ERDA-supported SPTL projects have had experience with the newer carbon-in-glass or capacitance thermometers which are now commercially available. We plan to purchase some of these for our own experimental work in the coming year, so as to become familiar with their use.

The general conclusion reported here, that thermometers will probably not be placed in high-field regions, would apply also to other types of sensors, e.g., pressure sensors.

2.3 Pressure Determination from Density and Temperature Measurements

The pressure in a single phase fluid can be uniquely determined from simultaneous measurements of density and temperature. This possibility, along with that of using other pairs of thermodynamic variables (e.g., sound velocity and temperature) was considered briefly in our previous publication [3] but dismissed as being not as promising as direct pressure measurement as discussed in section 2.4 of this report.

Since that time, Dr. C. T. Van Degrift, who initially stimulated our microwave cavity work, has moved from the University of California to the NBS Heat Division, and is currently pursuing this approach though inverting the procedure to obtain a secondary temperature standard from density and pressure measurements using a cavity. It is appropriate to review this question in more detail than was given in reference [3].

Dr. Van Degrift's secondary temperature standard is (will be) obtained by sealing a fixed quantity of helium into a high pressure chamber which has one wall in common with the microwave cavity, which operates in a vacuum. The helium pressure is determined by the cavity frequency measurement. The helium density is essentially constant, and is determined by calibration at a known temperature. Once the density is known, other temperatures can be determined just from cavity frequency measurement, knowing the equation of state for helium.

In order to invert his procedure, and determine a system pressure from density and temperature, one can make use of the fact that the dielectric constant is a simple monatonic function of density and that the resonant frequency will vary with dielectric constant if the helium permeates the

cavity. In this case the cavity is made with rigid walls so that the frequency does not change with pressure. To put this in quantitative terms, the dielectric constant is related to the density of helium by

$$\varepsilon \approx 1 + 4 \times 10^{-4} \rho. \qquad \text{[SI Units]} \tag{2.1}$$

For a cavity having rigid walls, a change in pressure will affect only the fluid density within the cavity, and the resonant frequency, f, will be proportional to $\varepsilon^{-1/2}$, or

$$\frac{df}{f} = -\frac{1}{2}\frac{d\varepsilon}{\varepsilon} . \tag{2.2}$$

In first order, $\varepsilon = 1$, so that

$$\frac{df}{f} \approx -2 \times 10^{-4}\, d\rho . \tag{2.3}$$

To relate a small density change, $d\rho$, to small pressure and temperature changes, dP and dT, we write

$$d\rho = \rho K \frac{dP}{P} + \rho\alpha \frac{dT}{T} , \tag{2.4}$$

where

$$K = \left(\frac{P}{\rho}\frac{\partial\rho}{\partial P}\right)_T \qquad \text{and} \qquad \alpha = \left(\frac{T}{\rho}\frac{\partial\rho}{\partial T}\right)_P .$$

Both K and α are equal to 1.0 for an ideal gas, but more realistic values for helium in the compressed liquid range are

$$K \approx 0.1 \quad \text{and} \quad \alpha \approx 0.5 .$$

Therefore, taking $\rho \approx 10^2$ Kg/m^3,

$$\frac{df}{f} \approx -.002 \frac{dP}{P} \; -0.01 \frac{dT}{T} .$$

Thus, to measure pressure to an accuracy of one percent, one must determine the resonant frequency to an absolute accuracy of about one part in 50,000. This is not hard to do in the laboratory, where a good counter can be used, but it would be difficult to do inexpensively, as, for example, with the voltage controlled oscillator circuit described in section 2.4 of this report. Further, the temperature would have to be measured, in this example, to an accuracy of 0.2 percent, or about 0.02 K, to obtain one percent pressure accuracy. Because temperature effects are so large, the readings of frequency and temperature would always have to be processed through the equation of state, in a minicomputer, to obtain the pressure. Finally, the method is not conveniently adaptable to differential pressure measurement, which would always require two separate microwave cavities, perhaps beating one against the other.

We still conclude that this would not be as practical for a field device as are the microwave cavities discussed in section 2.4 of this report.

2.4 Microwave Cavity Pressure Transducer

In simple concept, the microwave cavity pressure transducer is a sharply-tuned L-C circuit whose resonant frequency shifts with pressure. This is accomplished by building the circuit as a reentrant microwave cavity having one thin wall which deflects elastically when pressure is applied external to

the cavity. The cavity is so designed that the wall deflection causes an internal capacitance change and thus a shift in the natural resonant frequency, nominally about 1200 MHz, which can be detected by external circuitry. Potential advantages of this design are as follows:

(1) By building the cavity of a metal which is highly conducting at helium temperature, e.g., copper, or a superconductor, the resonant Q can be 4000 or more. This permits a very weak coupling between the resonant circuit and the measuring circuit, with corresponding insensitivity of the resonance to external parameters.

(2) The cavity can be made of all one metal, thus obtaining a rigid and rugged structure and avoiding differential thermal contraction and pressure seal problems associated with composite metal and insulating structures.

(3) Its output is essentially unaffected by external electromagnetic fields at power-line frequencies.

(4) It can be used as a differential pressure gauge by allowing helium within the resonant cavity itself. No loss in electrical performance results, but the volume of contained fluid does limit the sensitivity for high frequency pressure oscillations. Also, there is a significant zero shift as the absolute helium pressure within the cavity changes.

(5) It can be designed to be undamaged by large overpressures, though again, this is obtained at the cost of reduced hydraulic frequency response.

2.4.1 General Circuit Concept

The use of microwave cavities of this type as transducers was initially suggested by Dr. Craig Van Degrift [4, and private communication].

In Dr. Van Degrift's work the active element which maintains the oscillation and provides an output signal is a tunnel diode which is physically packaged with the cavity. The active circuit is supplied with d.c. power, and the circuit output is monitored with a frequency counter. When operated at low temperature, (typically below 30° K) this system can be made stable to one part in 10^8 or better, and can be applied to a variety of instrumentational problems. The difficulty with this system, for our application, is that noise on the d.c. power input shows up as frequency noise on the output, so that these leads would require very careful shielding.

In our work we have separated the passive L-C circuit (the cavity) from the active circuit which powers the oscillation and provides the analog output. We have chosen to make the active circuit a simple voltage-controlled oscillator, which is much less expensive, but also less precise, than the frequency counter required in Van Degrift's version. The connection between these 1.2 GHz components is made via a long coaxial lead. Low frequency noise, from d.c. to a few kilohertz, induced on this lead cannot perturb the analog output, so this system is to be preferred when the cavity and/or lead must be placed in an electrically noisy location. The disadvantage of this circuit is that the output signal can drift slightly in response to perturbations on the electrical characteristics of the coaxial cable if a precise electronic counter is used as the output device. However, a simple inexpensive readout device can provide adequate sensitivity if the diaphragm is designed for sufficient movement ($\approx$ 1 micrometer), and perturbations from the coaxial lead should be insignificant in this case.

2.4.2 Material

In order to obtain a sharp resonance (high Q) in the electrical circuit, and hence high resolution for small frequency changes, the cavity must be a

good electrical conductor. It is important also, that all of the cavity, pressure chamber, etc., be made of the same material so that differential thermal contractions on cooldown to 4 K will not lead to residual strains or distortions which could compromise the accuracy or calibration.

Our cavities are made of copper, chosen because it is a good electrical conductor at room temperature, becoming much better at 4 K. Thus the transducers should give a good and usable signal at room temperature and during cooldown, while best performance is obtained in the liquid helium temperature range. If only cold operation is desired, even better performance could be obtained by making them of niobium, which is superconducting below 9 K, or, as suggested by Zimmerman [5], tin-reacted niobium which is superconducting below 18 K.

One problem with copper cavities must be recognized. The stress-strain behavior of copper is strongly dependent on metallurgical condition, and linear elastic behavior, in particular, is obtained only for very small strains. This is discussed in more detail in section 2.4.4 of this report. Some sort of compromise may be worth consideration for future work, by selecting a material with lower conductivity but better elastic behavior.

2.4.3 Cavity Geometry

Two different geometries have been used for the design of the cavity. The first consisted essentially of a thin-walled pipe which was soldered into an axial hole in a specially machined piece, as illustrated in figure 2.2 (this is the same as figure 4.3 in our report last year [3]). While this type of cavity can be made to work, we concluded that delicate problems of machining and assembly of this type of cavity are significantly greater than that of the second type, illustrated in figures 2.3 and 2.4. The frequency, sensitivity, nonlinearity of response, etc., of this second type of cavity, can be calculated in a relatively straightforward manner.

Regarding the cavity as a simple LC resonant circuit, neglecting second-order contributions because of the finite cap thickness, and assuming a dielectric constant ε, the capacitance (referring to figure 2.3) is

$$C = 8.85 \times 10^{-12} \times \frac{\pi}{4} \frac{d^2}{g} \varepsilon \qquad (2.6)$$

and the inductance is

$$L = 2 \times 10^{-7} \ell \log \left(\frac{b}{a}\right) . \qquad (2.7)$$

where SI units are used throughout. Thus the resonant frequency, f_o, of the cavity is related to the cavity dimensions by

$$(2\pi f)^2 = \frac{1}{LC} = \frac{4}{\pi \times 17.7 \times 10^{-19}} \frac{g}{\varepsilon d^2 \ell \log\left(\frac{b}{a}\right)} \qquad (2.8)$$

The diameter of the capacitor cap (8.38 mm in figure 2.5) is a compromise between precise machining requirements and the goal of reducing the external cavity dimensions while retaining high sensitivity. A large cap diameter leads to a large capacitance between it and the closely spaced flexible wall which it faces. Thus for a given operating frequency, limited by availability of practical electrical components, a large cap allows a relatively small inductance, or cavity volume, to be used. On the other hand, with ordinary machining and assembly tolerances, the surface of this cap will not be exactly parallel to the wall which it faces, only about 0.06 mm away. One can see

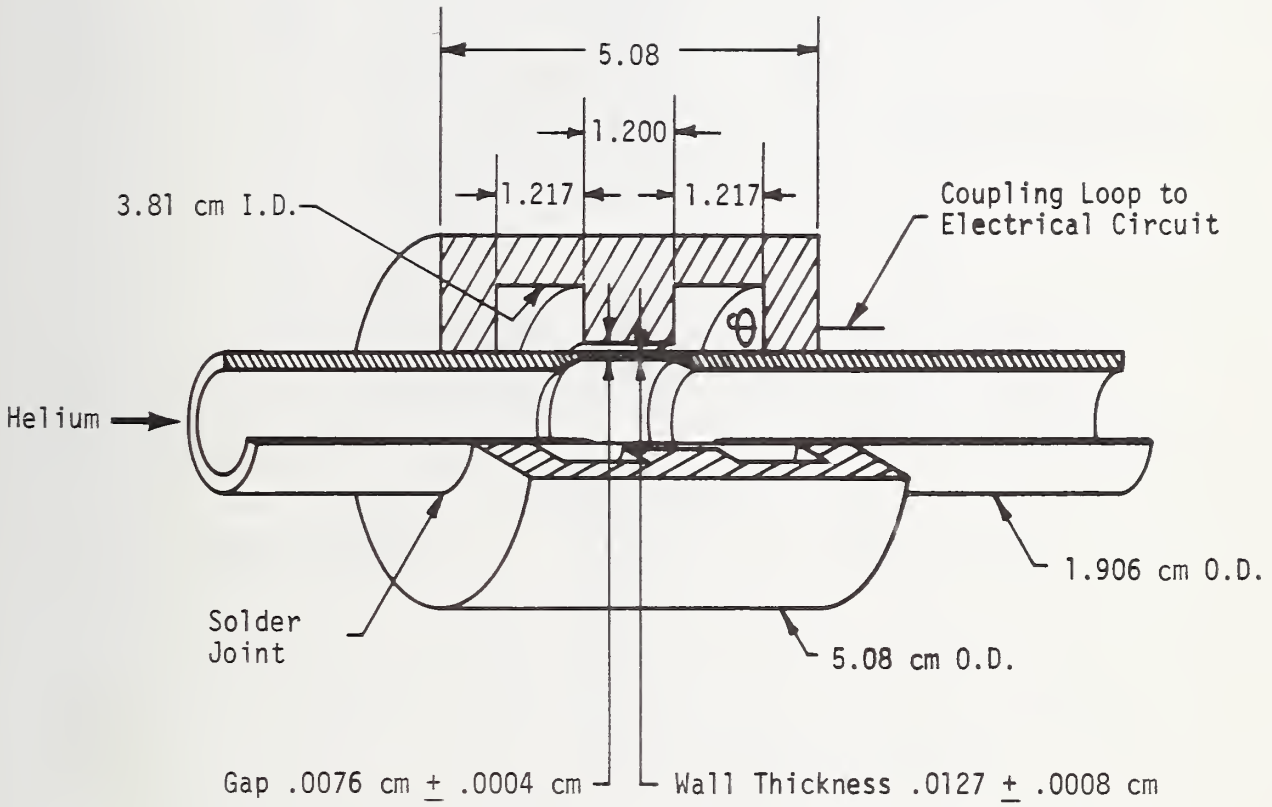

Figure 2.2. 440 MHz resonant cavity pressure sensor.

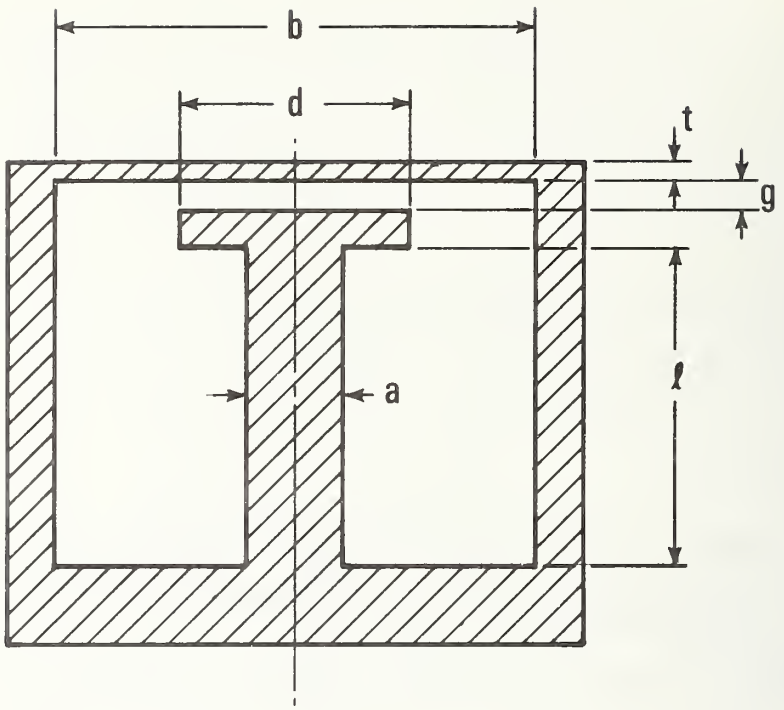

Figure 2.3. Geometrical parameters of the microwave cavity.

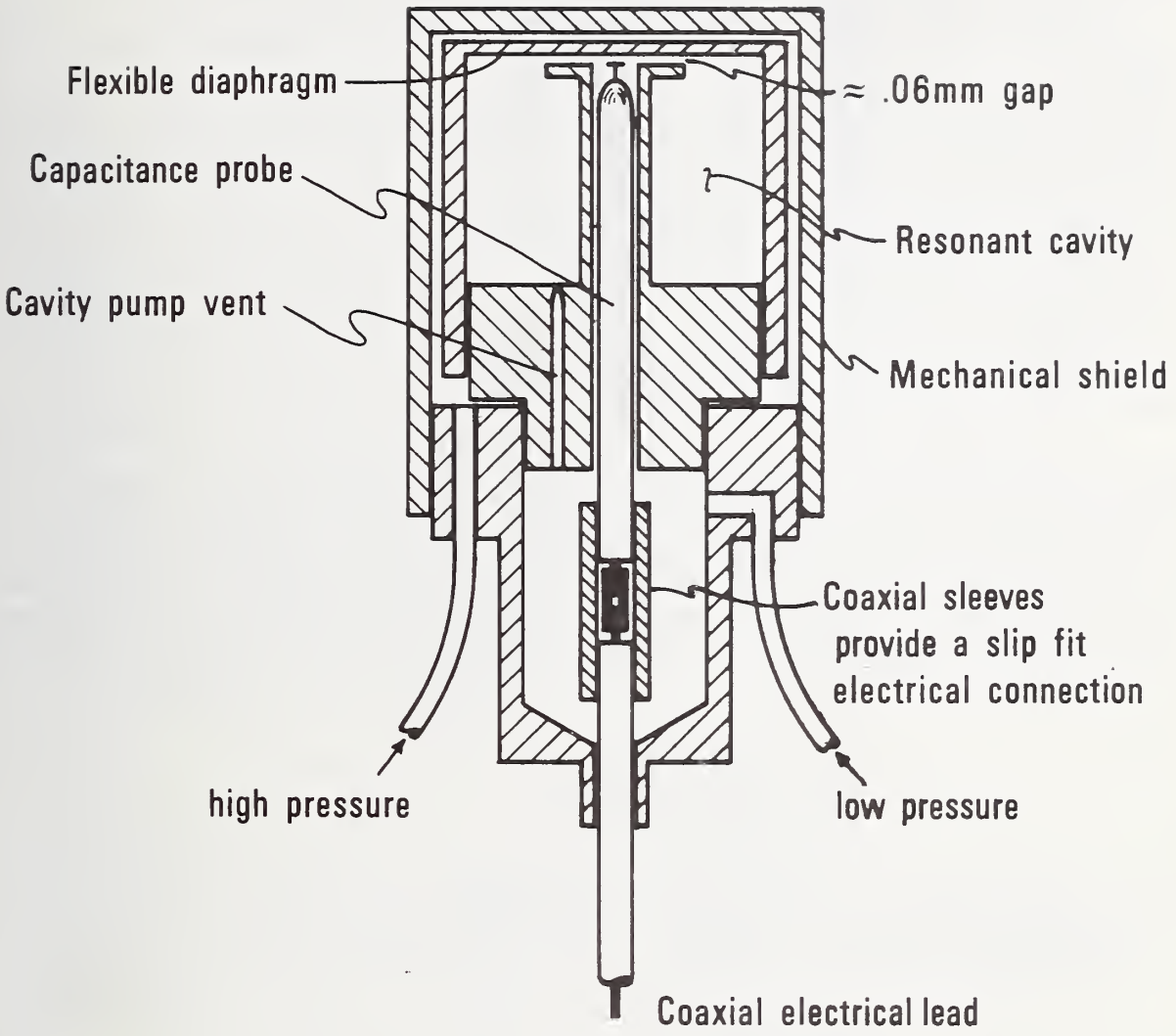

Figure 2.4. Assembly of the microwave cavity pressure transducer.

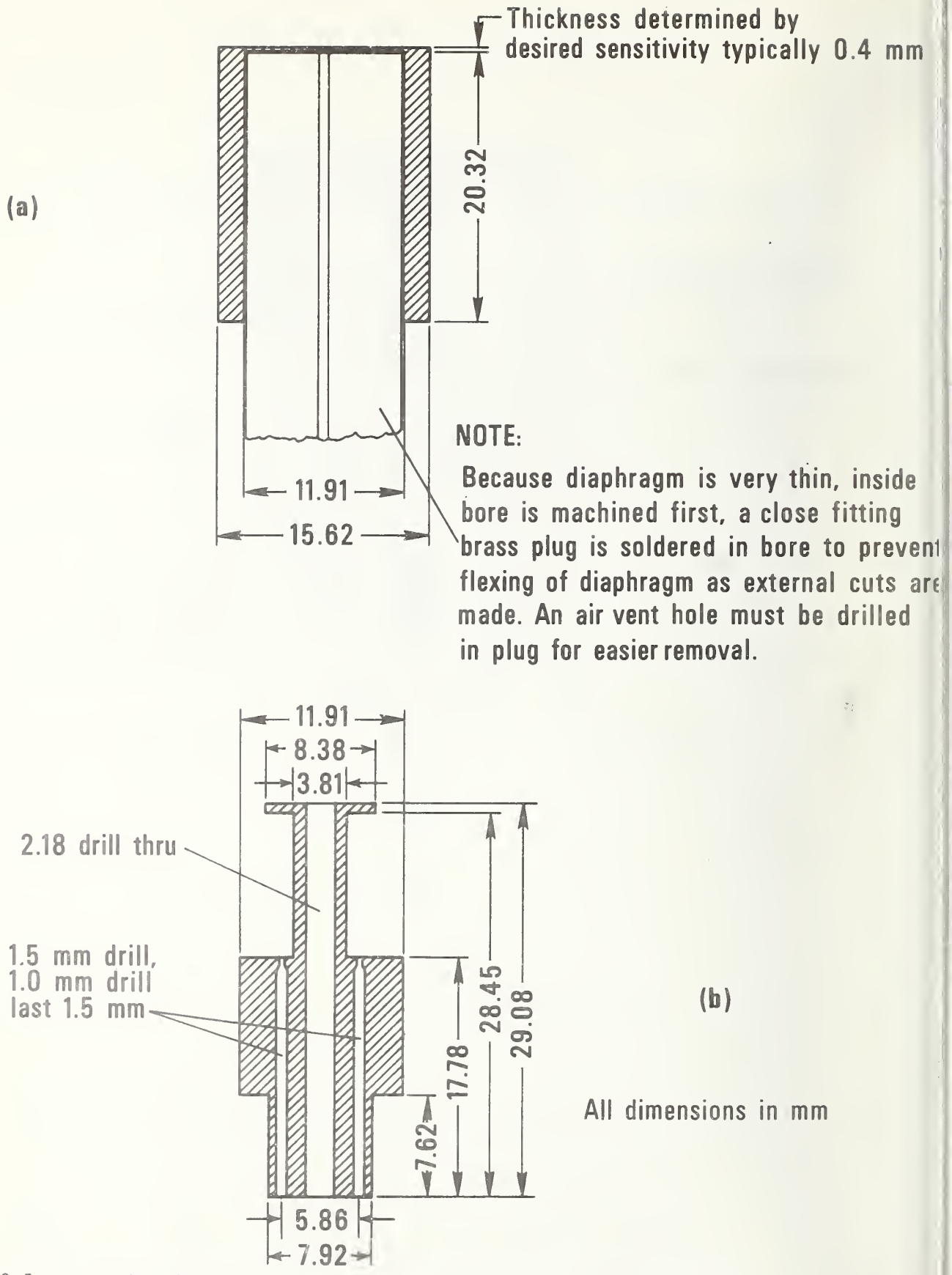

Figure 2.5. Design detail on the two pieces which are soldered together to form the cavity.

that a slight misorientation between the center lines of the two pieces in figure 2.5, will result in a closer than average spacing between some point on the cap rim and the opposite wall. Since the total capacitance is the integrated average of the reciprocal of the gap spacing, a relatively close spacing at the rim will have a dominant affect on the resonant frequency, degrading the sensitivity to wall movement if the cap diameter is too large.

Our experience suggests that if the gap, g, is much less than 0.05 to 0.07 mm, one encounters annoying difficulties with machining inaccuracies, precise control of f_o during assembly, cleaning of the cavity after assembly, etc. These difficulties can all be overcome, but the construction costs will rise in doing so. Our prototype cavities, to be installed for field tests in our helium flow loop, have been designed with a gap of about 0.06 mm. The gap spacing is controlled during assembly by a sliding motion of part b) inside part a) (of figure 2.5), observing the resonance with a temporarily installed probe connected to the electrical circuit. When the desired resonant frequency is obtained, the probe is removed, and the pretinned parts are heated to fix the final spacing. After this operation, the cavity is cleaned by forced flow of filtered ethyl alcohol, inlet through the 3.81 mm probe port.

The i^2R losses in the microwave currents broaden the resonance and reduce the ultimate sensitivity of the device. Since the microwave currents flow in a very thin layer over the metal surfaces, the surface finish should be kept as fine and clean as possible. It is also possible to minimize losses by geometric considerations, picking the cavity proportions to minimize the total resistance through which the currents must flow. Neglecting current flow in the facing surfaces of the capacitor plates (the current flow there is non-uniform as a given charge density builds up or decays), the resistance will be proportional to

$$\text{Resistance} \propto \frac{\ell}{\pi a} + \frac{\ell}{\pi b} + 2\int_{a/2}^{b/2} \frac{dr}{2\pi r} \quad . \tag{2.9}$$

Numerical experimentation with this equation (2.9) indicates that, for a given g and f_o, the losses are in fact a fairly weak function of geometry for reasonable variations of the parameters from the values shown in figure 2.5. Increasing the pillar diameter, a, would reduce the losses somewhat, but at the same time would result in a larger cavity, for a given frequency and capacitor gap.

2.4.4 Diaphragm Thickness and Transducer Sensitivity

The pressure sensitivity is controlled by the diaphragm thickness, t. An enlarged, out-of-scale sketch for calculation purposes is shown in figure 2.6. At a certain high pressure, P_m, the diaphragm contacts the opposite surface. As the result of this additional support, subsequently higher pressures will not linearly increase the maximum strain which the diaphragm experiences. If the design places this maximum strain within the elastic limit of the diaphragm material, overpressures, unless they are extreme, should not damage the subsequent performance within its design range. For a given pressure, P, the deflection of the center of the diaphragm is

$$z = \frac{3(1-\nu^2)}{256} \left(\frac{b}{t}\right)^3 b \frac{P}{E} \quad , \tag{2.10}$$

and the maximum stress in the diaphragm, which occurs at its circumference, is

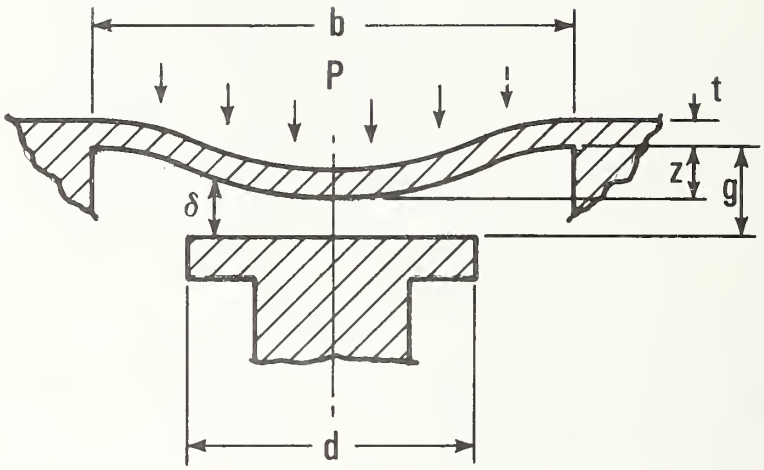

Figure 2.6. Schematic outline of the diaphragm distortion under pressure, defining relevant parameters (not to scale).

$$\sigma_{max} = \frac{3}{16}\left(\frac{b}{t}\right)^2 P \ . \qquad (2.11)$$

In equation (2.10) ν is Poisson's ratio and E is the elastic modulus.

If copper is stretched beyond its elastic limit, but not more than its tensile stress limit, it becomes work-hardened and will subsequently exhibit elastic behavior for stresses below the maximum value to which it has been subjected. In practice, the stress should be cycled between zero and the peak value several times in order to exhibit good linearity in the stress-strain curve over a major portion of this range. Also, depending on several metallurgical parameters, it probably should not be subjected to significant stresses in the opposite direction (leading to a phenomenon known as the Bauschinger effect [6]). The elastic limit of OHFC copper is a very strong function of the material condition, ranging from about 32×10^7 Pa (46 ksi) for material which has been cold draw down to 60%, down to 0.14×10^7 Pa in the annealed condition. Inspection of data for a number of OHFC and ETP coppers [7] shows that a reasonable tensile stress to which copper can be stretched without exceeding the tensile strength at room temperature is in the range 18 to 20×10^7 Pa. For our transducer design, it is realistic to adopt a conservative limit, namely $\sigma_{max} = 15 \times 10^7$ Pa. Thus, after construction, the transducer should be pressurized to reach this stress and then used only over, say, 50 percent of this range. In this way elastic, hysteresis-free performance should be obtained over its working range, provided that the diaphragm is not pressured in the opposite direction.

If we ask that this maximum stress, 15×10^7 Pa, occur just when the center deflection, Z, equals the initial gap, g, the thickness of the diaphragm must be

$$t = \frac{(1-\nu^2)}{16}\left(\frac{b}{g}\right)\frac{\sigma_{max}}{E}\, b \ . \qquad (2.12)$$

For our cavity dimensions, and with $E = 13 \times 10^{10}$ Pa (copper at room temperature), one finds

$$t = 0.15 \text{ mm}$$

corresponding to

$$P_{max} = 1.3 \times 10^5 \text{ Pa} \quad (1.3 \text{ atmospheres}).$$

Thus, using this technique, our differential pressure transducers with a nominal working range of $\lesssim 0.7 \times 10^5$ Pa should be undamaged by significant overpressures. For transducers of higher working range, σ_{max} would be reached before the diaphragm touched the opposite wall, so that this overpressure protection would not be available. This conclusion differs from that of Neubert, in his figure 3.22 [8], where it is stated that the response of a pressure diaphragm will be linear if the displacement z is less than 0.5 of the thickness, t: this latter can be true only if the ratio b/t exceeds a certain critical value, e.g., about 120 for copper.

The ability to sustain large overpressures without stressing the diaphragm beyond the design limit could be obtained by reversing the direction of diaphragm motion, i.e., by letting high pressure fill the cavity, and the low,

or reference, pressure be external to it. Thus an external, very closely spaced mechanical stop could be placed to support the diaphragm if it tries to deflect beyond a preset range. The free travel of the diaphragm could then be adjusted independently of the gap spacing, g, which controls the electrical characteristics of the cavity. The disadvantage of this procedure comes from the relatively large volume of fluid in the cavity, which reduces the mechanical response to high frequency fluid pressure oscillations. We have not built any transducers on this design, though it would be relatively straightforward to do so.

When the pressure is applied, the diaphragm distorts as sketched in figure 2.6 (not to scale), and the capacitance change is a function of Z, g, d, and b. To a very good approximation the capacitance is

$$C = \varepsilon \int_o^{d/2} \frac{2\pi r dr}{\delta} \tag{2.13}$$

where

$$\delta = g - Z(1 - 2\rho^2 + \rho^4)$$

and

$$\rho = r/(b/2) ,$$

Combining terms,

$$\frac{C}{C_o} = \frac{1}{\beta^2} \int_o^{\beta} \frac{2\rho d\rho}{1 - w(1 - 2\rho^2 + \rho^4)} \tag{2.14}$$

where

$$\beta \equiv d/b$$

and

$$w \equiv Z/g$$

and C_o is the capacitance when P = 0. Straightforward integration produces the result

$$C = \frac{C_o}{2\beta^2\sqrt{w}} \log \left[\frac{1 - (1 - \beta^2)\sqrt{w}}{1 + (1 - \beta^2)\sqrt{w}} \cdot \frac{1 + \sqrt{w}}{1 - \sqrt{w}}\right] . \tag{2.15}$$

Since w is proportional to pressure, and f is proportional to $\sqrt{1/C}$, this expression may be used to obtain the normalized frequency shift as a function of normalized pressure for any given diameter, β. Writing, to second order

$$\frac{\Delta f}{f} = \left(\frac{1}{f}\frac{\partial f}{\partial w}\right)_o w\ (1 + c_2 w) \tag{2.16}$$

the calculated initial sensitivity, $(1/f)(\partial f/\partial w)$, as a function of β, is given in figure 2.7. One can see that the sensitivity decreases as the diameter ratio increases, since in this case the electrode spacing approaches a constant value, independent of pressure, near its outer rim. Also shown is the second-order term, c_2, which does not vary greatly with diameter ratio. Based upon the yield stress limit and the cavity dimensions described above, a diaphragm designed for a maximum pressure of 10^5 Pa (1 atmosphere) will have a maximum normalized pressure, $w_m \approx 0.2$; for a maximum pressure of 20 x 10^5 Pa, $w_m \approx 0.045$. From the magnitude of c_2 calculated above, one can see that the calibration will be measurably nonlinear over the allowable range of the more

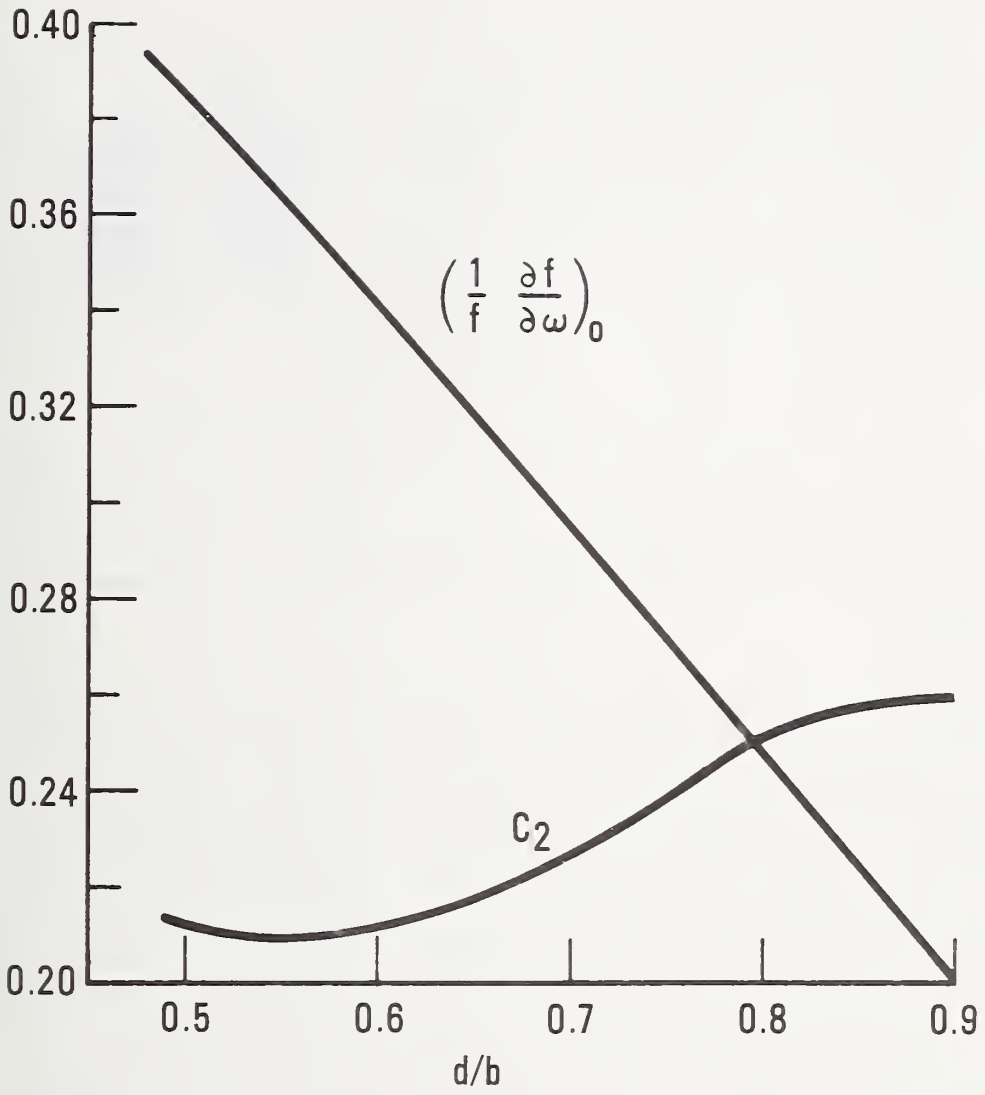

Figure 2.7. Normalized pressure sensitivity of the resonant frequency as a function of the diameter ratio d/b. Parameters are defined in the text.

sensitive gauges. In practice, the nonlinearity must be measured, since it will vary from this theoretical value if the capacitor plates are not exactly parallel. Also, the frequency-to-voltage circuits exhibit some nonlinearity which adds to this mechanical nonlinearity in the final readout.

2.4.5 Electrical Circuit

Our original design utilized inductive coupling to the H field within the cavity (as seen in figure 2.2), but we now use capacitive coupling to the E field, a technique which appears to offer a practical advantage. With inductive coupling, it is necessary to solder the center conductor of the coaxial pair to the inside wall of the cavity at some point so as to make a small loop perpendicular to the microwave H field. Once this operation is done, it cannot be removed and replaced without complete disassembly of the cavity. Further, in situ bending of the loop, to obtain a final adjustment on the coupling between the cavity and the outside circuit, will necessarily leave small stresses in the wire. These stresses react against the insulation holding the conductor centered within the outer conductor of the coaxial pair, and differential contraction during subsequent cooldown may cause erratic temperature-dependent motions of the coupling loop.

Capacitive coupling, on the other hand, involves a simple termination of the coaxial pair in a region of the cavity where the E field is high. No mechanical forces are applied to the center conductor other than those of the insulation which keeps it centered. Provided that axial stresses are not transmitted from the external lead to the short length of coax which serves as the coupling probe, there should be no tendency for relative movement between the probe and the cavity as the temperature is cycled. (It should be noted that the inductive probe would likewise be sensitive to axial forces along the center conductor).

Our capacitive probe design is illustrated in figure 2.8, and the assembly of the probe in the transducer is seen in figure 2.4. The epoxy seal at the end of the probe maintains a fairly rigid alignment between the inner and outer conductors when cooled to helium temperature. The regular insulation is marginal for this purpose, since it contracts much more than the outer conductor does, leaving a tiny radial gap at the inner diameter of the outer conductor, in principle allowing slight radial movement of the inner conductor. The conceptual design of this epoxy seal is similar to that of standard "Housekeeper" copper to glass seals. Adjustment of the coupling to the cavity is accomplished by axial movement of the probe assembly, which varies the capacitance between the center conductor and the opposite wall. This adjustment is made by monitoring the cavity resonance with an oscilloscope during assembly; we have not made any direct measurement of the spacing, but approximate measurements suggest that it is about 0.1 mm.

A schematic outline of the electrical circuit is shown in figure 2.9. The cavity is connected to the power supply and readout instrumentation by a single coaxial lead. The power supply contains a commercially available voltage controlled oscillator (VCO) whose output frequency as a function of applied voltage is given in figure 2.10. A feedback circuit senses the reflected microwave power from the cavity, and maintains the VCO input voltage at the value corresponding to the center of the cavity resonance. The readout circuit subtracts a controlled d.c. voltage (the zero set voltage) from the input voltage to the VCO, multiplies the result by either 1. or 10. at the operator's option, and transmits this to a digital voltmeter or other readout

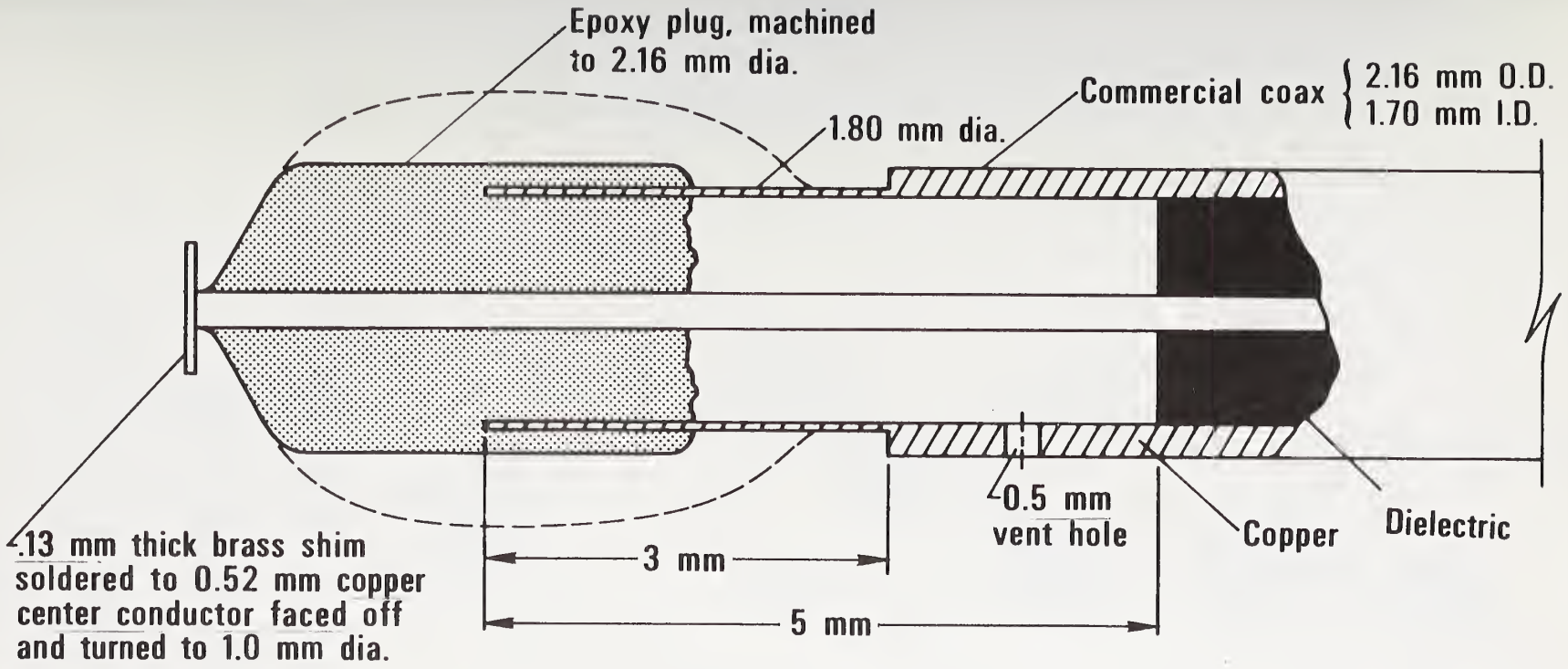

Figure 2.8. Design of the capacitive probe to the cavity.

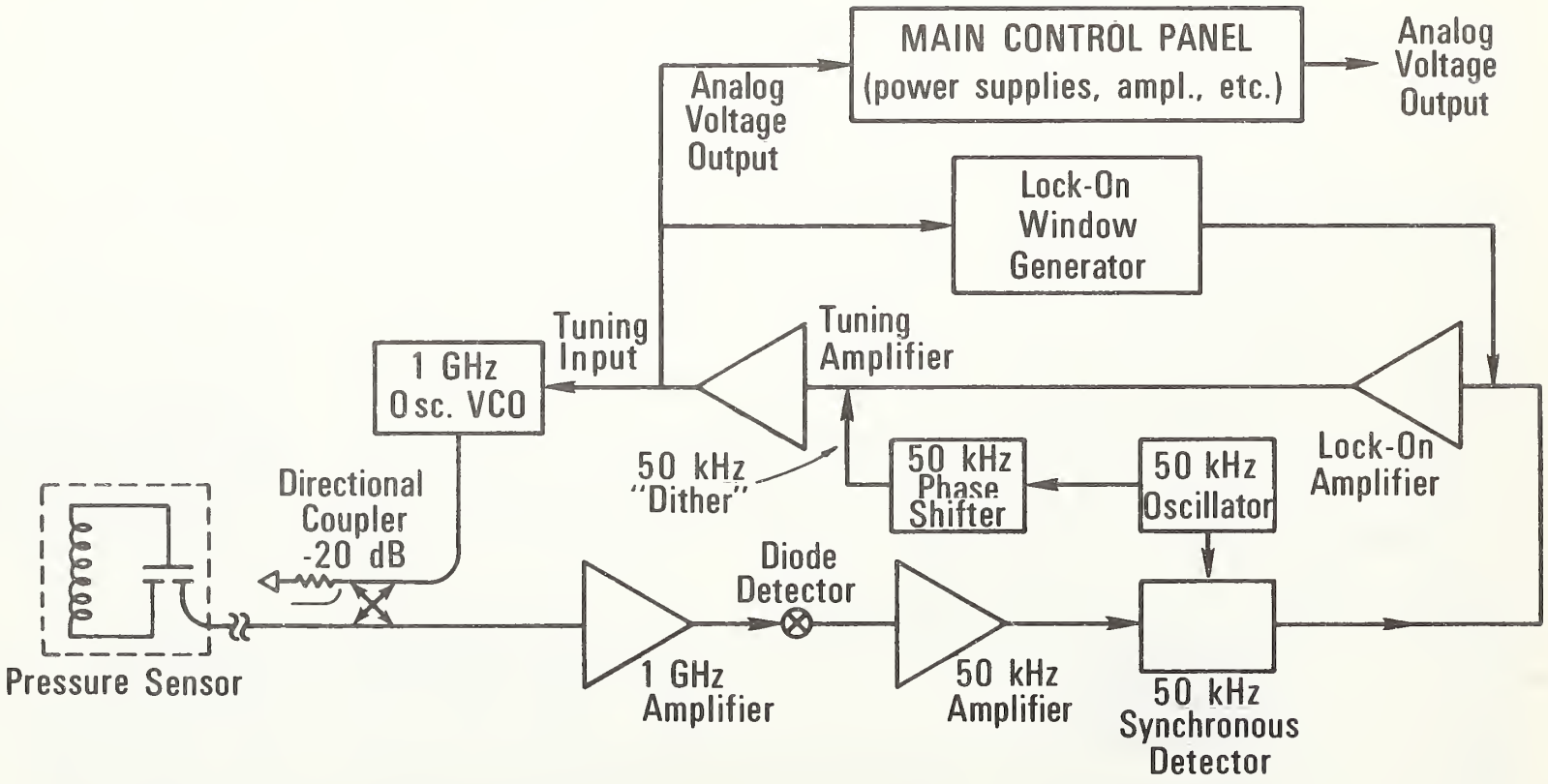

Figure 2.9. Block diagram of the electrical circuit.

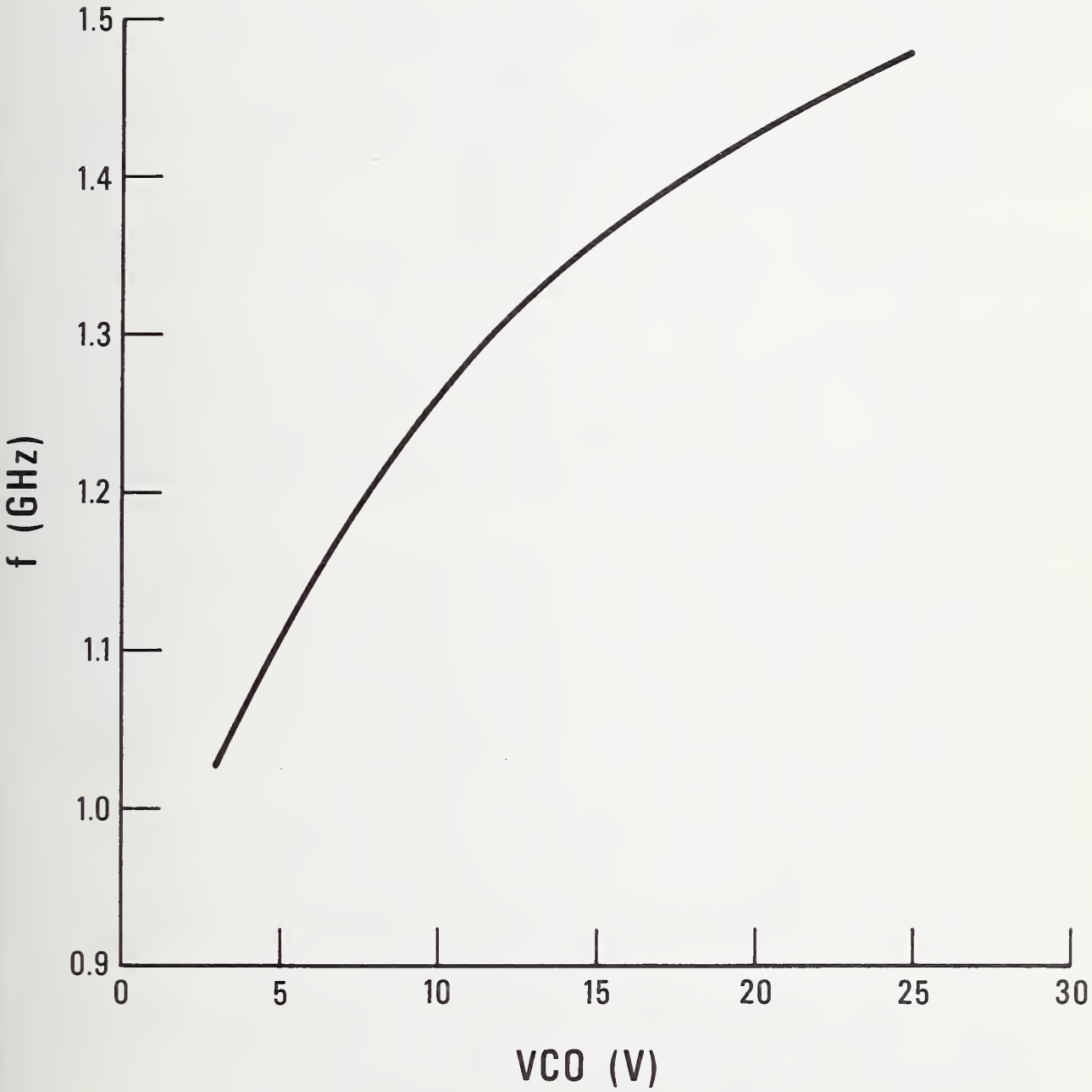

Figure 2.10. Output frequency of the voltage controlled oscillator as a function of applied voltage.

instrument with a range of ± 10 volts. With the signal strengths available, the circuits will lock on to the center of the resonance within 0.01 of the linewidth. For a typical cavity Q 4000, a frequency shift of one part in 4×10^5 can be thus resolved. From the VCO calibration curve in figure 2.10, and operating at 1200 MHz, this corresponds to about ± 0.001 volts at the output, on the x10 range.

During the cavity assembly and setup, the lock-on circuit is disabled, and the VCO is swept over a wider range, at the operator's selection, so that the resonance can be observed on an oscilloscope. When switched from set-up to run mode, the circuit automatically hunts for the resonant signal.

The basic circuit for producing an analog voltage output, determined by cavity frequency, has performed well in tests, but the peripheral circuits used to isolate the cavity resonance from unwanted reflected signals have gone through extensive revision.

Idealized curves of reflected power (measured by a diode detector) as a function of frequency are seen in figure 2.11(a). When the VCO frequency, f, differs significantly from the cavity resonant frequency, f_o, all of the incident power is reflected. As f approaches f_o, the cavity begins to absorb an amount of microwave power which depends on the coupling strength between the coax line and the cavity, and on the Q of the cavity. The coupling strength is controlled by the axial position of the probe, figure 2.8, in the cavity, figure 2.4. Assembly of the transducer involves setting the coupling so that the cavity is almost perfectly matched at 4 K, where the Q is the highest. Some trial and error is involved, since the adjustment requires a soldering operation on the warm transducer. Once this is set, the resonant curve with the copper cavity at room temperature will be somewhat like the "weak coupling" curve in figure 2.11(a).

In practice, however, the reflected power shows variations in addition to the cavity resonance, as illustrated in figures 2.11(b) and 2.11(c). These variations originate from the coherent addition of microwave power reflected by non-ideal components throughout all the 1200 MHz circuit. Of these, the most difficult for our purpose originate from signals reflected at or near the transducer mixing with signals reflected at or near the directional coupler. This latter mixing depends on the length of coax line, which is 0.5 meter for figure 2.11(b) and 2 meters for 2.11(c). Experiments with 250 meters of superconducting coaxial cable disclosed so much of this unwanted mixing that the electrical circuit was unable to lock on to the resonance.

In the original tests a discriminator circuit was added to prevent the lock-on circuit from operating when the magnitude of the reflected power was more than a preset value. This works well for short cable lengths, even with the cavity at room temperature, where the discriminator circuit could be set as the dotted line in figure 2.11(b) indicates. However, as the coax line length was increased the increasing number and amplitude of these unwanted reflections tended to obscure the signal from the resonant cavity at room temperature. The further addition of a sweep limiting circuit led to a cumbersome set of controls, compromised the flexibility of the original design, and displayed annoying transient effects. Consequently these have been recently replaced by a simpler circuit which precisely limits the search and lock-on circuit to operate only between two preset frequencies. Schematics for the complete circuit are given in figures 2.12 and 2.13. This new circuit has not been thoroughly tested as of this writing.

2.4.6. Transducer Tests

During this development, we assembled three different transducers and subjected them to various tests, and obtained parts for two more. Basic

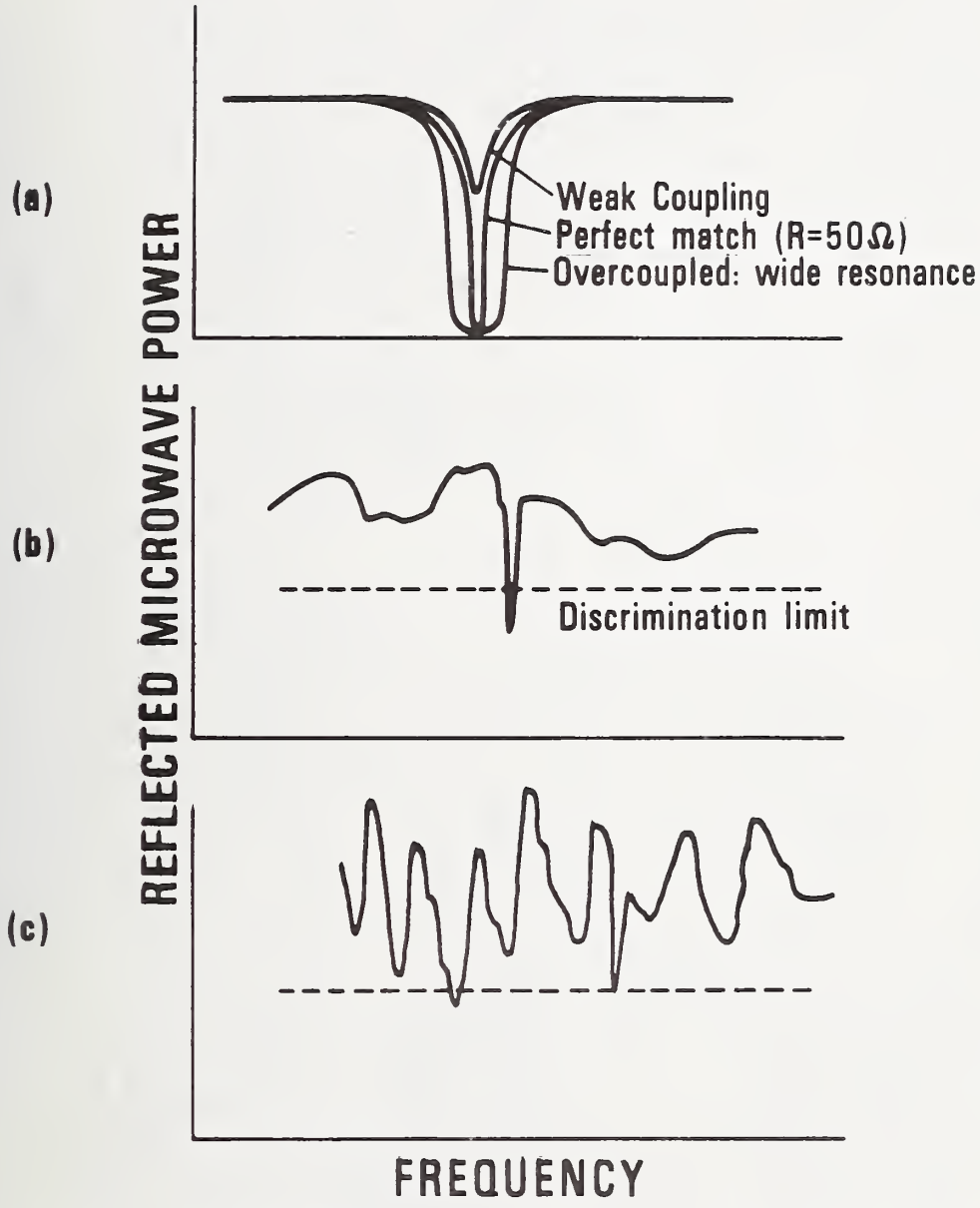

Figure 2.11. Approximate representation of the reflected electromagnetic power sensed at the diode detector as a function of frequency. The top curve represents the ideal case, for three different values of the coupling strength. The middle curve represents the curve obtained in practice with a short length of coaxial line between the cavity and the directional coupler. The bottom curve portrays the additional perturbations as the coaxial line length is increased. The dashed line represents the discriminator voltage cutoff as discussed in the text.

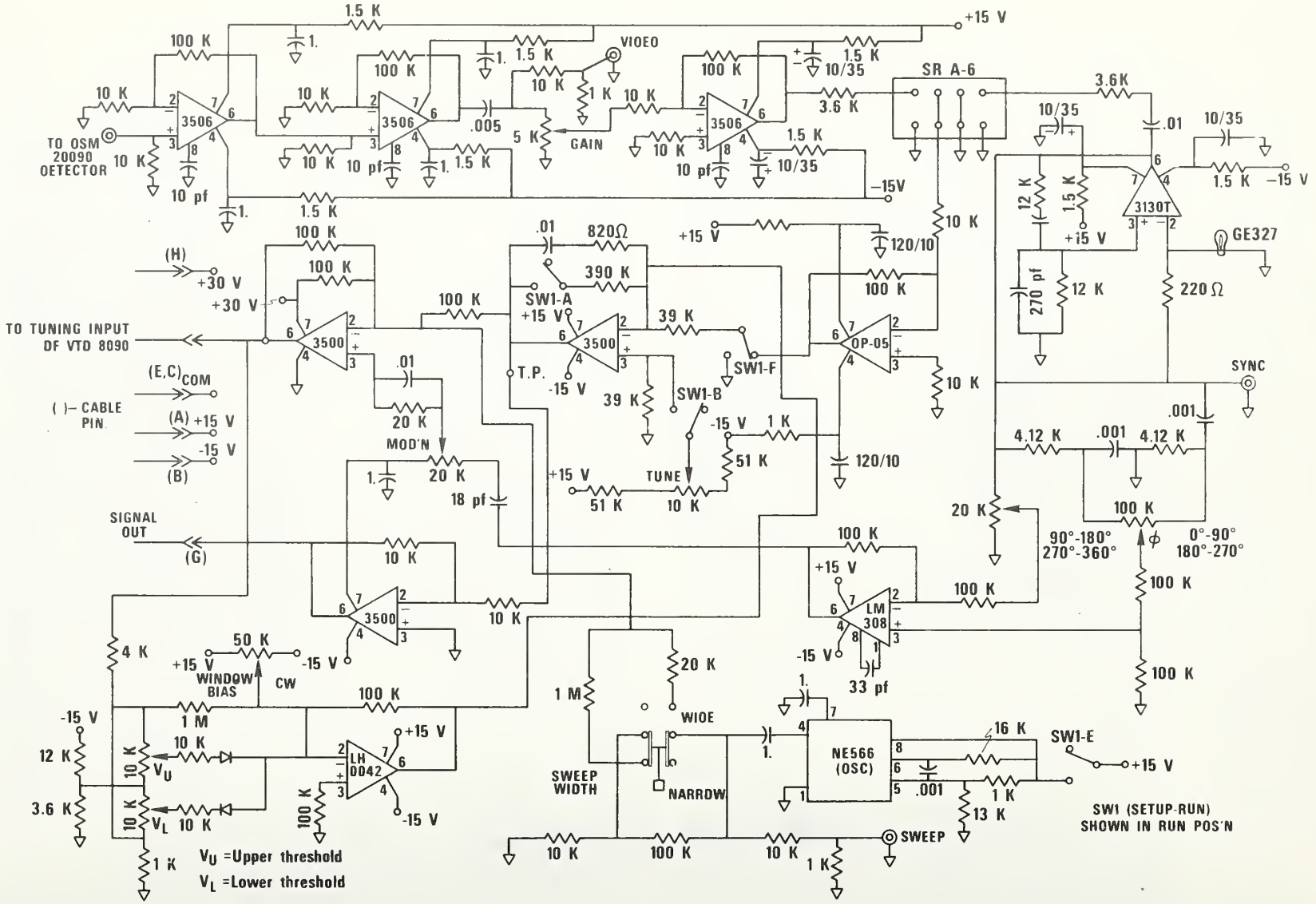

Figure 2.12. Detailed schematic diagram of the detection and demodulation circuits.

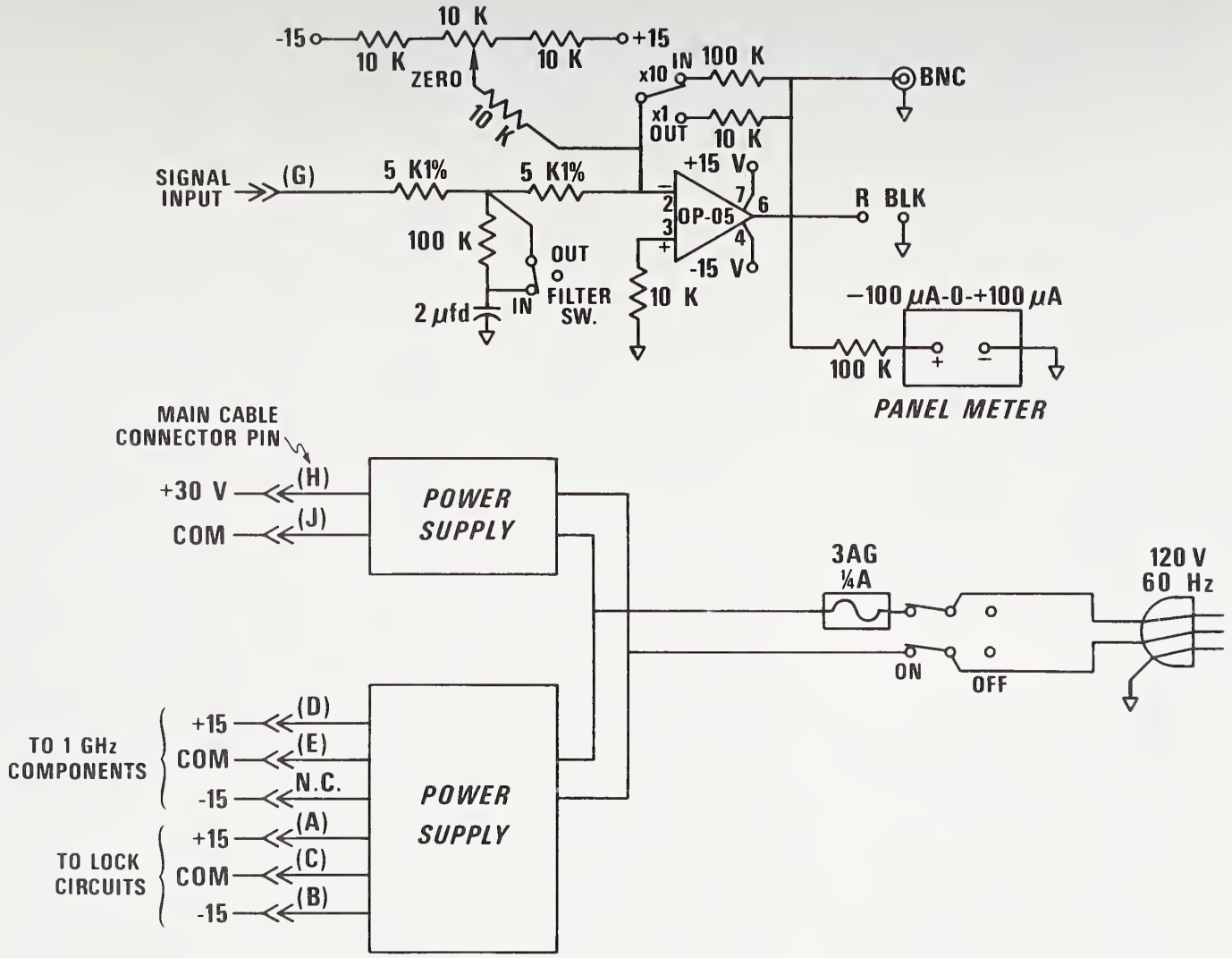

Figure 2.13. Schematic outline of the power supply connections and the analog output voltage circuit.

characterization of these is given in table 2.1. Not included are several earlier microwave cavities which were only for circuit tests, and did not function as pressure transducers.

Table 2.1. Transducers.

number	cavity dimensions (mm)		diaphragm		coupling probe
	length	diameter	thickness (mm)	construction	
1.A	15.24	9.144	0.25	soldered	machined and assembled
1.B	(cavity #1.A, reworked)		0.13	soldered	machined and assembled
2	10.40	11.91	0.14	soldered	sealed coax
3	10.40	11.91	0.46	integral	sealed coax
4	10.40	11.91	0.20	integral	(open coax)
5	10.40	12.19	1.02	integral	(open coax)

Transducer 1.A was relatively long and thin, with a diaphragm which was soldered in place. The solder fillet on the inside of the cavity, combined with a relatively large ratio of d/b = 0.90 (figure 2.3), resulted in some tight radial clearances necessitating some careful polishing and fitting during assembly. The coupling probe was assembled from several machined washers and small pieces. The performance agreed with design predictions, with a sensitivity of 4.3×10^{-5} volts/Pa at 76°K, and reproducibility of about $\pm$ 0.005 volts after some initial pressure cycles. Unfortunately, it developed a leak at a solder joint during testing and calibration in a water bath, and it ceased resonating. Attempts to dry it out and restore resonance did not work, though, from what we learned from subsequent tests, it is probable that we did bake it long enough.

This transducer was then disassembled and thoroughly inspected. No obvious problems were spotted, though discoloration on the cavity surface suggested that improved cleaning after the final solder operation may be helpful in maintaining a high Q.

Reassembly was made using a 0.13 mm diaphragm, about one half the thickness of the previous one, to obtain more sensitivity for differential pressure measurements. However, the reassembled cavity never did work well, being quite sensitive to mechanical shock and to thermal gradients. Using careful polishing and cleaning techniques, the Q of this cavity was about 2900 at 76°, about twice the previous value. (Screening and preliminary calibration tests were often made in a liquid nitrogen bath. The electronic circuits used at that time often would not lock on to the cavity resonance at room temperature, where the signal was relatively low. Liquid helium was used only after satisfactory performance in other ranges was obtained). After several attempts at calibration, tests of vibration, stress and thermal sensitivity, we concluded that the diaphragm must have been distorted slightly during soldering and that an additional support structure was necessary in order to eliminate cavity distortion by mechanical pressure from the coax and pressure lines.

Transducer number two was designed to be a little shorter and bigger diameter, with a different probe construction, and improved mechanical isolation of the cavity from external forces. The different geometry should

theoretically reduce the losses (increase the Q) slightly, and the coaxial probe (figure 2.8) was considerably simpler to build than was the old version. The 0.14 mm diaphragm was soldered on, as before. Though the performance as a transducer was less than could be desired, it was subjected to a number of tests.

In spite of careful cleaning, the measured Q's were 810 at room temperature, 1400 at 76°K, and 3100 at 4°K. The measured voltage shift at zero ΔP due to the dielectric constant of helium in the cavity was 4.7×10^{-7} V/Pa at 76°K, which is equal to the value calculated from the physical properties of helium, within measurement errors. Due to a cold leak across the solder which holds the diaphragm in place, the cavity was disassembled, cleaned and assembled again. After this operation, the measured Q rose to 2420 at 76°K, a more acceptable value. It is evident that, within a factor of two, the Q's are influenced by rather subtle factors.

Calibration data taken at 76°K (figure 2.14) shows good linearity over most of the range, but some hysteresis showed up as the ΔP approached zero. In the first helium test with this transducer, little data were obtained due to an external leak which slowly plugged one of the pressure lines with frozen air; the few points which were obtained suggested a sensitivity of approximately 0.53×10^{-4} V/Pa, though the validity of this conclusion could be questioned. However, a later, more thorough test gave a sensitivity 0.787×10^{-4} V/Pa, with a disappointing amount of hysteresis present (figure 2.15). Two factors from these tests suggest a fundamental problem with this transducer: (1) the sensitivity should be slightly less at 4°K than at 76°K since the elastic modulus of copper increases as the temperature drops, (2) more importantly, the sensitivity is an order of magnitude less than one would calculate for the ideal case. These two factors suggest that the capacitance gap within the cavity is too large, and perhaps non-uniform, and that the thin soldered-in-place diaphragm is afflicted with some sort of localized temperature dependent strain. Rather than attempting improvements in the technique of soldering the diaphragm in place, it was decided to take a more definite step and try machining the cavity and diaphragm out of one solid piece, as in figure 2.5(b).

Cavity number three was constructed essentially identical to cavity number two, except for the thicker diaphragm which was integral with the external wall of the resonant chamber. This is machined by first turning the inside dimensions (11.91 mm diameter by 20.32 mm deep, in figure 2.5(b)) from bar stock at least 30 mm long. After obtaining a good inside surface, a close fitting plug is soldered into this chamber to prevent flexing of the diaphragm as the opposite end is cut off at the desired diaphragm thickness. An alternative technique, suggested by E. Ballinger, is to fill the chamber with beeswax which provides adequate support as long as the piece is not heated by the subsequent machine operation.

Tests on this transducer provided considerable encouragement as to its basic design, and also allowed exploration of circuit problems which previously were smaller perturbations to the output. The circuit problems resulted in random background drifts in the output voltage of, roughly, .020 to .030 volts, and random jumps of roughly the same magnitude associated with making and breaking the coax circuit and with initiating the lock-on circuit. These problems, which are discussed in subsequent paragraphs, made it difficult to unambiguously test for mechanical performance to an accuracy greater than about $\pm$ .02 volts. However, on several occasions the observed background drift was opposite in direction to that expected from the effect of mechanical hysteresis. By making the assumption that this observed drift rate was constant during a calibration run, and subtracting it from the recorded data, we found calibrations at room temperature, 76 K, and 4 K were free from hysteresis and had standard deviations from a smooth (computer) fit of $\pm$ .002 to .003 volt, see figure 2.16. The observed sensitivities were

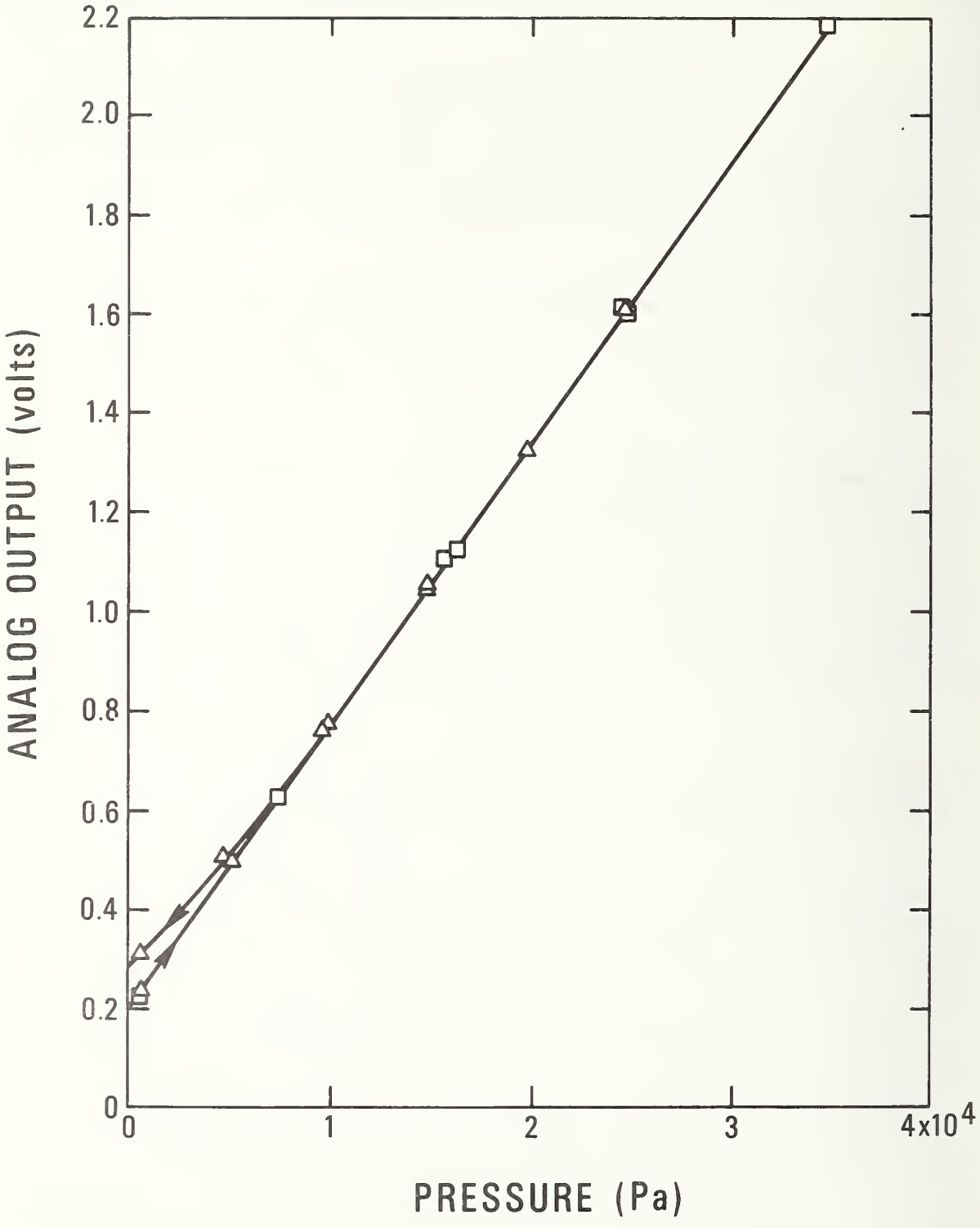

Figure 2.14. Calibration of cavity #2 at 76 K, showing some residual hysteresis.

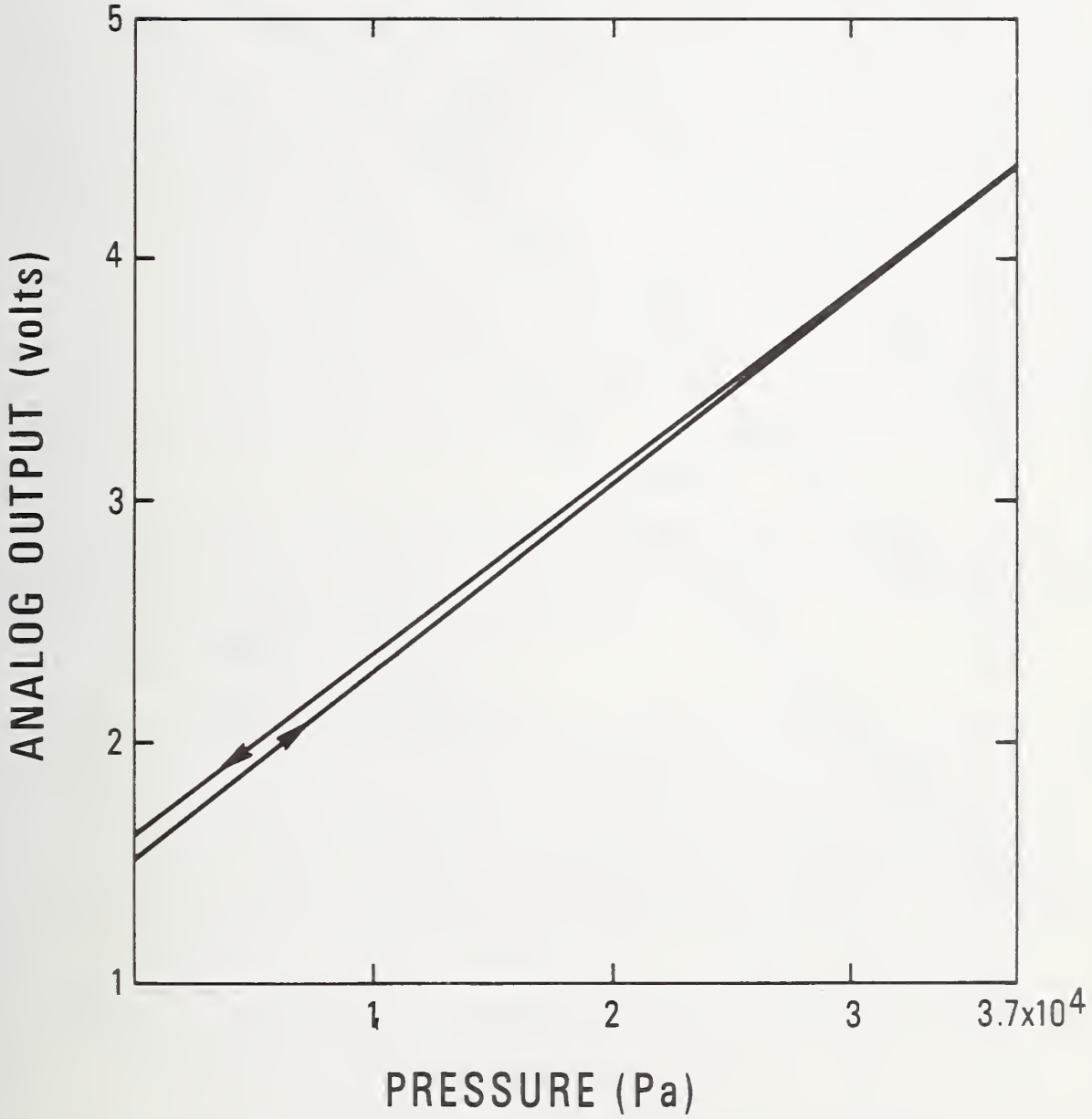

Figure 2.15. Calibration of cavity #2 at helium temperature, showing substantial hysteresis.

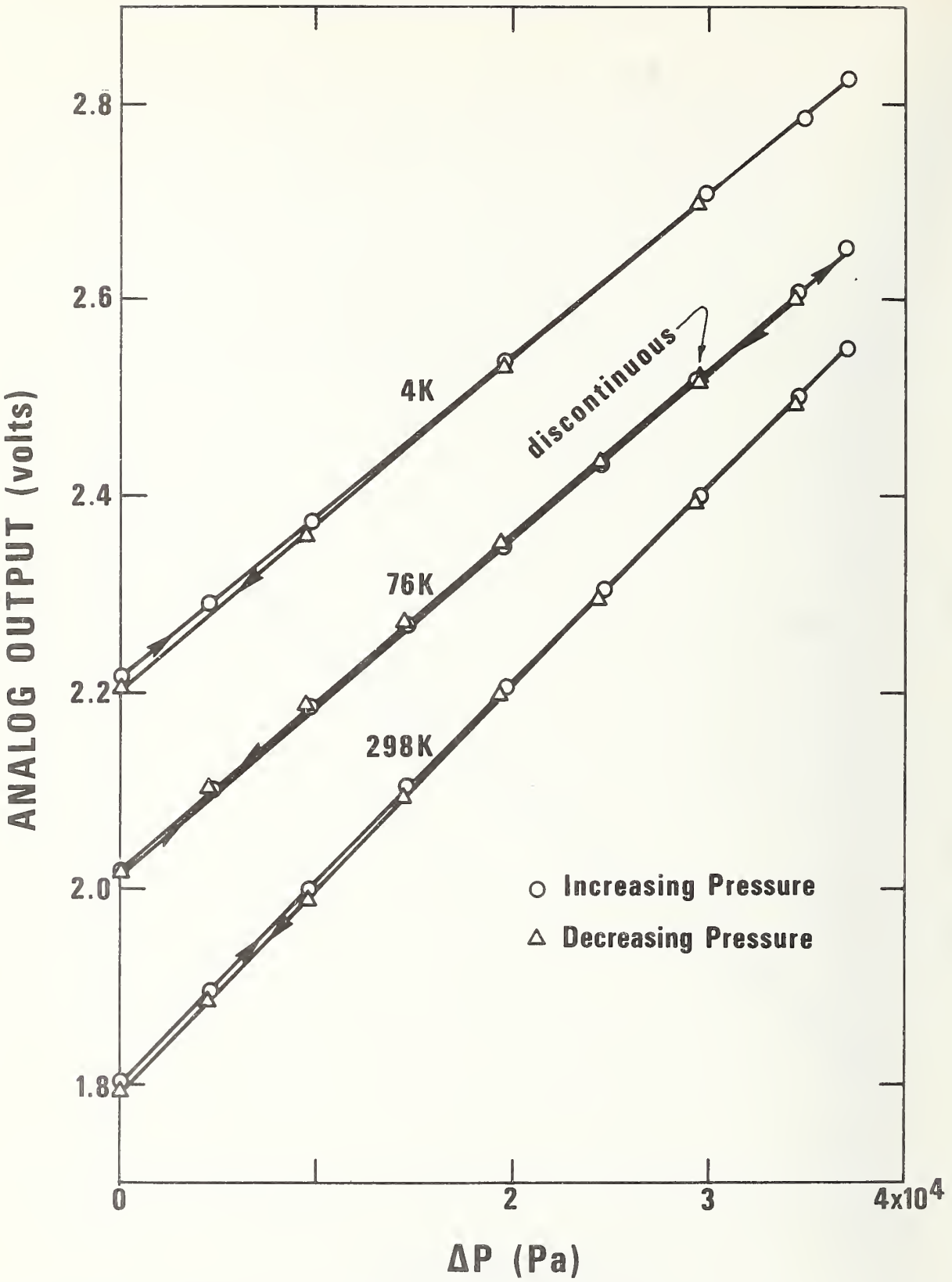

Figure 2.16. Uncorrected calibration data for transducer #3, for three different temperatures. The apparent irreversibility is opposite in direction to that expected from hysteresis, and is interpreted as drift in the electronics. The discontinuity in the 76 K data was observed during an experimental interruption.

2.085×10^{-5} V/Pa at room temperature (25 C)

1.707×10^{-5} V/Pa at 76 K

1.679×10^{-5} V/Pa at 4 K

which are consistent with the known increase in the elastic modulus of copper with decreasing temperature [9]. These will be confirmed when better circuit stability is obtained.

2.4.7 The Coaxial Connector

Evidence accumulated in various tests indicates that the connection of the coaxial conductor to the transducer is a critical design element. When the coax is cold, there is a tiny annular gap between the inside of the outer conductor and the outside of the dielectric spacer. This gap must be sealed to prevent residual vacuum (or pressure) leakage to the low pressure side of the transducer. At the same time mechanical forces from bending or differential thermal contractions of the coax must not be transmitted to the center conductor which terminates in the capacitance gap. Finally, the connector which must be used to eliminate the above mechanical problems should not reflect a significant amount of electrical power at 1200 MHz, i.e., it should match the 50 ohm characteristic impedance of the coax. In one case, cooldown stresses pushed so hard on the center conductor as to cause an irreversible shift to a severely overcoupled condition. After some trials, the connector in figure 2.4 was found to be satisfactory most of the time when installed in the line external to the transducer. However, they did not always stand up well under thermal cycling, and their construction was a slow hand operation. More recently a commercially available hermetic coaxial seal was found which is undamaged by fast immersion in liquid helium. It apparently uses a weakly magnetic material as the center pin, but we do not believe this will result in a measurable sensitivity of the transducer resonance to external magnetic fields.

Even using this commercial connector in place of the sealed coax connector, we occasionly encounter strange reflections which mix with the cavity signal and confuse the detector circuit. Also, successive making and breaking of the coax connections cause random variations of about $\pm$ .02 V at the analog output. These effects are still under study.

2.4.8. Summary and Conclusions

Our conclusion at this time is that the basic transducer design is working well. We have demonstrated hysteresis-free performance, a precision in agreement with theory, and the sensitivity expected from a high-Q resonant circuit. Some details deserve further study: performance with a simplified (less expensive) capacitance probe assembly, reduction of random electrical reflections from coaxial line connections, and reductions of background drifts in the electronics. Because of their insensitivity to electromagnetic noise at power line frequencies, they should be particularly useful for SPTL studies. Two prototype transducers are being installed in an NBS flow loop for field evaluation, and one or two may be delivered to an active SPTL project for furthru field tests.

Potential applications go beyond the needs of the sponsor, and NBS will be putting some funds into applying this technology for venturi flowmetering of cryogenic fluids in the coming year.

2.5. Helium Impurity Study

2.5.1. Assitance to Brookhaven National Laboratory

BNL is evaluating a screw compressor for use with their helium refrigeration system. Since this compressor is oil lubricated, relying on the presence of oil for sealing the impeller, the oil concentration in the helium

discharge must afterwards be reduced to a level acceptable for the following low temperature stages of the refrigerator. Thus in order to evaluate the performance of the oil removal system the impurity levels must be measured. We were asked to work with BNL in this task and have been doing so since November 1975.

At BNL a gas chromatograph is used to analyze for all helium impurities, including compressor oil. However, it would be extremely difficult to prepare calibration mixtures of oil in helium with standard techniques, eg., preparation by weight, because the saturated concentration level is in the parts per billion range. Therefore, we built a calibration apparatus which provides a reproducible oil-helium mixture. The apparatus, shown in figure 2.17, contains a windowed equilibrium cell where the recirculating helium at compressor discharge pressure bubbles through the oil and passes through a knockout pot; this pot serves two purposes. Firstly, the volume of the pot is large enough for the recirculating gas to have a residence time of nearly one hour to remove any entrained oil. Secondly, with the knockout pot and recirculation pump isolated, the large volume provides enough gas for many analyses of a constant composition mixture. All of the apparatus excluding the equilibrium cell is at ambient temperature. The equilibrium cell is submerged in a water bath which is below room temperature to minimize possible entrainment problems.

The apparatus was initially tested at NBS using n-butane instead of compressor oil. These tests showed that the apparatus provides a saturated mixture of butane in helium if the gas is recirculated for 1-1/2 to 2 hours. We found no evidence of entrainment as long as the equilibrium cell was kept below room temperature.

No attempt was made to check out the apparatus with compressor oil before shipping it to BNL since we do not yet have instrumentation for detecting ppb level impurities. Also BNL was in the process of changing grades of compressor oil.

It is not possible to determine the exact concentration of oil in the helium because the oil is such a complex mixture. However, the gas mixtures produced by the calibration apparatus can be used as a guide to the filtration system's effectiveness; this is because the best any filtration system can do is to reduce the oil level to saturation conditions.

The apparatus was delivered to BNL in June, 1976. Compressor oil which had been outgassed by heating in a vacuum for three or four days was put into the compressor and into the calibration apparatus. (The outgassing was required because any oxygen dissolved in the oil would oxidize the oil with one of the oxidation products being hydrogen. BNL had detected a buildup of hydrogen in a previous run when the compressor had been charged with oil directly from the drum). It was found that the oil level in the gas phase of the calibration apparatus was much higher than that taken from the compressor system which contains filters and a liquid-nitrogen-cooled adsorption bed. Next, a sample of oil from the compressor was put into the apparatus. The apparent vapor pressure of this oil was much lower than the original charge since the concentration of oil in the helium dropped nearly a factor of twenty compared with results of the first run. We suspect that the reduction would have been greater if all of the original oil could have been removed from the calibration apparatus. We have concluded that the oil contains volatile materials, relative to the vapor pressure of "pure" compressor oil, which can be removed by adsorption, but not by simply outgassing down to a pressure of 10 microns. If the vapor pressure of the oil can be reduced to the 10^{-11} mmHg range as stated by the manufacturer the saturation level of the oil in helium would be 10^{-14} or less -- far below the estimated maximum allowable concentration level of one ppb and also below the detectable level of any analytical equipment with the possible exception of a helium ionization detector.

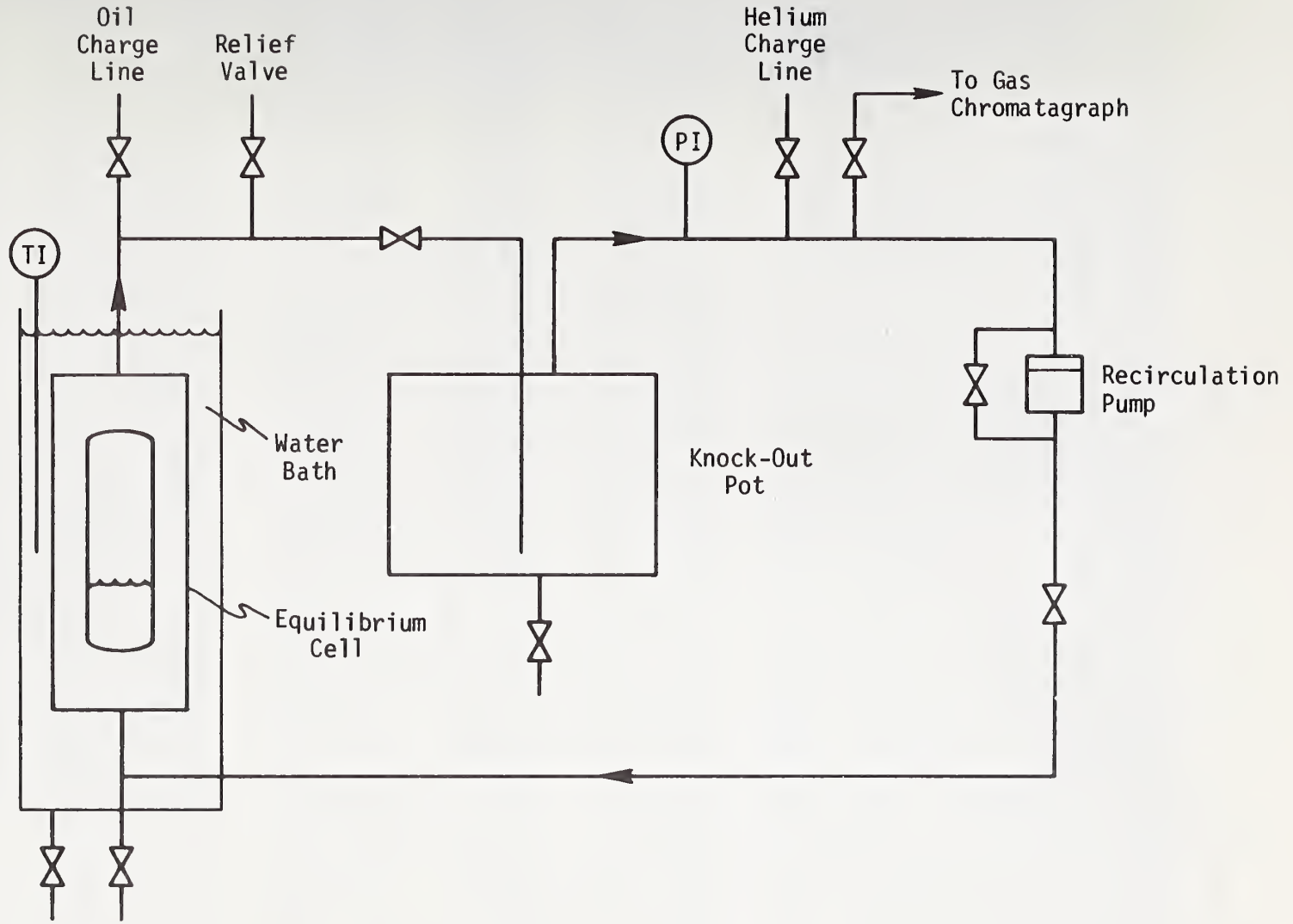

Figure 2.17. Schematic of helium impurity calibration apparatus.

2.5.2 Instrumentation for Air Impurities in Helium

Removal of impurities via filtration and adsorption is state-of-the-art technology (even if it is not fully understood), but instruments for on-line detection are not. Therefore, we are concentrating our efforts toward the low level detection of helium impurities with emphasis on the detection of air. At this stage we are considering methods to detect the adsorption bed breakthrough of air while keeping in mind the need for a rugged, reliable instrument which can be used in the field. A literature search revealed little information applicable to our particular requirements.

Both the concentration level and type of impurity dictate the kind of detector needed. If the level of air is in the parts-per-million range a conventional thermal conductivity detector with thermistors could be used. Also, it is possible that by replacing the thermistors with silicon diodes, the detector could be used in situ with a substantial increase in sensitivity. The thermal conductivity detector is a "rugged" device, insensitive to minor pressure and temperature fluctuations but more sensitive to flow fluctuations. Experimental work is necessary to determine how much the sensitivity would be enhanced by operating at the lower temperatures.

If the impurity is in the parts-per-billion range there presently are only two detectors which have the necessary sensitivity: helium ionization and electron capture. Helium ionization detectors can detect all trace impurities in the ppb range. However, they have the disadvantage of being very temperature and flow sensitive. Two of the three manufacturers of helium ionization detectors have stopped selling them because the maintenance costs were so high.

A more rugged and reliable detector is the electron capture detector. This instrument is used to detect trace quantities of oxides and halogenated hydrocarbons in the atmosphere. It is insensitive to nitrogen but very sensitive to oxygen. However, the detector increases sensitivity with increasing temperature and is normally operated in the 300 to 350° C range.

If air is the major contaminant in helium, the electron capture detector could be an attractive means of detecting bed breakthrough, especially if the packing is a molecular sieve, since oxygen breaks through the bed before nitrogen. Some work is needed to determine the minimum detectable level (MDL) of the electron capture detector to oxygen in a helium stream and also to determine how sensitive the detector is to flow, temperature and pressure fluctuations.

Finally, the thermal conductivity detector could be used to detect ppb of impurities if the impurities could be concentrated in some manner. One way would be to collect the impurities on another small adsorption bed at 80 K, warm the bed to room temperature or above and pass this gas through a detector. Also, a sample could be collected and put into a heated quartz tube which would allow the helium to diffuse out of the container. The residual gas could then be analyzed for impurities. Unfortunately, these concentration techniques could be difficult to adapt to automated field operation.

Currently, the only detector which can detect hydrogen and neon in the ppb range is the helium ionization detector. However, it might be possible to develop a detector sensitive to hydrogen in this low concentration range.

Future work planned on this project includes the evaluation of the electron capture detector; a manufacturer has tentatively agreed to loan us a detector for this work. Also, if it can be determined that its MDL is in the 100 to 1000 ppb range the thermal conductivity detector using silicon diodes will be investigated. Finally, methods for detecting low levels of hydrogen will be studied.

2.6 References

[1] Erez, A., A proposed light-coupled system for electrical measurements, Proc. Electro-Optical System Design Conf., pp. 183-188 (Sept. 1971).

[2] Morse, R.M., Staniforth, A., Morse, A.R., A data system for high voltage DC test lines, IEEE Trans. on Instrumentation IM-20, 285 (1971).

[3] Arp, V.D., Daney, D.E., Frederick, N.V., Jones, M.C., Ludtke, P.R., Parrish, W. R. and Powell, R.L., Helium research in support of superconducting power transmission, Nat. Bur. Stand. (U.S.) NBSIR 75-823 (October 1975).

[4] Van Degrift, C.T., A sensitive displacement transducer using an extremely reentrant 84 MHz cavity oscillator, Rev. Sci. Instrum. 45, 1171 (1974).

[5] Zimmerman, J.E., private communication.

[6] Timoshenko, S., Strength of Materials, Part II, Advanced Theory and Problems, D. Van Nostrand and Company, Princeton (1956).

[7] Reed, R.P. and Mikesell, R.P., Low temperature mechanical properties of copper and selected copper alloys, Nat. Bur. Stand. (U.S.) NBS Monograph 101 (1967).

[8] Neubert, H.K.P., Instrument Transducers, Oxford University Press (1963).

[9] Read, D.T. and Ledbetter, H.M., private correspondence; also, Ledbetter, H. M. and Weston, W.F., Low temperature elastic properties of some copper-nickel alloys, Ultrasonics Symposium Proc., IEEE Cat. No. 75 CHO 994-4SU (1975).

3.0 HELIUM PROPERTIES

In the early 1970's R. D. McCarty of our Laboratory collected and correlated all available data on the properties of helium. The output from this work is in the form of publications [1, 2] and computer codes which have been widely distributed throughout the world. However, some new data have become available, and advances have been made in the equations and computer codes which represent that data. We have maintained a low level of effort in this field and report here some recent developments.

3.1 Improved Helium Property Computer Codes

McCarty's basic equation of state uses density and temperature as the independent variables, whereas for many engineering calculations, pressure, enthalpy or entropy often occur as independent variables. New forms of helium equations, using these latter variables, were reported by Arp [3]. However, the residual inconsistency (typically about 0.02 K) between the McCarty and the Arp equations sometimes leads to problems when both equation sets are used in calculations which demand high internal consistency. In such cases it is necessary to use slow double-iteration techniques with McCarty's equations rather than to use Arp's equations.

At the Cryogenics Laboratory of the Department of Engineering Sciences in Oxford University, England, Hands revised the computer program based on McCarty's equations to convert them entirely to SI units, and to obtain faster computing time with very minor increase in required computer memory [4]. In addition, both Hands [4] and Arp [unpublished] independently developed some single and double iteration subroutines to be used when faced with the internal inconsistency problems mentioned in the above paragraph.

In the meantime, several workers have uncovered an error in the equation which McCarty used for the dielectric constant [Johnson, Acton and Kellner, private correspondence]. Equation 25 in reference [1] should read

$$\frac{3M}{4\pi}\ \frac{\varepsilon-1}{\varepsilon+2}\ \frac{1}{\rho} = p.$$

The factor $3M/4\pi$, which is missing in reference [1], essentially causes the published values of $(\varepsilon-1)$ to be about 4.6% lower than the true values ($M = 4.0026$ for helium).

Dr. Hands was a Guest Worker in our Laboratory during May and June of this year. During this time various subroutines in respectively the NBS and Oxford computer packages were compared, and the most efficient of them assembled into a single computer package, in SI units. The error in the dielectric constant subroutine was corrected. At the same time, we studied one other small problem with the basic equation of state used in [1].

The equations actually consist of a set of three mathematically separate equations, each valid in its own region of the density-temperature plane. The problem comes in obtaining a smooth transition from one region to another where the equations overlap, particularly in the region from 10 to 15 K at pressures greater than critical. Within this latter region one can find, for example, specific heats which waver unrealistically; more importantly, the equations are not thermodynamically consistent in that $\int_{10}^{15} C_p\, dT$ is not exactly equal to ΔH along an isobar. The error is negligible at 5×10^5 Pa (5 atmospheres) but about 20 percent at 100×10^5 Pa. Presumably one could find related errors in other thermodynamic functions and derivatives, but we have

not tested this. After some study, and discussion with McCarty, we conclude that there is no easy way to eliminate the inconsistency, but we can smooth the functions more effectively in this range by using a quadratic interpolation scheme between 9 and 16 K rather than the previous linear interpolation between 10 and 15 K. This has been done in the revised computer package, mentioned above.

To obtain this revised computer code, the reader (within the U.S.) should contact the NBS Cryogenics Division.

To put these equation of state problems in proper perspective, it is worth noting that the equation of state for helium is probably known more accurately and over a wider range (compared to its critical pressure and temperature) than is the equation of state for water, the most studied of all fluids. The next major advance in this field will probably come from the use of non-analytical terms to more accurately describe properties near the critical point.

3.2 Thermal Conductivity of Helium

Until very recently, no data have existed on the thermal conductivity of helium in the range from 4 to 20 K. This interval includes the critical point (at 5.2 K and 2.2×10^5 Pa), in the neighborhood of which it is known that all fluids exhibit markedly enhanced thermal conductivities. Our published tables [1] and computer codes in this region are based upon approximate scaling laws against C_p, developed several years ago for hydrogen. Our lack of confidence in this helium data has been stated on a number of occasions.

Acton and Kellner at Southampton University in England have measured the thermal conductivity of helium within this range during the past year. They do not plan to develop a data correlation, and have very kindly forwarded all of their data to us prior to their forthcoming publication. We find that their data is in fact generally within about 10 percent of our published values. We have begun to develop a correlation based upon currently accepted thermodynamic models, but have not yet completed the work. This work will be published, and added to the computer package of helium properties, only after the Acton and Kellner publication is completed.

3.3 References

[1] McCarty, R.D., Thermophysical properties of helium 4 from 2 to 1500 K with pressures to 1000 atmospheres, Nat. Bur. Stand. (U.S.) NBS Technical Note 631 (1972).

[2] McCarty, R.D., Thermodynamic properties of helium 4 from 2 to 1500 K at pressure to 10^8 Pa, Journal Phys. Chem. Reference Data 2, 923 (1973).

[3] Arp, V., New forms of state equations for helium, Cryogenics 14, No. 11, 593-598 (Nov. 1974).

[4] Hands, B.A., HEPROP, a computer package for the thermophysical properties of helium down to about 2 K, Cryogenics 13, 423 (1973).

4.0. FLOW FACILITY FOR MODELLING HELIUM FLOW PASSAGES OF HIGH ASPECT RATIO (L/D) ("LONG LINE" APPARATUS)

We have now completed construction and instrumentation of this apparatus. It is designed for investigations into steady state and time dependent fluid mechanical and heat transfer problems related to SPTL operation. Experiments planned include, first, measurement of friction factors during unheated steady flow of supercritical helium at a variety of pressures. In addition to supplying valuable data, this will serve to checkout the apparatus and prepare for the next phase -- studies of oscillatory behavior of supercritical helium flowing with uniform heating. These studies will require a systematic exploration of operating parameters and configurations. Inlet temperature, pressure, flow rate and total temperature rise of the helium will be varied, but, in addition, it is necessary to vary the flow impedance of equipment upstream and downstream of the heated channel. The final experiments will investigate the response of flow parameters to point and distributed heat pulses. Total length of channel will be variable in increments.

4.1. Apparatus

Because of the wide range of operating conditions anticipated during the course of the NBS experiments, the apparatus was designed for blow-down, or once-through operation, as illustrated in the flow schematic, figure 4.1. High pressure (120 atm) helium gas is regulated to near the operating pressure and then cooled to 80 K in the precooler. The helium then flows to the subcooler where it cools to near 4 K as it passes through a counter flow heat exchanger and a coil immersed in liquid helium. The temperature of the helium exiting the subcooler is at present controlled by a flow mixing valve. However, installation of a regulated heater is planned in order to achieve improved temperature control. After passing through the test section (in the experimental vessel) the helium cools, in succession, radiation shields in the experimental vessel and the subcooler transfer line. A general view of the apparatus is shown in figure 4.2. Appearing from left to right are the subcooler, precooler and experimental vessel.

The present test section, which is located in the experimental vessel (figure 4.3) is wound from 5 lengths of 4.008 mm I.D. x 0.41 mm wall stainless steel tubing. The total length is 182.9 m, giving a length to diameter ratio of $4.6\ (10)^4$, and the diameter of the helix is 77.5 cm, giving a value of 194 for the ratio of helix diameter to tube diameter. Epoxy-glass fiber spacers support the coil, and each coupling serves as a pressure and temperature station. All helium-temperature components are inside a copper radiation shield cooled by the exit gas, and this shield in turn is inside a liquid-nitrogen-cooled shield.

So that the flow impedance at either end of the test section may be varied, throttling valves and expansion pistons (7.6 cm diameter x 30 cm stroke) are provided as shown in figure 4.1.

The nominal range of the operating parameters is 0 to 30 atm inlet pressure, 4.5 to 100 K inlet temperature and 0 to 0.7 g/s mass flow rate.

4.2. Instrumentation

The position of the pressure and temperature instrument stations is given in figure 4.4 and the station details in figure 4.5. Although pressure taps

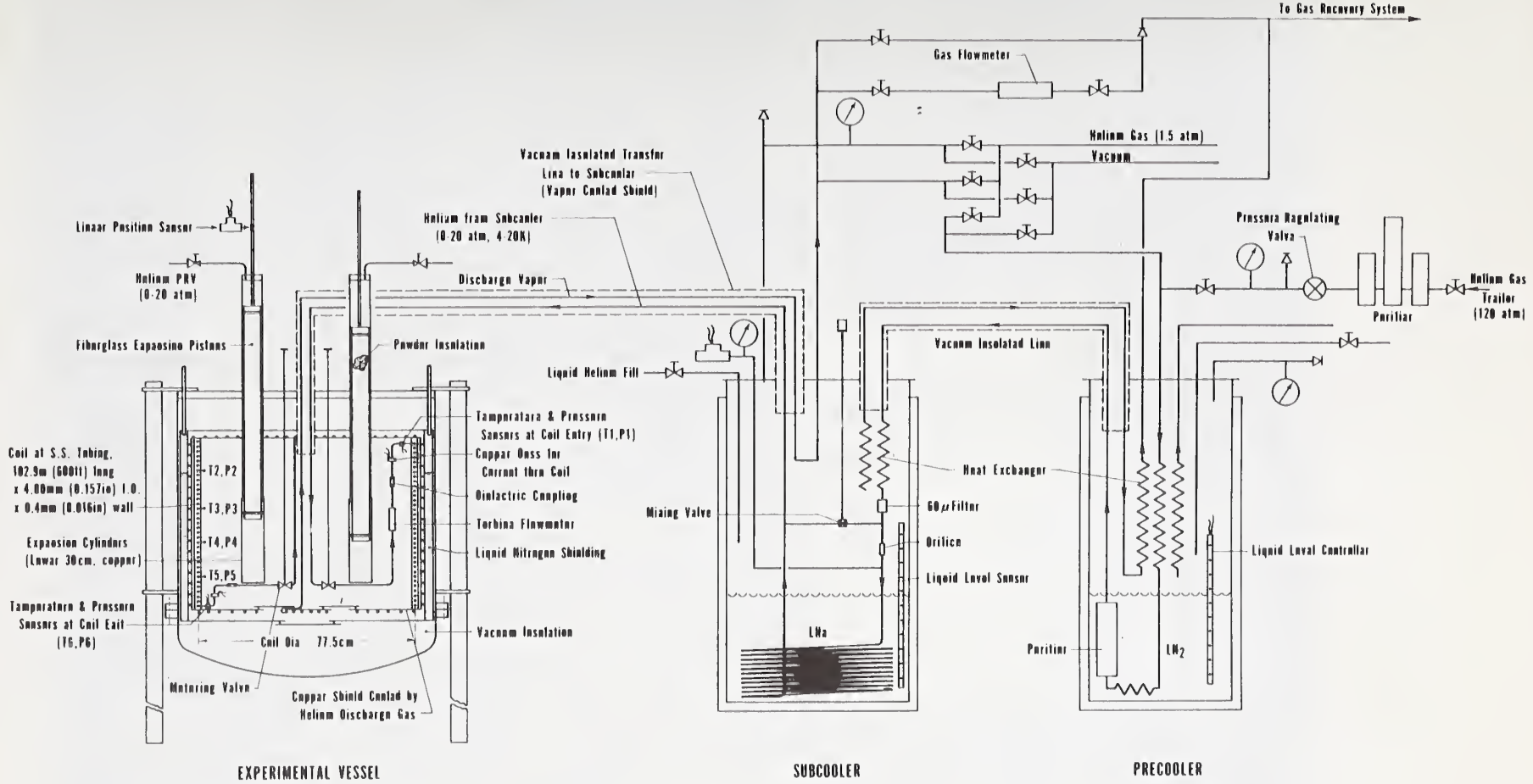

Figure 4.1. Flow schematic of Long Line apparatus.

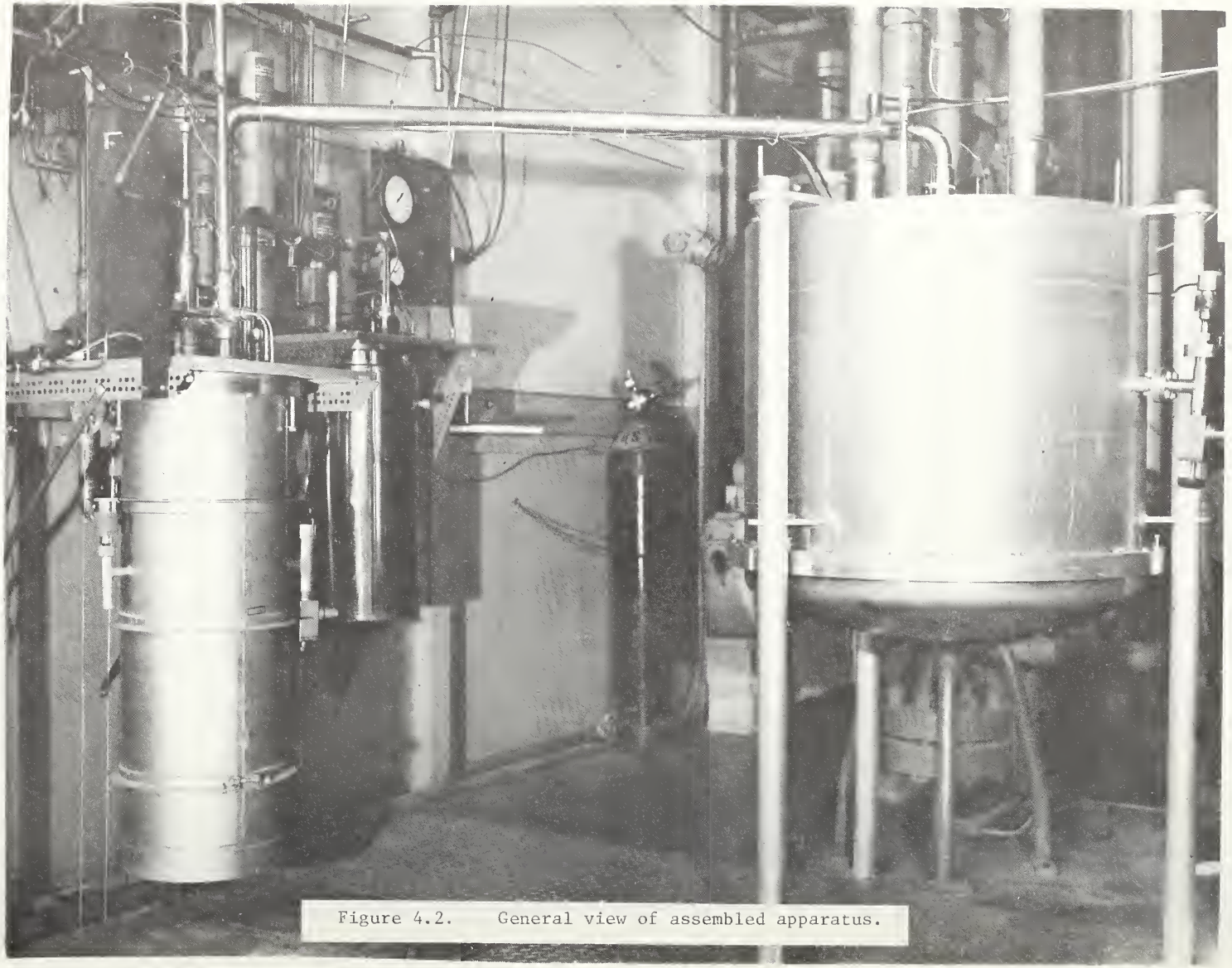

Figure 4.2. General view of assembled apparatus.

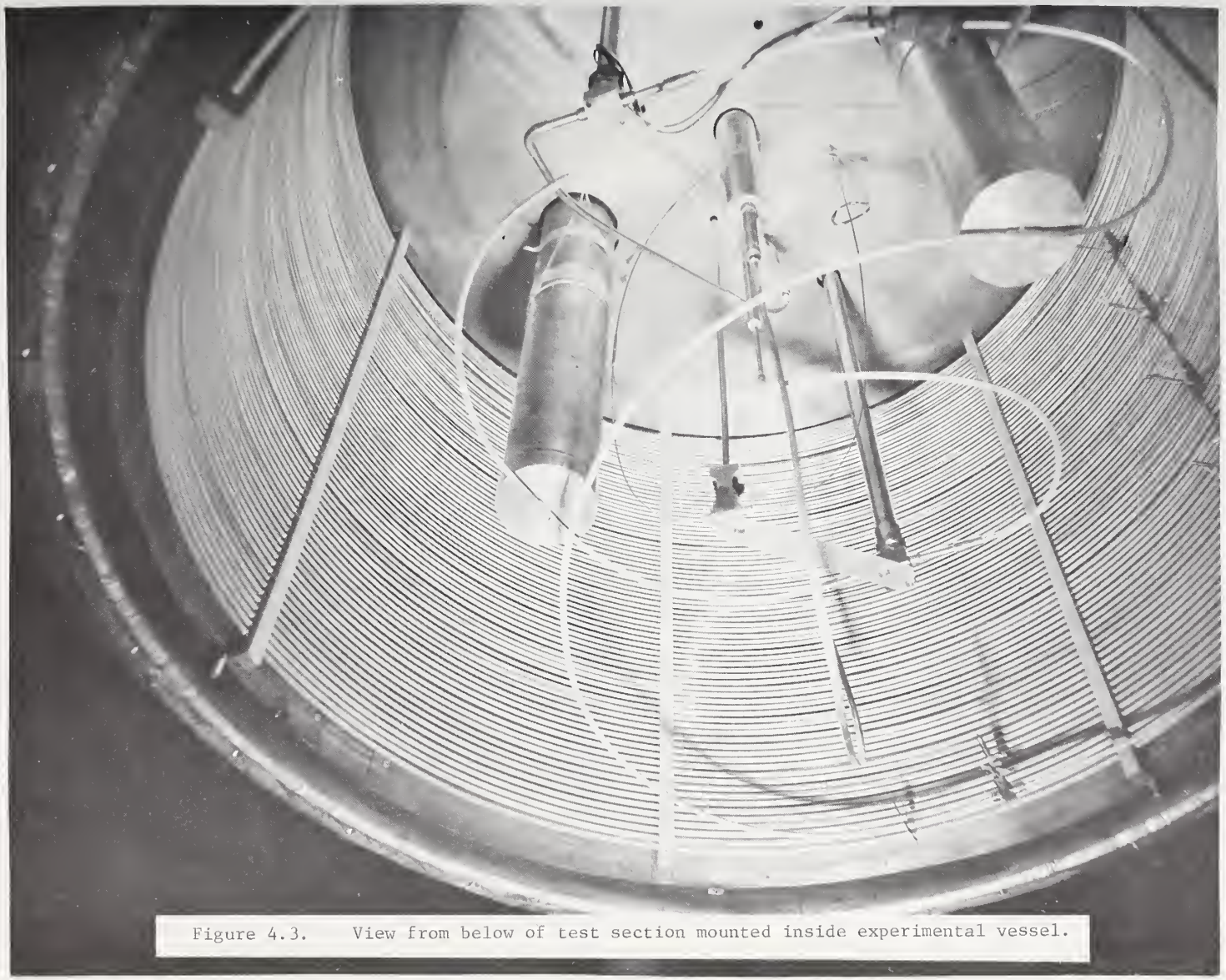

Figure 4.3. View from below of test section mounted inside experimental vessel.

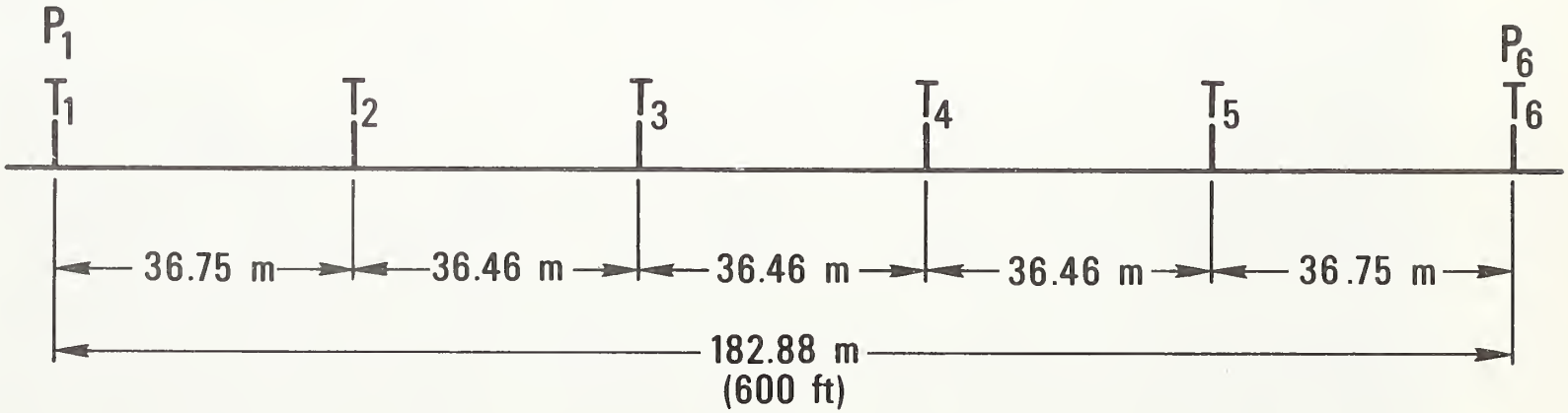

Figure 4.4. Positions of test section instrumentation.

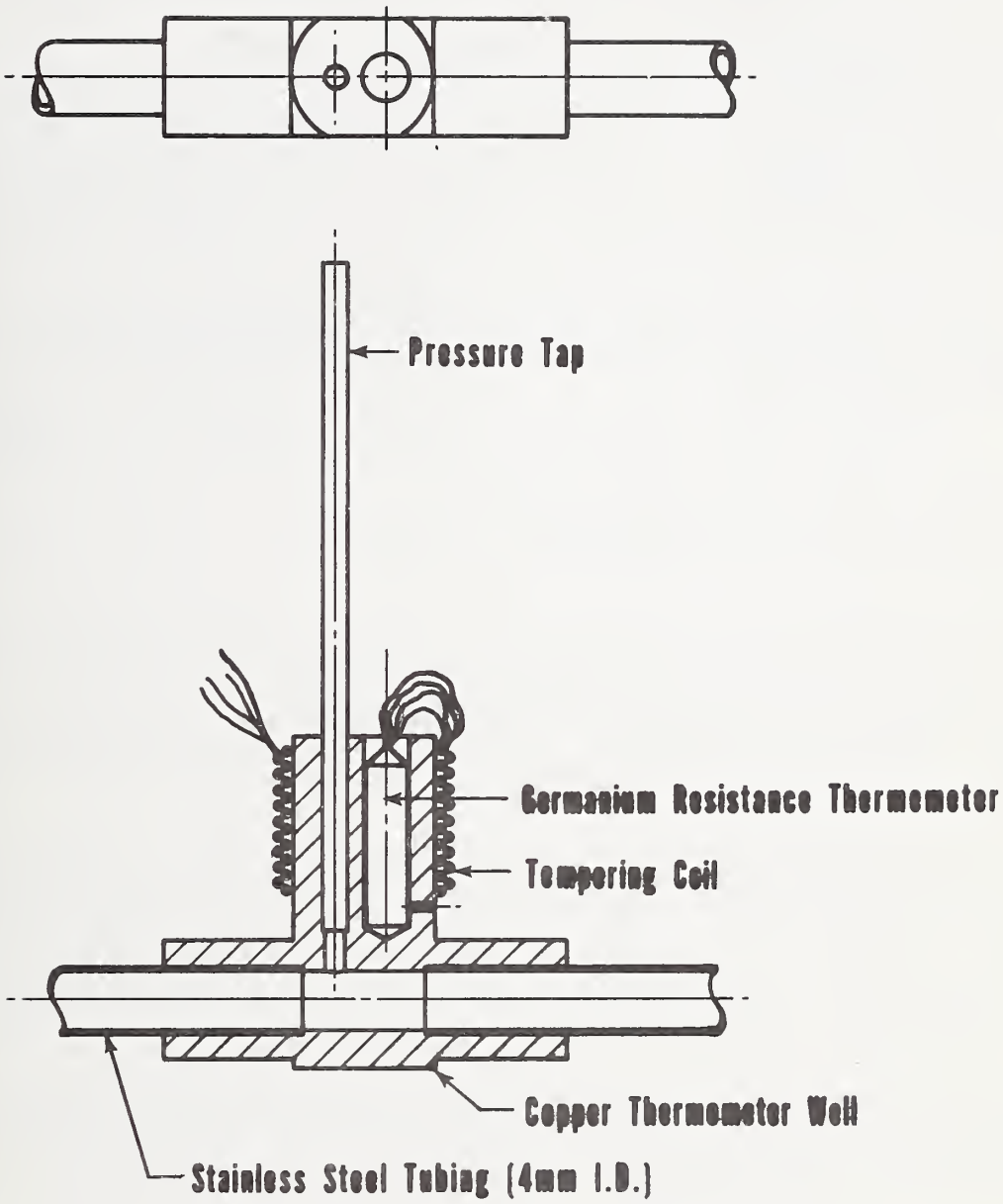

Figure 4.5. Thermometer well-pressure tap detail.

are provided at each station, only positions 1 and 6 are presently connected to pressure transducers. A variable reluctance diaphragm pressure transducer (in addition to a high precision bourdon tube gauge) is used to measure P_1. The pressure drop across the test section (P_1-P_6) is measured by a high precision capacitive-diaphragm type transducer. Future plans call for the installation of microwave cavity pressure transducers.

Temperatures at each station are measured with germanium resistance thermometers which are soldered into the wells with Wood's metal to assure good thermal contact. An electrical shunt around each well and 5 cm of tubing each side insures that thermal equilibrium between thermometer and helium will not be disturbed during heating runs when the stainless steel tubing will be directly heated by the passage of electric current.

The mass flow rate is determined by metering the exit gas at ambient temperature. At flow rates below 0.15 g/s a thermal type meter is used, and at higher rates a dry diaphragm type meter. Flow rate may also be measured with a turbine flowmeter at the inlet to the test section.

Data acquisition is by means of a mini-computer programmed to give on-line reduction of input emf's to temperatures, pressure, etc. Printout intervals as frequent as 20 s are possible, the principle limitation being the printer speed. Cathode ray tube display of the computer output is used during the general course of experimental operation until a permanent record is desired.

4.3. Status

Shakedown runs have been completed and have demonstrated successful operation of the system at 5 atm pressure and 6 K.

NBS-114A (REV. 7-73)

U.S. DEPT. OF COMM. BIBLIOGRAPHIC DATA SHEET	1. PUBLICATION OR REPORT NO. NBSIR 77-853	2. Gov't Accession No.	3. Recipient's Accession No.

4. TITLE AND SUBTITLE

HELIUM RESEARCH IN SUPPORT OF SUPERCONDUCTING POWER TRANSMISSION

5. Publication Date: February 1977

6. Performing Organization Code: 275.05

7. AUTHOR(S) M. C. Jones, V. D. Arp, W. R. Parrish, D. E. Daney, P. R. Ludtke, N. V. Frederick and B. A. Hands

8. Performing Organ. Report No. NBSIR

9. PERFORMING ORGANIZATION NAME AND ADDRESS

NATIONAL BUREAU OF STANDARDS
DEPARTMENT OF COMMERCE
WASHINGTON, D.C. 20234

10. Project/Task/Work Unit No. 2750551

11. Contract/Grant No. ERDA E(49-1)-3800

12. Sponsoring Organization Name and Complete Address (Street, City, State, ZIP)

U.S. Energy Research and Development Administration
Office of Conservation
Division of Electric Energy Systems
Washington, DC 20545

13. Type of Report & Period Covered: Annual Report July 1975 - Sept. 1976

14. Sponsoring Agency Code

15. SUPPLEMENTARY NOTES

16. ABSTRACT (A 200-word or less factual summary of most significant information. If document includes a significant bibliography or literature survey, mention it here.)

This report is the second annual report of research on helium related problems in support of superconducting power transmission development. The report is in four sections

In the first section; results are presented from experimental and computer modeling of the performance of current leads cooled with supercritical helium gas. Performance characteristics studied are burn-out conditions and existence of oscillation in the helium gas.

The second section, on helium measurements, reports some conclusions on the feasibility of data transmission from high-voltage regions to grounded read-out instrumentation, on thermometry and on helium impurity measurements. A major part of this section is a detailed description with test results of microwave cavity pressure transducers for use at helium temperatures.

A third section, on helium properties, reports some improvements in computer codes for helium properties and discusses some recent data on the thermal conductivity of helium.

In the final section, a description is given of a recently completed flow facility which has been built for research on flow and heat transfer dynamics of supercritical helium in channels of high aspect ratio modeling superconducting power transmission line channels.

17. KEY WORDS (six to twelve entries; alphabetical order; capitalize only the first letter of the first key word unless a proper name; separated by semicolons)

Burn-out; helium-cooled current leads; helium flow facility; helium impurities; microwave pressure transducer; thermal-acoustic oscillations.

18. AVAILABILITY

[X] Unlimited

[ ] For Official Distribution. Do Not Release to NTIS

[ ] Order From Sup. of Doc., U.S. Government Printing Office Washington, D.C. 20402, SD Cat. No. C13

[X] Order From National Technical Information Service (NTIS) Springfield, Virginia 22151

19. SECURITY CLASS (THIS REPORT)	21. NO. OF PAGES
UNCLASSIFIED	98
20. SECURITY CLASS (THIS PAGE)	22. Price
UNCLASSIFIED	$5.00

USCOMM-DC 29042-P74